# ASSESSING THE IMPACT OF SEA-SURFACE TEMPERATURE BIASES AND ERRORS ON TROPICAL CYCLONE SIMULATIONS AND PREDICTIONS

A Dissertation

by

WEI-CHING HSU

Submitted to the Office of Graduate and Professional Studies of
Texas A&M University
in partial fulfillment of the requirements for the degree of

DOCTOR OF PHILOSOPHY

| | |
|---|---|
| Chair of Committee, | Ping Chang |
| Committee Members, | Benjamin Giese |
| | Christina M. Patricola |
| | Robert Korty |
| Head of Department, | Shari Yvon-Lewis |

August 2018

Major Subject: Oceanography

# ABSTRACT

Tropical cyclones (TCs) are one of the most impactful natural hazards to people's life and economy, and improving forecast and future projection of TCs is one of the most important areas for the weather and climate research community. Previous studies show that sea surface temperature (SST) patterns both local to and remote from TC development regions are important drivers of the variability of TC activity on different timescales. Thus, reliable simulations and predictions of TC activity depend on a realistic representation of tropical SSTs. Nevertheless, severe SST biases are common to the current generation of global climate models, especially in the tropical Pacific and Atlantic, where TCs are active. Alleviating these SST biases has proven challenging, leading to the prospect that the bias problem may persist for decades, even with improvements in our understanding of the causes of the biases and in reducing the biases in the newer version of climate models. It is, therefore, crucial to understand and evaluate the effects of the biases on simulations of climate extremes. Using an atmospheric-only tropical-channel model (TCM), we investigated the impact of SST biases and uncertainties in SST prediction on TC simulations. The simulation results show significant influences from SST biases on TC simulations both in local basins and remote ocean basins. Moreover, ensemble dynamical downscaling experiments using TCM forced by SST anomalies derived from CESM Decadal Prediction Large Ensemble (CESM-DP-LE) experiments also reveal impacts from uncertainties in lateral boundary conditions, suggesting that uncertainties in tropical SST prediction may not be the only dominant factor limiting TC predictability. Last but not least, we explored the prospect of multiyear-to-decadal TC prediction by evaluating the skill of CESM-DP-LE in predicting TC-related environmental condition changes on multiyear-to-decadal time scales. The

results show that CESM-DP-LE is highly skillful in predicting TC genesis potential index (GPI) on multiyear to decadal timescales. In particular, it successfully predicted the decadal shift in the mid 1990s when the Atlantic TC activities increased abruptly. This result paves the way for further study of decadal TC forecast.

## CONTRIBUTORS AND FUNDING SOURCES

This work was supported by a dissertation committee consisting of Professor Ping Chang and Professor Benjamin Giese of the Department of Oceanography, and Dr. Christina M. Patricola and Professor Robert Korty of the Department of Atmospheric Science.

The CESM-DP-LE data was provided by Dr. Stephen Yeager at NCAR. And the control runs in Chapter II were conducted by Dr. Christina Patricola. All other work conducted for the dissertation was completed by the student independently.

The research was supported by U.S. National Science Foundation Grants OCE-1334707, AGS-1347808, and AGS-1462127, and National Oceanic and Atmospheric Administration Grant NA13OAR4310136. High-performance computing resources were provided by the Extreme Science and Engineering Discovery Environment (XSEDE). Simulations were performed at the Texas Advanced Computing Center (TACC) at the University of Texas at Austin and the Texas A&M Supercomputing Facility.

TABLE OF CONTENTS

Page

ABSTRACT ..... ii

CONTRIBUTORS AND FUNDING SOURCES ..... iv

TABLE OF CONTENTS ..... v

LIST OF FIGURES ..... vii

LIST OF TABLES ..... xii

CHAPTER I INTRODUCTION ..... 1

1.1 Importance of Tropical Cyclone Simulations ..... 1
1.2 Evolution of Tropical Cyclone Simulation and Prediction ..... 2
1.3 Importance of Sea Surface Temperature on Tropical Cyclone Activity ..... 3
1.3.1 Relationship Between Sea Surface Temperature and Tropical Cyclones ..... 3
1.3.2 Impact of SST Representation on TC Simulations ..... 5
1.4 Challenges and Objectives ..... 8

CHAPTER II THE IMPACT OF CLIMATE MODEL SEA SURFACE TEMPERATURE BIASES ON TROPICAL CYCLONE SIMULATIONS ..... 11

2.1 Introduction and Background ..... 11
2.2 Research Methods – Model Description and Experimental Designs ..... 14
2.2.1 Model Description ..... 14
2.2.2 Experimental Designs ..... 15
2.2.3 Quantifying TC Activity ..... 17
2.3 Results ..... 18
2.3.1 Atlantic SST Biases ..... 18
2.3.2 Pacific SST Biases ..... 23
2.3.3 Atlantic and Pacific SST Biases ..... 26
2.4 Discussion and Summary ..... 28

CHAPTER III UNCERTAINTY AND FEASIBILITY OF DYNAMICAL DOWNSCALING FOR TROPICAL CYCLONE PREDICTION AT SEASONAL-TO-DECADAL TIME SCALES ..... 53

3.1 Introduction and Objectives ..... 53
3.2 Model Description and Experimental Designs ..... 55
3.2.1 CESM-DP-LE ..... 56
3.2.2 WRF-Based TCM ..... 58
3.2.3 Experimental Design ..... 59

3.2.3.1 Two Cases: 1997/1998 and 2015/2016 ..... 60
3.2.3.2 SSTA Representations During the Two Cases ..... 61
3.2.3.3 Experiment Description ..... 63
3.3 Results ..... 64
3.3.1 TCM2's Potential TC Forecast Skill ..... 64
3.3.2 Impact of Predicted SST Errors on TC Hindcast ..... 66
3.3.2.1 Model Skills with Predicted SST ..... 66
3.3.2.2 Insensitivity of ACE to Errors in Predicted SSTA ..... 68
3.3.3 Uncertainty from Lateral Boundary Conditions ..... 69
3.3.3.1 ACE, TC Counts, and Track Density Anomalies ..... 70
3.3.3.2 GPI Analysis of DPs and BC ..... 70
3.3.3.3 Heat Transport Analysis ..... 72
3.3.4 Uncertainty from Atmospheric Internal Variability (Initial Conditions) ..... 74
3.4 Summary and Future Work ..... 74

CHAPTER IV EXPLORING LONG-TERM PREDICTABILITY OF TROPICAL CYCLONES USING CESM DECADAL PREDICTION LARGE ENSEMBLE (CESM-DP-LE) ..... 95

4.1 Introduction and Objectives ..... 95
4.2 Data and Research Method ..... 97
4.2.1 CESM-DP-LE ..... 97
4.2.2 Genesis Potential Index ..... 98
4.3 Results ..... 100
4.3.1 Evaluating Skills of CESM-DP-LE in Predicting Decadal Changes of TC Environment Condition ..... 100
4.3.1.1 GPI from CESM-DP-LE ..... 101
4.3.1.2 Diagnosing GPI Terms ..... 102
4.3.2 MDR GPI and TC Time Series Analysis ..... 104
4.3.2.1 MDR GPI Time Series ..... 104
4.3.2.2 Decomposition of GPI ..... 105
4.4 Summary and Discussion ..... 107

CHAPTER V CONCLUSIONS AND FUTURE WORK ..... 122

5.1 Conclusions ..... 123
5.2 Future Work ..... 124

REFERENCES ..... 127

LIST OF FIGURES

Page

Figure 1.1. A summary of the large ensemble TCM experiment. Each row in this figure represents Atlantic ACE variability in response to SST forcing of a particular mode of climate variability with the bottom row representing observed ACE variability based on HURDAT .....10

Figure 2.1. The April-November averaged multi-model mean tropical SST biases (°C) .....34

Figure 2.2. The differences between track density ensemble means of Atlantic (a) warm (*AtlWB*), (b) cold (*AtlCB*), (c) total (*AtlTB*) bias runs, and that of control (*CTRL*) runs. Hatched regions passed the two-sample student t-test at 5% significance level .....35

Figure 2.3. Boxplot of simulated Accumulated Cyclone Energy (ACE) ((a) to (c)) and number of TCs ((d) to (f)) from control (*CTRL*), Atlantic warm (*AtlWB*), cold (*AtlCB*), and total (*AtlTB*) bias runs (16 ensemble members each) in different ocean basins. The horizontal line between light and dark shading represents the median of the ensemble values, while the upper boundary of the light color box represents the 75 percentile and the lower boundary of the dark color box represents the 25 percentile. The whiskers show the maximum and minimum ensemble values .....36

Figure 2.4. The differences between GPI ensemble means of Atlantic (a) warm (*AtlWB*), (b) cold (*AtlCB*), (c) total (*AtlTB*) bias runs, and that of control (*CTRL*) runs. Hatched regions passed the two-sample student t-test at 5% significance level .....37

Figure 2.5. The contribution on the differences of GPI ensemble means between Atlantic cold (*AtlCB*) bias runs and control (*CTRL*) runs from different GPI terms. Hatched regions passed the two-sample student t-test at 5% significance level .....38

Figure 2.6. The wind cross-section along 15°N (averaged from 12.5°N to 17.5°N), where the *AtlCB* shear contribution (to GPI anomaly) and cold bias induced zonal wind anomalies at 200hPa and 850hPa show the largest values. (a) shows the ensemble-averaged anomalous wind profile (in arrows [m/s]) calculated from zonal (u) and vertical (w) wind (times 6000 for scaling) differences between *AtlCB* and *CTRL* runs, and the zonal wind anomalies (in shaded color) from *AtlCB* comparing to *CTRL*, while (b) shows the *CTRL* ensemble-averaged wind profile, and (c) shows the *AtlCB* wind profile .....39

Figure 2.7. JJAS accumulated precipitation (a) and seasonal-mean vertical-integrated (1000hPa to 500hPa) moisture convergence (b) differences between *AtlCB* and *CTRL*. Red colors in (a) indicate more precipitation in *AtlCB* than *CTRL*.

While red colors in (b) indicate anomalous moisture convergence, blue colors indicate anomalous moisture divergence ..... 40

Figure 2.8. Same as Figure 2.2, but results from Pacific bias runs instead of Atlantic bias runs are shown. The colorbar is identical to that in Figure 2.2 ..... 41

Figure 2.9. Same as Figure 2.3, but results from Pacific bias runs instead of Atlantic bias runs are shown ..... 42

Figure 2.10. Same as Figure 2.4, but results from Pacific bias runs instead of Atlantic bias runs are shown ..... 43

Figure 2.11. Similar to Figure 2.5, but with results from Pacific warm bias runs showing on left panels, and those from Pacific cold bias runs showing on right panels ..... 44

Figure 2.12. Similar to Figure 2.2, showing the differences between track density ensemble means of Atlantic and Pacific total bias (*AtlPacTB*) runs, and that of control (*CTRL*) runs ..... 45

Figure 2.13. Same as Figure 2.3, but results from Atlantic total bias (*AtlTB*), Pacific total bias (PacTB), and combined Atlantic and Pacific total bias (*AtlPacTB*) runs instead of Atlantic bias runs are shown ..... 46

Figure 2.14. Similar to Figure 2.4, showing the differences between GPI ensemble means of combined Atlantic and Pacific bias (*AtlPacTB*) runs and that of control (*CTRL*) runs ..... 47

Figure 2.15. The mechanism of remote influence of the Atlantic cold bias *(AtlCB)* on ENP TCs ..... 48

Figure 3.1. Anomaly correlation coefficient of seasonal mean (MJJASON) SST anomalies derived from CESM-DP-LE (averaged over lead time 6 to 12 months) and the observation (CFSR) ..... 77

Figure 3.2. Anomalies of number of TCs, ACE, and number of hurricanes in Atlantic. Blues lines show the observational values from IBTrACS, and red lines show the ensemble-mean values from 10-member ensemble runs generated by improved TCM ..... 78

Figure 3.3. Seasonal-mean Niño3.4 region-averaged SST anomalies ..... 79

Figure 3.4. Observed (*CTRL*), Persisted (*PSST*), and CESM-DP-LE predicted (*DPm*) seasonal SSTA in 1997 and 1998 ..... 80

Figure 3.5. Observed (*CTRL*), Persisted (*PSST*), and CESM-DP-LE predicted (*DPm*) seasonal SSTA in 2015 and 2016 ..... 81

Figure 3.6. ACE anomalies in different (Atlantic, Eastern North Pacific, and Western North Pacific) ocean basins for all experiments (1997 and 1998). Horizontal lines show the observed values calculated from IBTrACS .....82

Figure 3.7. ACE anomalies in different (Atlantic, Eastern North Pacific, and Western North Pacific) ocean basins for all experiments (2015 and 2016). Horizontal lines show the observed values calculated from IBTrACS .....83

Figure 3.8. Anomalies of TC number in different (Atlantic, Eastern North Pacific, and Western North Pacific) ocean basins for all experiments (1997 and 1998). Horizontal lines show the observed values calculated from IBTrACS .....84

Figure 3.9. Anomalies of TC number in different (Atlantic, Eastern North Pacific, and Western North Pacific) ocean basins for all experiments (2015 and 2016). Horizontal lines show the observed values calculated from IBTrACS .....85

Figure 3.10. Track density differences between El Niño (1997) and La Niña (1998) years for all six (*CTRL*, *PSST*, *DPm*, *DPs*, *BC*, and *CSST*) experiments.....86

Figure 3.11. Track density differences between El Niño (2015) and La Niña (2016) years for all six (*CTRL*, *PSST*, *DPm*, *DPs*, *BC*, and *CSST*) experiments.....87

Figure 3.12. GPI differences between *BC* and *DPs* runs for the four simulation years .....88

Figure 3.13. Term contributions on GPI differences (*BC* comparing to *DPs*) for 1997.....89

Figure 3.14. Term contributions on GPI differences (*BC* comparing to *DPs*) for 1998.....90

Figure 3.15. Term contributions on GPI differences (*BC* comparing to *DPs*) for 2015.....91

Figure 3.16. Term contributions on GPI differences (BC comparing to DPs) for 2016.....92

Figure 3.17. Seasonal (JJASON)-mean (a) meridional heat transport (MHT) and (b) its standard deviation calculated from NCEP2. (a) shows the MHT for four different years, and (b) shows the standard deviation of the 4 years in red, and of climatology (1979 to 2017) in blue .....93

Figure 4.1. Correlation coefficients of 5-year running mean GPI calculated from CESM-DP-LE and NCEP. Each figure showing results for different lead years from CESM-DP-LE, while (j) demonstrating the results of lead year 2 to 10 mean. The yellow box in (j) shows the region of conventional Atlantic MDR. All the regions with values passed the 95% student t-test are hatched.....109

Figure 4.2. Identical to figure 4.1, but for results of interannual values instead of 5-year running means.....110

Figure 4.3. Correlation coefficients of 5-year running mean vorticity terms calculated from CESM-DP-LE and NCEP. The yellow box shows the region of conventional Atlantic MDR, and all the regions with values passed the 95% student t-test are hatched....111

Figure 4.4. Same as figure 4.3, but showing results for interannual values instead of 5-year running means....112

Figure 4.5. Correlation coefficients of 5-year running mean humidity terms calculated from CESM-DP-LE and NCEP. The yellow box shows the region of conventional Atlantic MDR, and all the regions with values passed the 95% student t-test are hatched....113

Figure 4.6. Same as figure 4.5, but showing results for interannual values instead of 5-year running means....114

Figure 4.7. Correlation coefficients of 5-year running mean potential intensity (maxPI) terms calculated from CESM-DP-LE and NCEP. The yellow box shows the region of conventional Atlantic MDR, and all the regions with values passed the 95% student t-test are hatched....115

Figure 4.8. Same as figure 4.7, but showing results for interannual values instead of 5-year running means....116

Figure 4.9. Correlation coefficients of 5-year running mean shear terms calculated from CESM-DP-LE and NCEP. The yellow box shows the region of conventional Atlantic MDR, and all the regions with values passed the 95% student t-test are hatched....117

Figure 4.10. Same as figure 4.9, but showing results for interannual values instead of 5-year running means....118

Figure 4.11. Normalized time series of 5-year running mean HURDAT2 TC counts and Atlantic MDR GPI calculated from CESM-DP-LE and NCEP. (a) shows the 5-year running mean of observed (HURDAT2) TC counts in black, NCEP-based MDR GPI in blue, and CESM-DP-LE-based GPI in red. (b) shows the 5-year running mean TC number in black, and different color lines showing 5-year running GPI from different lead years in CESM-DP-LE....119

Figure 4.12. Normalized 5-year running mean time series of TC counts (in black) and each term ((a)shear, (b) humidity, (c) vorticity, and (d) potential intensity terms) in GPI calculated from NCEP (in blue) as well as CESM-DP-LE (in red)....120

Figure 4.13. Regression coefficients of 5-year running mean global SST onto 5-year running mean Atlantic MDR GPI time series. Results from both NCEP (a) and CESM-DP-LE (b) are shown .....121

LIST OF TABLES

Page

Table 2.1. Experiment names for control and bias runs, and the associated SST biases that included in the SST forcings for each experiment ....49

Table 2.2. Ensemble means (from 16 ensemble members each) of ACE and the number of TCs from control (*CTRL*) and Atlantic bias (*AtlWB*, *AtlCB*, and *AtlTB*) runs in both real number and percentage difference from *CTRL* (only shown if the difference from *CTRL* is significant at the 5% level)....50

Table 2.3. Identical to Table 2.2, but showing the results for control and Pacific bias (*PacWB*, *PacCB*, and *PacTB*) runs ....51

Table 2.4. Identical to Table 2.2, but showing the results for control, Atlantic total bias (*AtlTB*), Pacific total bias (*PacTB*), and combined Atlantic and Pacific total bias (*AtlPacTB*) runs ....52

Table 3.1. List of experiments and associated SST forcing, lateral boundary conditions, and initial conditions ....94

# CHAPTER I

# INTRODUCTION

## 1.1 Importance of Tropical Cyclones Simulations

Tropical cyclones (TCs) are one of the most destructive natural hazards that strongly influence life and economy. For example, hurricane Katrina (2005), Sandy (2012), Harvey, Irma, and Maria (2017) are among the most damaging and deadliest Atlantic TCs that made landfall in the U.S. (Blake et al. 2011; Blake et al. 2013; Emanuel 2017; Shuckburgh et al. 2017; Klotzbach et al. 2018). Therefore, improving forecast and future projection of TC activity is one of the highest priority research areas. While projections of TC activity under future climate change scenarios remain uncertain (e.g., Emanuel 2005; Holland and Webster 2007; Bender et al. 2010), an emerging consensus regarding several aspects of future TC changes has developed thanks to the increased computer capabilities (Knutson et al. 2010; Camargo and Hsiang 2016). Based on current TC projection under future climate-change scenarios using high-resolution models, we are expecting a slightly reduced number of TCs, but a likely increase in high-intensity tropical cyclones (Knutson et al. 2010). Nevertheless, no robust projection is shown for future TC location changes, such as TC tracks and landfall frequency, and sub-regional projections remain highly uncertain (Camargo and Hsiang 2016). Further research on providing reliable climate model simulations of TC response to future climate change is needed for both the scientific community and society.

## 1.2 Evolution of Tropical Cyclone Simulation and Prediction

Attempt to forecast TC variability on seasonal time scales started in the early 1980s (e.g. Gray 1984b), and the predictions were based on statistical models (Camargo et al. 2007). Predictors such as El Niño Southern Oscillation (ENSO), regional sea surface temperature (SST), and sea level pressure are used to predict basin-wide TC activity (e.g. Gray 1984b). Nevertheless, only specific regions (northern Atlantic and Pacific basins for instance) can be benefited from the statistical predictions, and only specific aspects of TCs (such as seasonal TC number) can be predicted. With dramatically improvements in computational capabilities, dynamical (atmospheric only or coupled atmosphere-ocean) models are now utilized to make experimental seasonal TC forecasts (e.g., Wang et al. 2009; LaRow et al. 2010; Murakami et al. 2016; Zhang et al. 2017). One forecasting approach is based on atmospheric only models with predicted SSTs as a boundary condition. For this approach, important aspects of TC-ocean interactions (e.g., Lin et al. 2013) are not represented. Other dynamical seasonal TC frameworks use coupled atmosphere-ocean models in which TC-ocean interactions are captured. However, the coupled modeling approach is faced with two challenges, one of which is severe model biases in the tropics and another of which is the much higher computational cost. To overcome some of these challenges, statistical-dynamical hybrid based forecasting approach has been recently proposed. Vecchi et al. (2014) demonstrated that this hybrid approach produces higher forecast skills than those of the solely dynamical model based forecast, at least in the North Atlantic. While ensemble means of model forecasts were treated as the best estimate for their TC forecasts, Vecchi et al. (2014) noted the importance of developing error models, other than the internal variability (inter-ensemble spread), to quantify the uncertainty of TC forecasts.

Even though the seasonal (one to three seasons) prediction of basin-wide TC activity has been well developed (e.g.. Gray 1984a,b; Camargo et al. 2007; Zhao et al. 2010; Vecchi et al. 2014), research on the possibility of predicting TC frequency on decadal or longer timescales (under warming climate) is still in its infancy (e.g., Emanuel et al. 2008; Knutson et al. 2010). Some initial studies have started to investigate TC changes over the intermediate (multiyear to decadal) timescales, as external (radiative) forcing and internal variability of climate system can both contribute to the changes in TC activity (e.g., Vecchi et al. 2013). From a socio-economic standpoint, developing a capability of decadal TC forecast can have enormous value. In practice, however, since large ensemble of climate model simulations for timescales longer than a season can only be achieved currently in low resolutions (larger than 1°), statistical models are used based on large-scale environmental condition changes predicted by dynamical simulations to demonstrate the possible modulation of large-scale fields (mostly SSTs) on TC activity (Zhang and Delworth 2006; Smith et al. 2010; Vecchi et al. 2013; Caron et al. 2014).

## 1.3 Importance of Sea Surface Temperature on Tropical Cyclone Activity

### *1.3.1 Relationship Between Sea Surface Temperature and Tropical Cyclones*

SST both local to and remote from the TC development region is one of the most important environmental variables for TC activity. In the Atlantic region, for example, TC intensity is a function of local SST in the northern tropical Atlantic with maximum potential intensity directly related to SST (Emanuel 1986). In addition, non-local SSTs (e.g., those in the southern tropical Atlantic) may remotely influence Atlantic TC activity by driving changes in northern tropical Atlantic mid-tropospheric humidity and tropospheric vertical wind shear (e.g., Vimont and Kossin 2007). Pacific TC activity also strongly depends on SST. For example,

Webster et al. (2005) showed that with an increasing global SST, strong TCs (category 4 and 5) in the North Pacific may be significantly increased.

On seasonal-to-decadal time scales, it is well known that tropical Atlantic and Pacific SST variability exerts a significant influence on TCs. The El Nino-Southern Oscillation (ENSO) in the Pacific and the Atlantic Multidecadal Oscillation (AMO) (on decadal timescale) as well as the Atlantic Meridional Mode (AMM) (on interannual to decadal timescales) in the Atlantic can impact TC activity through not only changing local SSTs, but also modulating vertical wind shear, low-level vorticity, and tropospheric moisture (Gray 1984a,b; Tang and Neelin 2004; Emanuel 2005; Webster et al. 2005; Emanuel 2007; Vimont and Kossin 2007). ENSO is the most dominant mode of climate variability on interannual timescales. It is well known that warm phase of ENSO (El Niño) can suppress Atlantic TC activity, because of the warming in the eastern tropical Pacific that enhances vertical wind shear in the Atlantic through changes in the Walker Circulation (Gray 1984a,b; Tang and Neelin 2004). Furthermore, the impact of ENSO has a 'see-saw' effect on Atlantic and Eastern North Pacific TCs (Elsner and Kara 1999). During El Nino, while TC activity is suppressed in Atlantic, it is enhanced in the Eastern North Pacific (ENP). Even though the relationship between ENSO and TC frequency in the ENP is still uncertain, increase in intense ENP hurricane numbers has been related to El Niño events (Gray and Sheaffer, 1991; Whitney and Hobgood, 1997). Collins and Mason (2000) and (2003) suggested an enhancement in TC strengths caused by increased humidity and SST during El Niño in the western (west of 116°) ENP, while they suggested general climatologically favorable conditions for TC genesis in the eastern portion of the ENP regardless of ENSO phase. Fu et al. (2017) demonstrated a reduction in TC frequency in the nearshore ENP during El Niño due to

Changes in low-level vorticity induced by strengthened gap winds, and further clarifies the relationship between ENSO and ENP TC activity.

Moreover, during the negative (positive) phase of AMM, which is characterized by warm (cool) SST anomalies in the southern tropical Atlantic and cool (warm) anomalies in the northern tropical Atlantic, the TC activity in the Atlantic MRD is suppressed (enhanced) (Patricola et al. 2014). Besides the local effect of AMM on TC activity, a teleconnection between AMM and TC activity in the ENP is shown in both observation and model simulations. Patricola et al. (2016) suggested a reduction in the ENP TC activity during positive AMM through a Walker Circulation-type response. While the AMM represents the SST variability in both northern and southern tropical Atlantic, the AMO represents the SST variability in the subtropical and mid-latitude North Atlantic (Vimont and Kossin 2007), and the variability of Atlantic TC activity on longer timescales (multidecadal) is linked to the variability in AMO (e.g., Zhang and Delworth 2006).

### *1.3.2 Impact of SST Representation on TC Simulations*

TC variability can come from external source (e.g., SST variability) and internal atmospheric dynamics. The SST-induced TC variability defines the predictable component of TC variability, because tropical SST anomalies tend to have long persistent memory and are potentially predictable on seasonal or longer time scales (Zhao et al. 2010). Previous studies suggest that the skills in representing SSTs can be translated into model predictability on TC activity, especially in the Atlantic, at least on seasonal time scales. For example, Chen and Lin (2013) forced their high-resolution (25km) atmospheric only model with persisted SST, and showed an extremely high predictability in interannual variability of Atlantic TCs. The

correlation between the predicted and the observed interannual TC (or hurricane) counts over the period from 1990 to 2010 is as high as 0.89 in the Atlantic (Figure 4a in Chen and Lin (2013)). However, the model representation of TC activity in the Pacific is not as good, with very low correlation skills in the Western Pacific Ocean. They suggest this reduction in TC interannual predictability can be contributed from either the low skill in representation of Pacific interannual variability of SST using persisted SST, or the lower predictability in Pacific TCs. Zhao et al. (2010) also emphasized the importance of SSTs on seasonal TC forecasts by comparing forecasts using persisted-SST and observed-SST in their high-resolution (50km) atmospheric model simulations. They suggested that coupled model based TC forecast depends strongly on the ability of the models to predict the relative change of SST in TC main development region (MDR) to tropical mean SST.

Other than the direct impact of tropical SST on TC simulations, the representations of the associated climate modes are also crucial. Figure 1.1 shows observed and simulated Atlantic Accumulated Cyclone Energy (ACE) (Bell et al. 2000) in a large ensemble of WRF runs forced with idealized El Nino and AMM SST forcing (Patricola, personal communication, 2016). The bottom row shows the observed variability of Atlantic ACE from the Atlantic hurricane dataset (HURDAT), while other rows show the simulated ACE variability forced by El Nino- and AMM-like SSTs. In Figure 1.1, the observation (HURDAT) covers a wide range of variability while the range of the simulated variability in the absence of anomalous SSTs is considerably smaller, suggesting that much of the observed ACE variability is attributed to SST variability induced by various climate modes of variability in the tropics. For example, the SST forcing from El Nino and cold phase of the AMM seem to lower the ACE, while the SST forcing of warm phase of the AMM seems to increase the ACE. Only when the effect of all climate modes

is considered can the full range of observed ACE variability be reproduced by the model simulations, confirming again that much of the observed ACE variability is tied to interannual SST variability related to the AMM and ENSO. Furthermore, figure 1.1 shows that TC internal variability may also depend on SST forcing. For example, the inter-ensemble spread of ACE in AMM warm phase appears to be greater than that in either El Nino or AMM cold phase. Since seasonal TC predictability is determined by the ratio between external TC variability and internal TC variability, it is possible that SST forcings can have impact on TC predictability. Therefore, reliable simulations of TC activity depend on a realistic representation of SSTs and associated climate modes.

SST changes on longer time scales (for example, multiyear to decadal time scales) are suggested to be predictable, partly because of the warming trend associated with the radiative forcings (e.g., van Oldenborgh et al. 2013) and partly because of the long ocean memory associated with the ocean's meridional overturning circulation, particularly in the Atlantic (Yeager et al. 2018). There is also an observational evidence that the variability of TC activity on decadal timescale is related to the decadal SST variations, especially in the north Atlantic basin (Zhang and Delworth 2006; Knight et al. 2006). Moreover, studies suggest TC forecast skill on multiyear to decadal timescales may arise from both SST predictability and initialization (e.g., Smith et al. 2010). However, a possible break down in the statistical relationship between SST and basin-wide TC activity (such as TC number) is suggested for future climate (Caron et al. 2014), due to a possible change in SST threshold for TC genesis (e.g., Knutson et al. 2008). Therefore, further studies are needed to establish a more robust relationship between SSTs and TCs on longer timescales.

### 1.4 Challenges and Objectives

One of the most well known problems in state-of-the-art climate model simulations and projections is the SST biases in almost all ocean basins, especially in the eastern tropical oceans and the Southern Ocean regions. Figure 1a in Wang et al. (2014) shows the annual-mean (1900 to 2005) SST biases, averaged from 22 models of the Coupled Model Intercomparison Project phase 5 (CMIP5). If we compare the SST bias map to the TC track locations and frequency around the globe, many of the TC active regions are subject to severe SST biases. Large warm biases can be seen in the southeastern basin of the tropical Atlantic and Pacific. In particular, the Atlantic warm SST bias can be as large as 6°C in some of the CMIP5 models (Xu et al. 2014). Other than the severe warm biases, prominent cold SST biases of more than 1°C also occur in northwestern Atlantic and Pacific, where most of the TCs occur, even though with smaller amplitudes. The SST biases have persisted from CMIP3 to CMIP5, but the spread of bias amplitudes among different models is smaller in CMIP5 than in CMIP3 (Richter et al. 2014), suggesting that all CMIP5 models are producing more similar SST biases than CMIP3 models.

The causes for these SST biases are complex and have been subject to considerable investigations. Studies suggest that the causes of the biases can be traced to simulation biases in coastal winds (and thus coastal upwelling), stratocumulus decks (and thus shortwave radiation), mesoscale eddies (and thus offshore transport), equatorial westerly wind, and thermocline (Richter and Xie 2008; Li and Xie 2012; Patricola et al. 2012; Xu et al. 2013; Xu et al. 2014; Ritcher et al. 2015; Small et al. 2015; Patricola et al. 2016). In order to efficiently remove the SST biases, higher resolutions (both horizontally and vertically) in climate models and more oceanic observations (especially for tropical subsurface) are needed, both require tremendous amount of resources (e.g., Ritcher 2015; Small et al. 2015). Even with the improvement in our

understanding of the causes of the biases and progress made to reduce the biases in the newer version of climate models, it is suggested that the SST biases may persist for decades (Ritcher 2015). Therefore, it is crucial to account for the impact of SST biases on model simulations of TCs, although few studies have been focused on this subject (e.g., Vecchi et al. 2014).

The main objective of this dissertation is to investigate the impact of model SSTs, including both their biases and predictions, and the TC-associated environmental variables on TC simulations. And the main focus of each chapters of this dissertation is as follows: Chapter two: Quantifying the impact of state-of-the-art climate model (CMIP5) SST biases on TC simulations; Chapter three: Examining the feasibility of dynamical seasonal prediction of TCs using predicted SST information from a large ensemble of climate model decadal predictions; Chapter four: Exploring the predictability of TC environmental condition changes on subdecadal time scales using a large ensemble of climate model decadal predictions. Every chapter starts with an introduction section, following by methodology, data, and experimental designs. The results and summary (discussion) for each project will then complete each Chapter. Through these three projects, we hope to potentially improve our understanding on the influence of SST representations on seasonal to decadal TC predictability. In the end of this dissertation, we will summarize the major findings of this study and discuss possible future work.

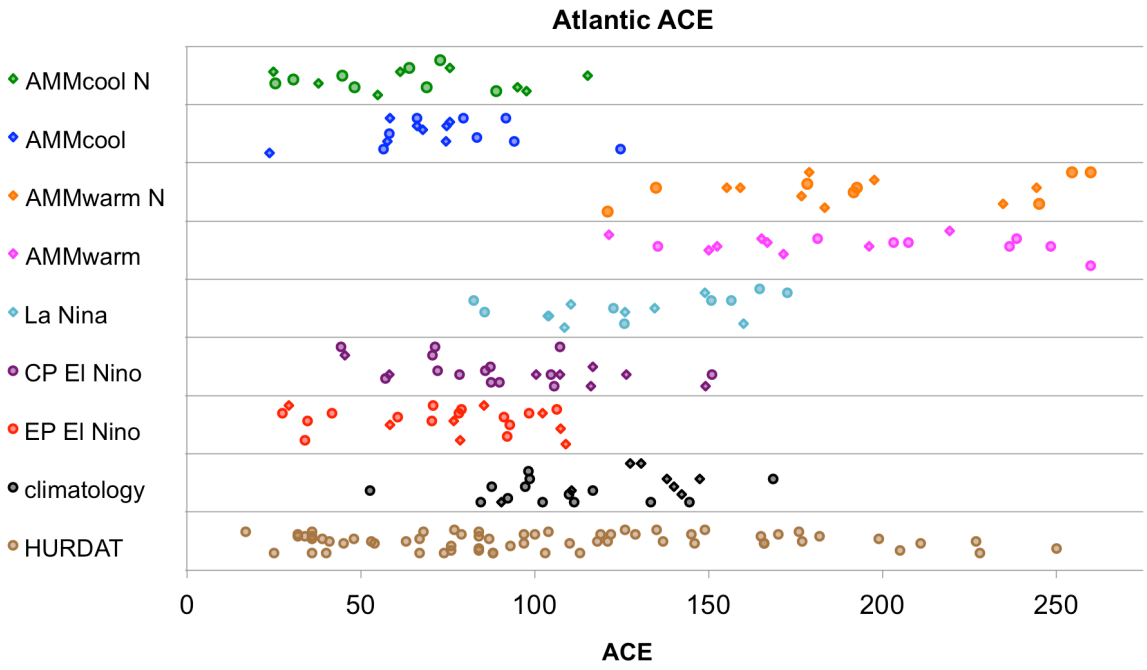


Figure 1.1. A summary of the large ensemble TCM experiment. Each row in this figure represents Atlantic ACE variability in response to SST forcing of a particular mode of climate variability with the bottom row representing observed ACE variability based on HURDAT.

# CHAPTER II

# THE IMPACT OF CLIMATE MODEL SEA SURFACE TEMPERATURE BIASES ON TROPICAL CYCLONE SIMULATIONS

## 2.1 Introduction and Background

Reliable climate model simulations of TC activity depend on a realistic representation of modes of climate variability on seasonal to multi-decadal timescales, as well as climatological mean SSTs. However, severe SST biases exist in the tropical Pacific and Atlantic in most of the Intergovernmental Panel on Climate Change (IPCC) coupled global climate models (CGCMs) (e.g., Richter 2015). Figure 2.1 shows the multi-model ensemble-averaged seasonal mean (April to November) of the tropical SST biases in the Atlantic and Pacific from the Coupled Model Intercomparison Project Phase 5 (CMIP-5) models (details in Methodology). The SST bias in the Indian Ocean is not shown, since its magnitude is relatively small. Very large warm biases cover the southeastern tropical Atlantic and Pacific (Wang et al. 2014), with the Atlantic bias reaching 6°C in some models (Xu et al. 2014). In addition, cold SST biases occur in the northwestern Atlantic and Pacific, albeit with weaker amplitudes. Wang et al. (2014) and Zhang et al. (2014) suggest interhemispheric links of the biases in Atlantic and Pacific.

Several mechanisms have been identified to cause the SST biases, which can vary from region to region (Richter and Xie 2008; Li and Xie 2012; Patricola et al. 2012; Xu et al. 2013). The tropical cold biases mainly originate from atmospheric errors in cloud cover (Li and Xie 2012) and trade winds (Liu et al. 2012), and can be largely reduced by increasing model resolution (Zuidema et al. 2016). The mechanisms for the warm biases in eastern Pacific and Atlantic are more complex. While the processes driving the warm bias in the Atlantic are mostly

rooted in the narrow near-shore winds along the Benguela coast (Xu et al. 2014; Small et al., 2015; Patricola and Chang, 2016), errors in marine stratocumulus and associated short wave radiation can contribute significantly to the southeastern Pacific warm bias (Masunaga et al. 2002; Painemal and Minnis 2012; Zuidema et al. 2016), even though the patterns of the biases are similar in the two ocean basins. Moreover, nonlinear processes associated with ocean mesoscale eddies may contribute to the warm biases in the eastern ocean basins (Colas et al. 2012; Toniazzo et al. 2010). Atlantic equatorial westerly wind biases can also remotely influence the eastern warm SST biases through oceanic Kelvin waves (Richter 2015).

Even though the mechanisms that cause the SST biases have been widely studied, the impact of the biases on TC simulations and seasonal predictions has not been fully understood. Dynamical climate models are now utilized to make experimental seasonal TC predictions, owing to model developments and improvements in computational capabilities (e.g., Wang et al. 2009; LaRow et al. 2010; Murakami et al. 2016; Zhang et al. 2017). One forecast approach is based on atmosphere-only models with predicted SSTs as boundary condition. For this approach, important aspects of TC-ocean interactions (e.g., Lin et al. 2013) are not represented. Another forecast approach uses coupled atmosphere-ocean models. However, the severity of the tropical SST biases can potentially have considerable impacts on TC simulations and predictions. Vecchi et al. (2014) show improvements in simulated TC genesis and track by reducing SST biases in a high-resolution CGCM simulation through adjusting momentum, enthalpy, and freshwater fluxes. They suggest that the improved TC representations are likely achieved by improvements in simulated large-scale climatological conditions and interannual variability. Zhao et al. (2010) suggested the importance of SSTs on seasonal TC forecasts using persisted and observed SST anomalies in a high-resolution (50km) atmospheric-only model. Their results

potentially indicate that coupled model TC forecast skill strongly depends on the ability of the models to represent the relative change of SST in the TC main development region (MDR) to tropical mean SST.

The SST biases can also introduce large uncertainties into future projections of TC activity based on climate models. There is no consensus on projected changes in future TC frequency, although the most recent simulations suggest a slight reduction in overall TC numbers but an increase in the percentage of intense TCs (e.g., Emanuel 2005; Holland and Webster 2007; Bender et al. 2010; Knutson et al. 2010; Camargo and Hsiang 2016). Nevertheless, projections of future TC location changes, such as TC tracks and landfall frequency, are not robust, and sub-regional projections remain highly uncertain (Camargo and Hsiang 2016). A clear understanding of future changes in TCs requires reliable simulations of the mean and variability of SST.

Given that the SST biases problem is likely to persist in models for at least a decade or longer (Richter 2015), it is crucial for us to take into account the impact of these biases on simulations of TCs activity. In this Chapter, we will address the question: How do Atlantic and Pacific SST biases impact the simulated TC climatology? By conducting suites of TC-permitting model simulations with and without SST biases, we hope to improve our understanding of how the warm and cold SST biases individually influence simulated TC activity, and through what mechanisms. Moreover, we will also consider how the Atlantic and Pacific SST biases jointly influence TC simulations and assess their relative importance in affecting TC simulations in different regions, as modes of tropical Pacific and Atlantic variability are known to exert joint influences on Atlantic TC activity (Patricola et al. 2014). By splitting the biases up by region and by sign, we will attempt to identify which biases are most detrimental to

TC simulations and what their impacts are for basin-wide TC activity. Moreover, while keeping in mind that relationships occur between biases in different ocean basins, we would like to address the question: how can SST biases from basins outside of the region of interest impact TC activity? Although previous studies have shown that SST biases can impact TC simulations, the impact has not been systematically quantified and the pathways by which the biases influence TCs have not been understood. The objective of this study is to gain insight into the impact of the SST biases on TC simulations at seasonal-to-interannual timescales. More importantly, we will shed light on underlying dynamics of SST biases' impact on TC simulations.

This chapter is organized as follows. Section 2 describes the modeling tool and experiment design. Section 3 presents the results of the model experiments where SST biases are specified either individually or jointly in different tropical ocean basins. Section 4 discusses the implications of the results and summarizes the main conclusions.

## 2.2 Research Methods – Model Description and Experimental Designs

### *2.2.1 Model Description*

We utilized a Tropical Channel Model (TCM) configuration (Patricola et al. 2016; Patricola et al. 2017) of the Weather Research and Forecasting (WRF) Model (Skamarock et al. 2008) developed by the National Center for Atmospheric Research (NCAR). This model is more suitable for this study compared to many global climate models (GCMs) due to its non-hydrostatic dynamical core and finer resolution. The TCM extends around the global tropics from 30°S to 50°N, and has 27 km TC-permitting horizontal resolution and 32 levels in the vertical. While the horizontal resolution of the TCM is too coarse to resolve the details of the individual TCs, it is sufficient to investigate the statistics of TC activity. By setting the model

domain to the global tropics, we allow atmospheric responses to SST forcings to propagate around the globe in the tropics and subtropics. Moreover, by setting the northern boundary at 50°N, atmospheric teleconnections that affect the MDR from outside the tropics can be considered, as teleconnections between different tropical ocean basins can be linked through regions outside of the tropics (Nobre and Shukla 1996).

The sensitivity of physical parameterizations of the WRF model was well tested over the Atlantic MDR (Patricola et al. 2014), and the TCM was tested over both the Atlantic and Pacific basins (Patricola et al. 2016; Patricola et al. 2017). However, we note some problems with the model. For example, the TCM tends to generate too much rainfall over Africa and the Amazon, underestimate the maximum near-surface wind speed of TCs, and overestimate the number of Atlantic and ENP TCs (Patricola et al. 2016). Despite these issues, the TCM reproduces the atmospheric responses to ENSO and AMM reasonably well (Patricola et al. 2016; Patricola et al. 2017). Therefore, with these known problems, the TCM is a suitable tool for this study.

*2.2.2 Experimental Designs*

We conducted extensive WRF TCM experiments forced by surface boundary conditions with and without SST biases. By prescribing the SST forcings to the TCM, we can isolate the atmospheric response to specific regions of SST bias, which is important as different mechanisms generate the SST biases in different regions. The SST biases were calculated from the CMIP-5 (Taylor et al. 2012) multi-model (37 models) ensemble mean subtracted from the National Oceanic and Atmospheric Administration (NOAA) Optimum Interpolation (-OI) observed SST (Reynolds et al. 2007), and were then interpolated to 6-hourly from monthly, and to the 27km grid of the TCM. A suite of simulations (Table 2.1) were conducted to quantify

individual and joint effects of SST biases on TC activity by separating the Atlantic and Pacific SST biases into warm, cold, and total (combining warm and cold) biases. The biases near the lateral boundaries were smoothed over 5 degrees in the latitudinal direction. Even though the amplitudes of seasonal variation of the biases are smaller than the biases themselves (Wang et al. 2014), we included the annual cycle of the SST biases in our simulations.

The biases were added to the control SST to produce the warm, cold, and total bias simulations. Figure 2.1 shows the seasonal mean (from April to November, to focus on the TC season) of the SST biases that we used in the experiments. While the SST biases were calculated based on the 1984-2004 NOAA-OI SST, the control SST was based on the monthly 1950-2014 climatology from the Hadley Center Global Sea Ice and Sea Surface Temperature dataset (HadISST) (Reyner et al. 2003). HadISST was utilized for the control SST because the product covers a longer time period, whereas the NOAA-OI SST was used to calculate SST biases because the resolution is finer. We do not expect details between HadISST and NOAA-OI SST to significantly impact the results of this study, as the SST biases have much larger amplitude than the difference between the two SST products.

To quantify the impact of SST biases, the ensemble of control simulations (*CTRL*) serves as a reference for experiments including the Atlantic warm bias (*AtlWB*), Atlantic cold bias (*AtlCB*), Atlantic total bias (*AtlTB*), Pacific warm bias (*PacWB*), Pacific cold bias (*PacCB*), Pacific total bias (*PacTB*), and the combined Atlantic and Pacific total bias (*AtlPacTB*) simulations (Table 2.1). Initial conditions (ICs) and lateral boundary conditions (LBs) were provided by the 6-hourly NCEP-U.S. Department of Energy (DOE) Atmospheric Model Intercomparison Project II (AMIP-II) Reanalysis (NCEP-2) from the years 1989 and 1996 (Kanamitsu et al. 2002). The two years were chosen since climate modes such as AMO were in

a neutral phase (Patricola et al. 2014). To focus on the TC season in the northern hemisphere, the simulations were started in April and ended in November. The first two months were discarded as spin up, with analysis covering June to the end of November. An ensemble of 16 runs was generated by altering the start date to generate different ICs for each ensemble member of each experiment in order to quantify the statistical significance of the results.

*2.2.3 Quantifying TC Activity*

The tracking algorithm from Walsh (1997) was used to identify simulated TCs, including tropical storms and hurricanes or typhoons (depending on the ocean region). To be identified as a tropical cyclone, the system must generate south of 30°N, last at least two days, and have a warm core. Moreover, an identified TC must have a closed surface pressure minimum, a minimum 10-meter wind speed of 17.5 $ms^{-1}$, and satisfy a 850-hPa vorticity threshold over its center. The resolution used to calculate the track density is 2° longitude by 2° latitude. A comparison between the track density from the Revised Atlantic Hurricane Database (HURDAT2) (Landsea et al. 2015) and from TCM ensemble of the climatology simulation in the ENP and Atlantic is shown in Supplementary Figure 6 in Patricola et al. (2016).

To investigate the impact of SST biases on TC activity, we calculated the simulated accumulated cyclone energy (ACE), which accounts for TC strength, number, and duration (Bell et al. 2000). ACE is the summation of the square of the 6-hourly maximum sustained wind speed of TCs over a TC season. Furthermore, to understand the underlying dynamics linking SST biases to TC simulations, we examine the Genesis Potential Index (GPI) (Emanuel and Nolan, 2004). By calculating GPI, we can quantitatively estimate how various environmental variables influence changes in TC activity:

$$GPI = |10^5\eta|^{\frac{3}{2}}\left(\frac{H}{50}\right)^3\left(\frac{V_{pot}}{70}\right)^3(1+0.1V_{shear})^{-2}.$$

The GPI is calculated from the monthly mean of absolute vorticity at 850 hPa (η), relative humidity at 600 hPa (H), potential intensity ($V_{pot}$), and vertical wind shear between 850 and 200 hPa ($V_{shear}$). The potential intensity (PI) is computed based on atmospheric (temperature and specific humidity) vertical profiles, sea level pressure, and SST. While GPI does not explain all variability associated with TCs, it is a suitable index for investigating the conditions that influence the TC activity (Camargo et al. 2007; Patricola et al. 2014).

## 2.3 Results

### *2.3.1 Atlantic SST Biases*

Figure 2.2 shows the differences in ensemble means of the TC track density between the Atlantic bias runs and the control simulation. The Atlantic warm bias produced no significant impact on TC track density (Figure 2.2a) and genesis locations (not shown). However, the Atlantic cold bias caused a marked decrease in Atlantic TC track density, and a remote increase in ENP TC track density (Figure 2.2b), with an insignificant change in Atlantic genesis density and a positive genesis density anomaly near the coast of the ENP (not shown). Note that the positive anomaly in track density in the ENP is slightly offshore, and the magnitude of the anomaly is even larger than that in the Atlantic. *AtlTB* impacts the track density in a similar way as *AtlCB*, but with smaller magnitudes (Figure 2.2c). Moreover, the Atlantic SST biases produced no statistically coherent response in WNP track density.

Figure 2.3 shows the values of ACE and the number of TCs in the Atlantic, ENP, and WNP basins computed from the control simulation and the Atlantic bias experiments. Both

*AtlCB* and *AtlTB* generate lower ensemble median values and lower ensemble mean values (Table 2.2) of ACE and TC number in the Atlantic and higher values in ENP compared to *CTRL*. The simulated basin-wide decrease in Atlantic TC activity and increase in ENP TC activity in response to the Atlantic cold and total biases are all significant at the 5% level (two-sample student t-test). Both *AtlCB* and *AtlTB* generate a decrease in Atlantic TC intensity (not shown), corresponding to the smaller ACE values, and an increase in ENP TC intensity that co-occurs with larger ACE values. Moreover, similar to the impact on track density, the impact of Atlantic cold and total biases on ACE and TC number is stronger in the ENP basin (remotely) than in the Atlantic basin (locally) (Table 2.2).

On the other hand, the Atlantic warm bias does not significantly (5% level) impact ACE and TC number in any of the tropical ocean basins. Furthermore, the Atlantic SST biases insignificantly influence WNP ACE and TC number. Note that even if we consider the internal variability (or the range of the values of the ensemble members), the values of ACE and number of TCs generated by *AtlCB* and *AtlTB* in the Atlantic and ENP are considerably different from those of *CTRL* (Figure 2.3).

To understand the underlying dynamics linking SST biases to TC simulations, we examined the GPI (Figure 2.4) and the associated atmospheric variables. The patterns of significant GPI changes are consistent with the changes in ACE and number of TCs. The cold (Figure 2.4b) and total (Figure 2.4c) SST bias forcings induce a decrease in ensemble-mean GPI in the Atlantic MDR and Gulf of Mexico (GoM), and an increase in the ENP. The Atlantic warm bias alone insignificantly impacts GPI (Figure 2.4a). Therefore, we focus on *AtlCB* and *AtlTB* to investigate the dominant GPI terms (atmospheric variables) that contribute to the GPI change driven by Atlantic SST biases. The impact of AtlTB is not significantly different from

that of AtlCB, suggesting that the cold bias, rather than the gradient generated by both the cold and warm biases, mainly contributes to the anomalous GPI patterns.

GPI changes forced by Atlantic SST biases can be further diagnosed by computing contributions from environmental variables including vertical wind shear, mid-tropospheric relative humidity, potential intensity, and vorticity. To estimate the contribution from each factor, we calculated the GPI by setting one term in GPI to the value from one of the perturbed simulations, and other terms to values from the control simulation, and then compared to the *CTRL* GPI (Camargo et al. 2007; Patricola et al. 2014; Patricola et al. 2016). Only the result for *AtlCB* (Figure 2.5) is shown due to the similarity between the GPI responses in the *AtlCB* and *AtlTB* experiments. In both the Atlantic cold and total bias runs, the mid-tropospheric humidity, vertical wind shear, and potential intensity all contribute to the decrease in Atlantic GPI, while only the shear term contributes to the increase in ENP GPI. (The negative contribution from the humidity and vorticity terms compensates the large positive contribution from the shear term by a small magnitude along the coast of the ENP.) Moreover, the weakly positive GPI anomalies in the central Pacific in *AtlCB* and *AtlTB* arise from the humidity term. The response in atmospheric conditions (e.g., mid-tropospheric relative humidity and vertical wind shear) is consistent with the associated GPI term (not shown). For example, the vertical shear is enhanced by the *AtlCB*, consistent with the relationship found in previous studies: with cold anomaly in northern Atlantic SST, the strengthened subtropical high can induce easterly low-level wind anomalies in the MDR, and further enhance the local vertical wind shear (Vimont and Kossin 2007). Moreover, the change in tropospheric humidity can be locally linked to the change in surface latent heat flux generated by SST anomalies in the Atlantic (Vimont and Kossin 2007). Note that in order to test the robustness of the results, all of the above analyses (and those for

Pacific and combined Atlantic and Pacific SST bias experiments) were repeated by randomly choosing 8 out of the 16 ensemble members. There is little difference in the results, suggesting that the ensemble size is sufficiently large to generate robust findings.

It has been shown that SST anomalies in the tropical Atlantic can remotely influence atmospheric circulations and SSTs in the tropical Pacific on interannual to centennial timescales (Kucharski et al. 2016). On interannual timescales, previous studies have shown that the teleconnection generated by Atlantic SST variability can impact the Pacific basin through a Walker-type circulation response (Patricola et al. 2017; Zhang et al. 2017), consisting of near-surface wind anomalies triggered by equatorial Kelvin waves (Polo et al. 2014; Ding et al. 2012; Rodriguez-Fonseca et al. 2009), and/or Rossby wave responses (Ham et al. 2013; Ham et al. 2013). In our *AtlCB* simulations, while a Walker-type circulation response similar to the negative AMM experiment in Patricola et al. (2017) can be seen (Figure 2.6a), the remote impact of Atlantic cold bias on ENP TC activity, especially the shear contribution, is also strongly influenced by the change in regional circulation inducing by the topography.

In *CTRL* simulations (Figure 2.6b), a low-level easterly, which is generated by trade wind and the associated Caribbean low level jet (CLLJ), appears in the Caribbean/Atlantic region with the corresponding westerly on top around 200hPa induced by the occurrence of the Central America mountain. On the lee-side of the Central America topography, a low-level westerly occurs with an easterly in upper levels. Circulations on the lee-side and in the Caribbean region (windward side) both contribute to an ascending wind on top of the Central America mountain region, generating a maximum rainfall region in the TCM. (Note that in observation, the lee-side circulation/shear is much weaker, therefore the precipitation pattern is different from that in the TCM.) Moreover, in the western part of the ENP, a circulation cell (or double cell, as it is

generated by both the Hadley Cell and Walker circulation) exists, with a low-level easterly occurring with an upper-level westerly. A descent motion band around 120°W is then generated by the double cell and the lee-side circulation.

In the *AtlCB* simulations (Figure 2.6c), a stronger low-level easterly occurs in the Caribbean/Atlantic region with an enhanced upper-level westerly. This strengthening of the circulation on the windward side of the mountain is contributed by strengthening of the CLLJ. The strength of the CLLJ is correlated to the SST difference between the tropical Atlantic and ENP, and is also strongly controlled by the land-sea temperature difference between the Caribbean and the northern part of the southern America land (e.g., Whyte et al. 2008). With the Atlantic cold bias, the pressure gradient is enhanced between the ocean basins and between the land and sea, and therefore the CLLJ is strengthened. However, since the air coming from the Atlantic/Caribbean region is colder and dryer (due to the cold SST bias) compared to *CTRL,* the latent heat release associated with the orographic lifting is weaker than that in *CTRL*. This leads to a weakened ascending motion in *AtlCB* than in *CTRL*, resulting in an anomalous descending wind over the mountain and the windward region. Figure 2.7 shows rainfall and vertical-integrated moisture convergence differences between *AtlCB* and *CTRL*. A decrease in the regional rainfall over the Central American is indicative of a weakening in the diabatic heating, while a decrease in the moisture convergence from windward side to coastal leeward side of the mountain suggests a reduced moisture supply in the region. Note that due to the complexity of the terrain, the spatial pattern of moisture convergence over the mountain is messy. As a result, the cold SST bias in *AtlCB* produces a clockwise anomalous vertical circulation above the mountainous region in the Central America (Figure 2.6a), which acts to strengthen the circulation over the Caribbean and Atlantic and weaken the circulation over the far eastern ENP

(Figure 2.6b). As such, the vertical wind shear is strengthened over the Caribbean and Atlantic and reduced over the ENP. This offers an explanation for the sharp change in sign of vertical shear induced GPI anomaly over the Central America (Figure 2.5b), which dominates the GPI difference between *AtlCB* and *CTRL* (Figure 2.4b).

### *2.3.2 Pacific SST Biases*

Unlike the Atlantic cold bias, which significantly impacts both the Atlantic and eastern Pacific basins (Figure 2.2), the Pacific cold bias has no significant impact on TC track density in these ocean basins (Figure 2.8). (However, a positive anomaly in track density occurs in the Pacific region around 180°W.) The Pacific warm bias and total bias significantly increase the track density and genesis density (not shown) locally in the ENP, but the positive anomaly pattern has a different shape and location from that of the *AtlCB* experiment. While the maximum magnitudes of the track density anomaly from *PacWB* and *PacTB* are about half of that from the Atlantic cold bias, the positive TC track density anomaly in the central Pacific (around 180°W) is much larger in *PacCB* and *PacTB* compared to *AtlCB*. A positive track density anomaly in the central North Pacific occurs with a negative anomaly in the central to eastern Atlantic basin in both *PacCB* and *PacTB* (Figure 2.8b and c). Since the positive anomaly in the central Pacific is accompanied by a negative anomaly in the western (coastal) Pacific, an eastward shift of TCs in the WNP is generated by the Pacific total SST bias (Figure 2.8c).

This eastward shift also appears in genesis density (not shown), and a similar shift in WNP TCs is observed during El Niño events (eg. Chan 1985, 2000; Wang and Chan 2002). Wang and Chan (2002) suggest that the equatorial westerlies associated low-level shear vorticity and upper-level divergence induced by the intensified WNP subtropical high during El Niño

events can both contribute to a southeastward shift of TCs, by enhancing TC generation in SE WNP and suppress generation over the NW quadrant of the WNP. In our case, similar anomalous westerlies can be generated by the zonal SST gradient induced by the zonal gradient in cold and warm biases north of the equator, and the intensification of the subtropical high can be generated by the local decrease in SST induced by the northwestern part of the Pacific cold bias. Therefore, with both the warm and cold biases combined, PacTB generates the most significant eastward shift in TCs. However, the SST bias pattern in the Pacific is more complex than El Niño related SST anomalies, and further work is required to fully understand their impact on the shift of TC locations, and how the mechanism is different from that during El Niños.

Consistent with the impact on the track density, the Pacific cold bias alone insignificantly influences ACE and number of TCs in both the Atlantic and Pacific basins (Figure 2.9 and Table 2.3). The warm bias, on the other hand, locally increases ENP TC activity (Figure 2.9b and e). Similarly, the ensemble means in ACE and number of TCs increase (Table 2.3). Furthermore, the *PacWB* runs generate stronger TCs in the ENP (not shown), consistent with the larger ACE values. The remote impact of the Pacific warm bias on the TC activity in Atlantic is evident, with a slight decrease in ACE and number of TCs (Figure 2.9a and d). However, the ensemble-averaged Atlantic ACE in *PacWB* is significantly different from that of *CTRL* in the Atlantic basin, whereas the change in number of TCs is insignificant (Table 2.3). Moreover, there is no significant change in the ensemble mean of both ACE and number of TCs in the Atlantic basin in *PacTB*. The ensemble means show that while the Atlantic SST biases have a larger impact on TCs remotely in the ENP compared to locally in Atlantic (Table 2.2), the Pacific biases have a larger impact locally in the ENP (Table 2.3).

Even though the Pacific SST bias has no significant impact on WNP ACE and number of TCs, the probability density function of TC intensity (not shown) indicates that *PacCB* shifts the TCs to lower intensity compared to CTRL. A similar result is obtained by separating out strong TCs when calculating the ensemble ACE and the number of TCs. While the ensemble-averaged values of ACE and number of TCs in *PacCB* are insignificantly different from those in *CTRL* (Table 2.3), the *PacCB* ensemble mean of ACE for TCs stronger than category 3 shows a 61% decrease from *CTRL* in WNP. Besides the change in ACE, the number of TCs stronger than category 3 also decreases in *PacCB* (by 75%), indicating that a significant decrease in TC intensity in the WNP can be caused by the Pacific cold bias.

GPI and associated atmospheric variables are also analyzed for Pacific bias experiments. Locally, PacWB and PacTB strongly increase GPI in the ENP, corresponding to an increase in ACE and number of TCs in that region (Figure 2.10). *PacCB* remotely increases GPI in the western Atlantic near the Caribbean Sea (Figure 2.10b), corresponding to an insignificant increase in ACE in Atlantic basin (Table 2.3). *PacTB* has the combined effect of *PacWB* and *PacCB* in the ENP and Atlantic basins, where GPI increases strongly in the ENP, but changes insignificantly in the Atlantic. Both *PacWB* and *PacCB* (and thus *PacTB*) generate a positive GPI anomaly in the central Pacific near 10° to 15°N and 160°E to 150°W, and a negative anomaly north of the positive anomaly in central Pacific as well as in the WNP. Note that a similar pattern is shown in the track density anomaly for *PacTB* (Figure 2.8), except for a westward shift compared to the GPI anomaly pattern.

The contributions from each factor in GPI indicate that the warm bias generates an increase in GPI in the ENP mainly through PI (Figure 2.11). *PacWB* and *PacCB* have similar GPI anomalies in the central Pacific derived from similar physical causes: both humidity and

shear terms make a positive GPI anomaly. This similarity between the GPI term contributions in *PacWB* and *PacCB* suggests that it is the gradient of the SST, rather than the SST anomaly, that influences the atmospheric circulation and condition (Graham and Barnett 1987; Wang and Li 1993), which further induce changes in TC activity. Nevertheless, the negative GPI anomaly in central and WNP is much weaker in *PacWB* than *PacCB*, with the anomaly attributed to all GPI terms. Although the *PacCB* generates a stronger eastward shift in the WNP TC tracks and GPI anomaly, with the cold bias in western WNP, TCs do not seem to intensify further even with a longer distance to travel over the ocean (which can potentially intensify TCs (eg. Wang et al. 2002; Camargo and Sobel 2005; Wang et al. 2013)). This could be related to the coarse resolution of the model used in this study that does not fully resolve TC dynamics. As a result, the TC activity (ACE and TC number) of strong TCs decreases in *PacCB*. As for the Atlantic bias experiments, all the analyses for the Pacific SST bias experiments have been repeated by randomly chosen 8 ensemble members, and the results remain similar to those with all (16) ensemble members.

### *2.3.3 Atlantic and Pacific SST Biases*

Given the importance of joint SST variability (Patricola et al. 2014), we expect the Atlantic and Pacific biases to jointly influence the TC simulations. Both Atlantic total bias (*AtlTB*) and Pacific total bias (*PacTB*) generate an increase in track density in ENP (Figure 2.12), with *AtlTB* from about 10°N to 20°N (Figure 2.2c), and *PacTB* from about 20°N to 30°N (Figure 2.8c). Note that while the strongest increase of the track density in *PacTB* is along the west coast of Central America (corresponding to the bias location), the anomaly in *AtlTB* is slightly offshore in the ENP (due to the local topographic impact). The impact of the combined Atlantic and

Pacific SST biases (*AtlPacTB*) is shown to have combined effects of *AtlTB* and *PacTB*. Figure 2.12 shows the TC track density difference between *AtlPacTB* and *CTRL*. Compared to *AtlTB* and *PacTB*, it is clear that the positive track density anomaly in the ENP is more widespread in *AtlPacTB*. In the Atlantic region, SST biases in both *AtlTB* and *PacTB* contribute to the negative anomalies in TC track density in *AtlPacTB*. However, the positive track density anomalies in the central Pacific and negative anomalies in the WNP appear to mainly come from the Pacific SST biases (*PacTB*), with minor contribution from the Atlantic biases (*AtlTB*).

The combined Atlantic and Pacific SST biases significantly reduce ACE and TC number in the Atlantic basin, and this suppression of TC activity is mainly dominated by the Atlantic bias (Figure 2.13 and Table 2.4). In the ENP, both *AtlTB* and *PacTB* significantly increase the values of ACE and TC number, resulting in a significantly large increase in TC activity (199% and 88% compared to CTRL for ensemble mean ACE and TC number, respectively) in *AtlPacTB* runs. However, the ensemble mean ACE and TC number show relatively minor changes in the WNP in *AtlPacTB* compared to *AtlTB* and *PacTB* (Table 2.4). Interestingly, there is an indication that the ensemble spread, which is a measure of atmospheric internal variability, is reduced in WNP when the Atlantic and Pacific SST biases are combined in *AtlPacTB* compared to that in *AtlTB* and *PacTB* respectively. Whether this change in internal variability is robust requires further research.

To investigate the environmental condition changes associated with the impact of combined bias on TC simulations, we also computed GPI for the *AtlPacTB* experiment (Figure 2.14). According to the GPI anomalies induced by individual Atlantic and Pacific SST biases (Figure 2.4 and Figure 2.10, respectively), the negative GPI anomalies in Atlantic basin in *AtlPacTB* are mainly driven by the Atlantic cold bias, whereas the positive GPI anomalies in the

ENP are caused by joint impacts from the Atlantic cold bias and Pacific warm bias. In the central and WNP region, the GPI anomaly in *AtlPacTB* shows a similar pattern and magnitude to the Pacific bias experiments, indicating the dominant influence from the Pacific biases, rather than the Atlantic biases, on the GPI in these regions. This GPI anomaly pattern is generally consistent with TC changes measured by other TC activity indexes, including track density, ACE, and number of TCs. It shows that TC activity is (1) strongly enhanced in the ENP, (2) suppressed in the Atlantic, and (3) generally increased in central Pacific and decreased in the WNP because of an eastward shift in TC locations, under the combined influence of SST biases in both basins.

**2.4 Discussion and Summary**

Large ensembles of TC-permitting tropical-channel WRF simulations show that tropical SST biases common to current generation climate models can have a significant impact on TC simulations, predictions, and projections both locally in and remotely from tropical Atlantic and Pacific basins. Even though previous studies have suggested impacts of SST biases on simulated TCs (Vecchi et al. 2014), the influence of individual biases (and biases in each basin) has not been systematically investigated. In this study, we investigate the local and remote TC responses to individual biases by separating warm and cold biases in each ocean basins, and the results allow us to identify which biases have the most significant impact on TC simulations. Our study shows that tropical SST biases can cause an overestimation of ACE (by ~200%) in the ENP and underestimation of ACE (by ~60%) in Atlantic, while the impact on WNP ACE is insubstantial. Considering the basin-wide TC activity, TCs in the ENP appear to be most affected by SST biases because of the joint influence from the tropical Atlantic and Pacific. In contrast, Atlantic

TC activity is mostly affected by the cold bias in the Northern Tropical Atlantic, whereas TC activity in the WNP seems to be dominated by the local influence of Pacific SST biases. Therefore, the results of this study suggest that reducing the Atlantic cold SST bias and Pacific SST warm biases could have the strong impact on improving TC representation in climate simulations, especially in the ENP and Atlantic. Moreover, even though the spatial patterns and magnitudes are similar between the Atlantic and Pacific SST biases, the mechanisms of how these biases exert their influence on simulated TC activity are different.

The Atlantic cold SST bias causes decreases in mid-tropospheric humidity and potential intensity, and increases in vertical wind shear, all of which contribute to decreases in the North Tropical Atlantic GPI, leading to decreases in track density, ACE, and number of TCs in the region. In addition, increase in ENP GPI (together with increase in track density, ACE, and TC numbers) primarily comes from decreases in vertical wind shear due to the remote influence of the Atlantic cold SST bias that produces a walker-type response (Patricola et al. 2017) forced by a diabatic heating anomaly associated with orographic lifting along Central America mountain ranges. The terrain-induced circulation anomaly enhances vertical wind shear over Atlantic sector and reduces vertical wind shear in the near coast region of ENP. Figure 2.15 shows a schematic diagram illustrating the mechanism behind the anomalous circulation. In response to the cold bias in Atlantic (*AtlCB*), the CLLJ intensifies because of the increase in both inter-basin SST gradient and land-sea temperature contrast. At the same time, atmospheric moisture content also decreases due to the surface cooling, which is the strongest in the Southern Caribbean (Figure 2.1). The drier and colder winds carried by the CJJL reduces the orographic lifting induced diabatic heating, which in turn produces a clockwise anomalous vertical circulation over Central America (Figure 2.15b). The anomalous circulation acting on the mean circulation

(Figure 2.15a) produces intensified vertical wind shear on the Atlantic side and reduced shear on the Pacific side of Central America, which is primarily responsible for the enhanced TC activity over the ENP and reduced TC activity over the Caribbean and Atlantic in *AtlBC*. This remote influence of Atlantic SST is supported by observational analysis that shows an increase in ENP TCs during cold AMM phase (Patricola et al. 2017). Both observations and simulations from TCM show a decrease in vertical wind shear in ENP during negative AMM events. Furthermore, even though the impact of Atlantic SST biases on WNP TCs is insubstantial, Yu et al. (2015) noted a possibility of the influence of Atlantic SST variability on the circulation in Pacific Ocean. Therefore, accurate simulations of Pacific TCs will require a realistic representation of Atlantic SST.

The spatial distribution of the SST biases and the known influence of tropical SST on TCs (e.g., Vimont and Kossin 2007; Patricola et al. 2014; Patricola et al. 2017) together suggest that the Atlantic SST biases, which have a similar spatial structure to the negative phase of AMM, is a leading cause for failure of climate models to accurately simulate Atlantic and ENP TC activities. On the other hand, the impact of the equatorial Pacific biases is more complex than ENSO's impact on TCs because the SST biases have a more complex spatial structure along the equator than ENSO SST anomalies. The SST bias in the northwestern Pacific has a similar pattern to its counterpart in the north tropical Atlantic, but its impact on TCs is different from the Atlantic because, unlike the Atlantic, SST anomalies in the WNP have a limited influence on western Pacific TCs (Chan 2005), suggesting that dynamic processes controlling SSTs' influence on TCs are different between these two regions. We further note that the net effect of the Atlantic and Pacific biases on TCs simulated by AtlPacTB cannot be simply deduced by linear superposition of the effects from *AtlTB* and from *PacTB*, although some compensation between

the effects of different SST biases on TC activity is observed. This suggests that the SST biases on TCs are inherent nonlinear.

In contrast to Atlantic SST biases, the Pacific SST biases do not exhibit as strong remote influence on Atlantic TCs as Atlantic biases on Pacific TCs. The warm SST bias off the west coast of Mexico has a significant impact on ENP TCs, which is mainly driven by local change in potential intensity (which is further a function of SST variability). Moreover, anomalies in the WNP suggest an eastward shift of the TCs due to the Pacific SST biases, possibly through a mechanism similar to the southeastward shift of WNP TCs that attributes to El Niño events (Wang and Chan 2002). While our results show no significant impact of Pacific SST on Atlantic TCs, previous studies have shown a remote influence of ENSO variability on the TC activity in the Atlantic basin. Given that the regions with larger SST biases in the Pacific basin are not in the El Niño regions, it suggests that the location of the maximum SST anomalies (or biases) may play an important role controlling the impact on TCs, as suggesting by Wang and Chan (2002). However, further research is required to reach a conclusion.

Our results suggest that SST biases can change TC tracks, and thus TC landfall locations. In other words, tropical SST biases can introduce biases to our forecast of regional TC landfall. For example, the Pacific biases introduce an eastward shift in the WNP TC tracks, suggesting a reduced possibility of TC landfall in the Asian region. Therefore, projections of future TC changes over the Asian region, particularly TC landfall over East Asia, may be subject to considerable uncertainties because of SST biases in coupled models. A similar shift in WNP TC tracks is shown in Figure 1 in Vecchi et al. (2014). By removing the SST biases through flux adjustment, the WNP TCs are generated more toward the Asian region and less in the Central Pacific region. Moreover, both our result and that from Vecchi et al. (2014) suggest an increase

in track and genesis of TCs in near-coastal region of ENP in the presence of SST biases, indicating a possible overestimation of Northern and Central American TC landfall from the Pacific Ocean. Nevertheless, while our simulations with Atlantic biases show a basin-wide decrease in TC tracks, indicating no significant change in the TC locations, Vecchi et al. (2014) show a southeastward shifted in tracks and genesis locations, suggesting a less possibility of TCs making landfall over US and Mexico from GoM and western Atlantic Ocean. We should note that Vecchi et al. (2014) consider the SST biases not only in the tropic, but also in extratropics, and the sample size in their simulations is about twice of our TCM simulations.

Even though our ensemble size is shown to be sufficient for computing basin-wide TC activities, it is possible that our sample size is not large enough to thoroughly investigate systematic shifts in the Atlantic TC tracks and genesis locations caused by SST biases. Moreover, we utilized a TC-permitting atmospheric-only model, while Vecchi et al. (2014) utilized a high-resolution atmospheric model coupled to a low-resolution ocean model. Due to the differences in experimental designs between this study and Vecchi et al. (2014), it is difficult to directly compare the results. Furthermore, while our results suggest the importance of the response in the Caribbean and western north Atlantic, the model we utilized (TCM) is known to have convection biases in these regions. Therefore, an oversensitivity of TC responses may be present in our TCM. However, this problem of regional convection biases is also a general problem among many AGCMs (Biasutti et al. 2006; Ryu et al. 2014). One should keep these convection biases in mind when interpreting our results.

In conclusion, our results suggest the SST biases can influence simulations, seasonal forecasts and future projections of TCs not only in local basins, but also in remote ocean basins. Therefore, we should take the SST biases and their impact into account when analyzing TC

projections from coupled AOGCMs. Many previous studies focus on the origins of these SST biases (Richter and Xie 2008; Li and Xie 2012; Paticola et al. 2012; Xu et al. 2013; Small et al., 2015), and some progress has been made to improve the SST biases, even though the improvement has shown to be difficult and challenging in some specific regions such as the eastern ocean basins (Xu et al. 2014; Richter 2015, Small et al. 2015, Zuidema et al. 2016). Nevertheless, the bias problem is unlikely to be resolved in the near future and the climate modeling community will continue to confront with this problem (Richter 2015). Moreover, since tropical SST biases can have remote effects on biases in other regions, it could potentially hinder the effort to improve regional processes to address local SST biases, making the reduction of SST biases more challenging (Wang et al. 2014). This means that we need to develop strategies of coping with the impact of these model biases at least in the near future. With only few studies focusing on the impact of SST biases on TC simulations and predictions, more future investigations are needed to have a comprehensive understanding of local and remote influence of the SST biases on TC simulations on seasonal to decadal timescales.

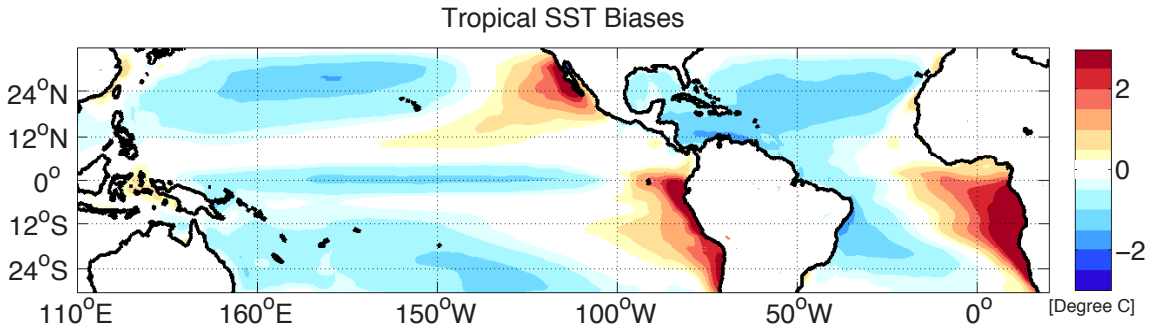


Figure 2.1. The April-November averaged multi-model mean tropical SST biases (°C).

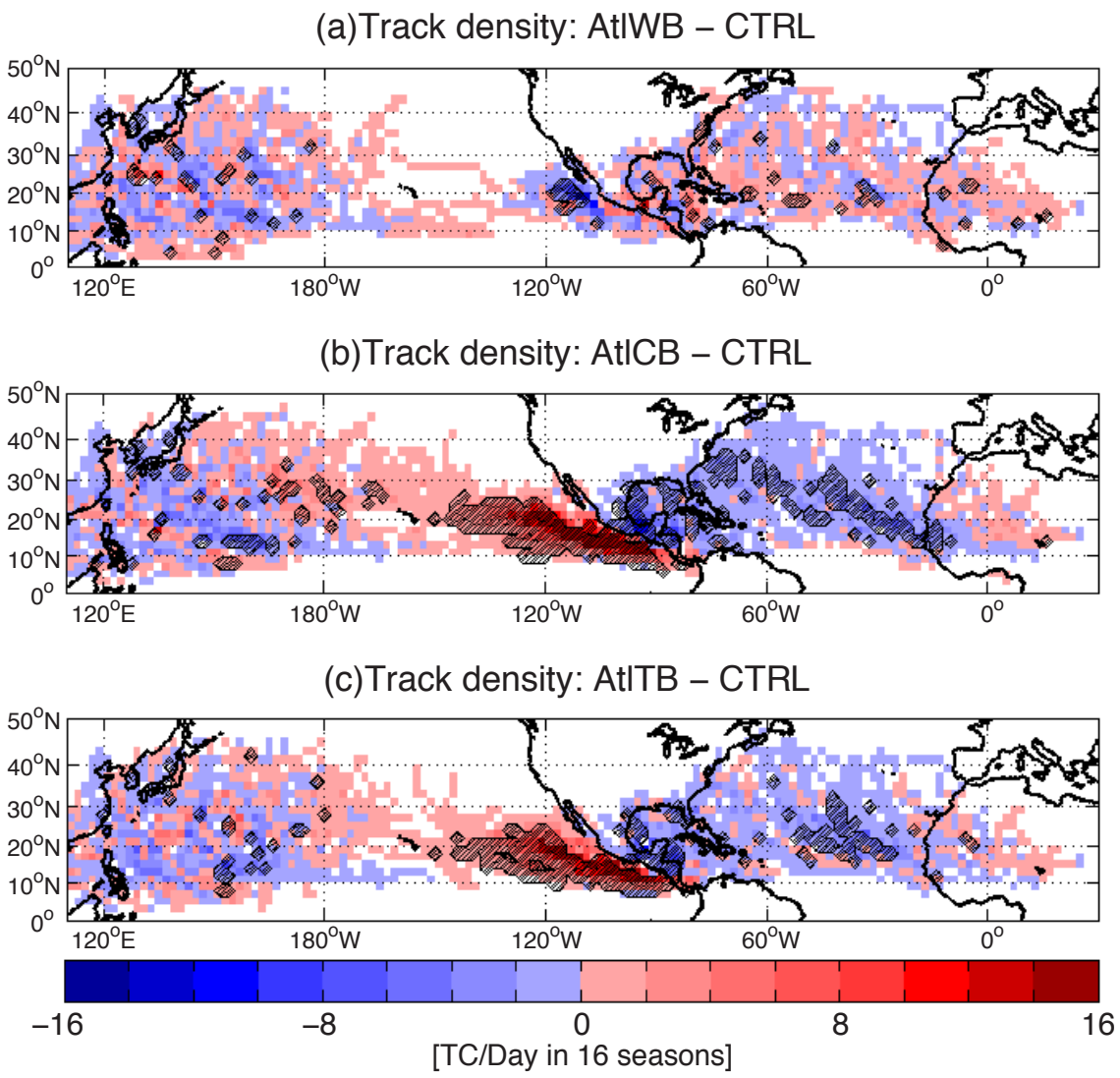


Figure 2.2. The differences between track density ensemble means of Atlantic (a) warm (*AtlWB*), (b) cold (*AtlCB*), (c) total (*AtlTB*) bias runs, and that of control (*CTRL*) runs. Hatched regions passed the two-sample student t-test at 5% significance level.

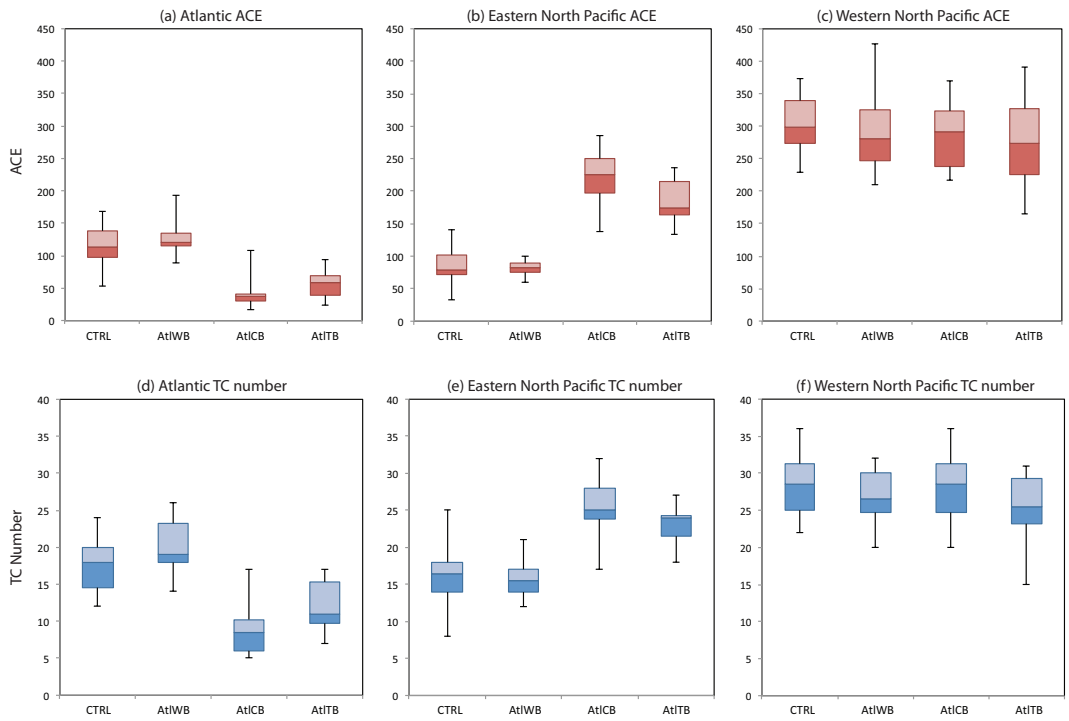


Figure 2.3. Boxplot of simulated Accumulated Cyclone Energy (ACE) ((a) to (c)) and number of TCs ((d) to (f)) from control (*CTRL*), Atlantic warm (*AtlWB*), cold (*AtlCB*), and total (*AtlTB*) bias runs (16 ensemble members each) in different ocean basins. The horizontal line between light and dark shading represents the median of the ensemble values, while the upper boundary of the light color box represents the 75 percentile and the lower boundary of the dark color box represents the 25 percentile. The whiskers show the maximum and minimum ensemble values.

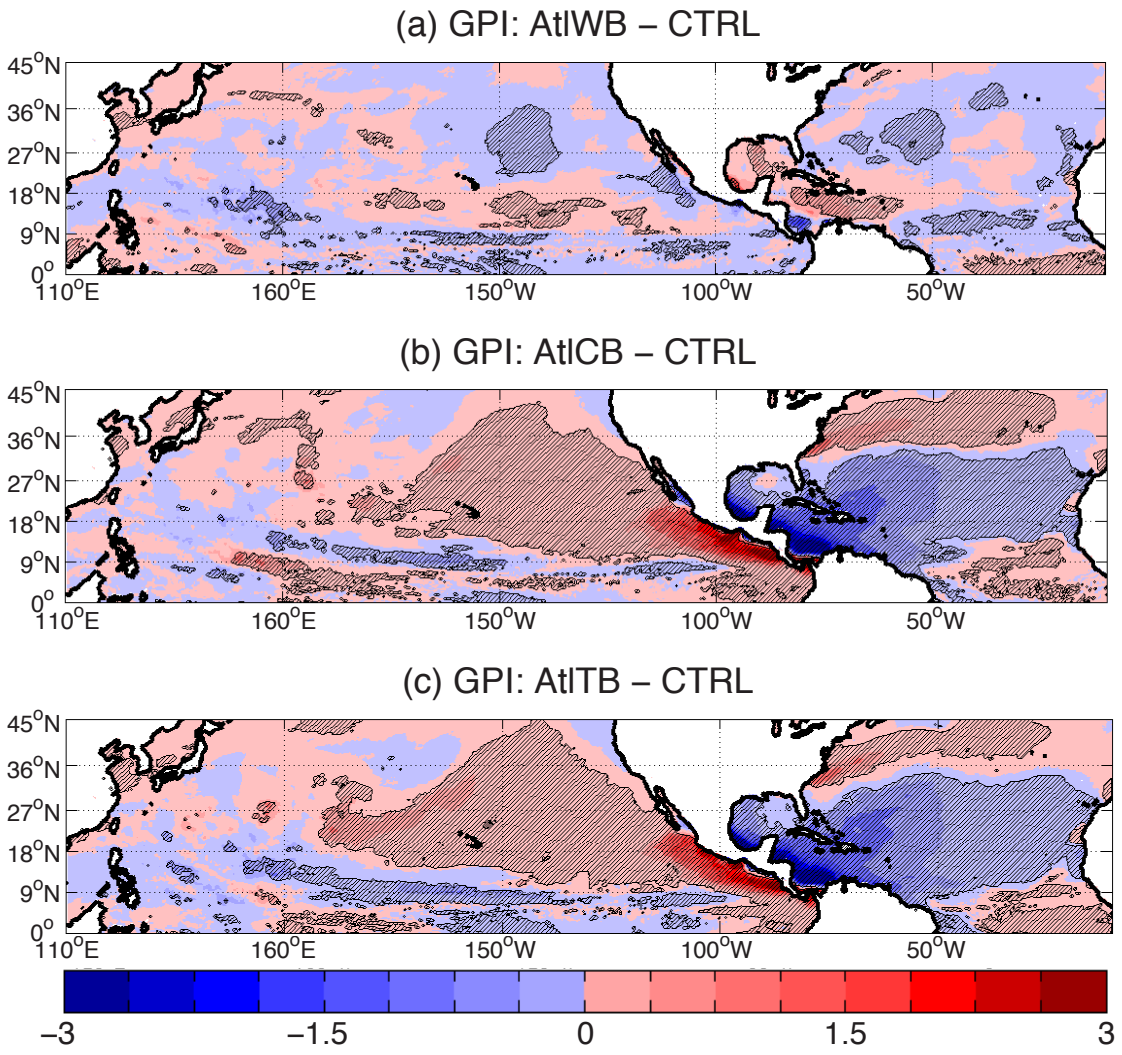


Figure 2.4. The differences between GPI ensemble means of Atlantic (a) warm (*AtlWB*), (b) cold (*AtlCB*), (c) total (*AtlTB*) bias runs, and that of control (*CTRL*) runs. Hatched regions passed the two-sample student t-test at 5% significance level.

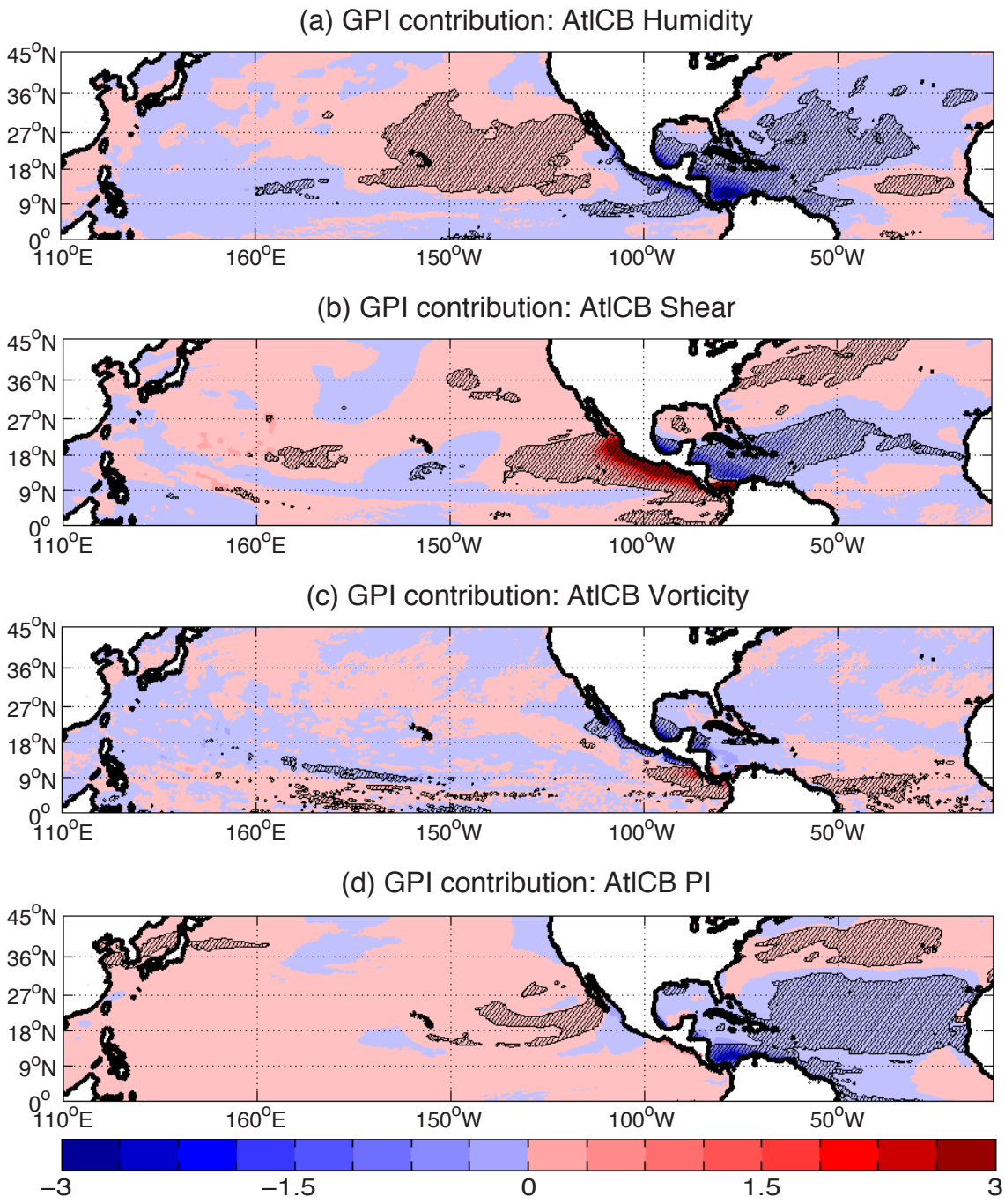


Figure 2.5. The contribution on the differences of GPI ensemble means between Atlantic cold (*AtlCB*) bias runs and control (*CTRL*) runs from different GPI terms. Hatched regions passed the two-sample student t-test at 5% significance level.

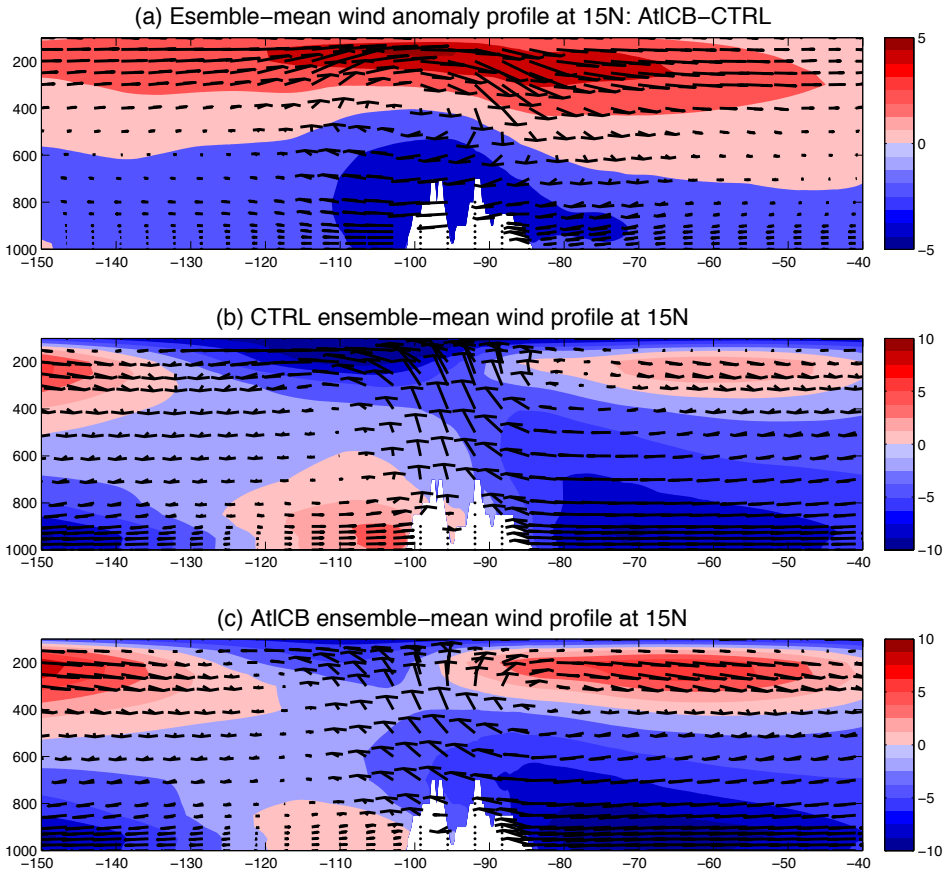


Figure 2.6. The wind cross-section along 15°N (averaged from 12.5°N to 17.5°N), where the *AtlCB* shear contribution (to GPI anomaly) and cold bias induced zonal wind anomalies at 200hPa and 850hPa show the largest values. (a) shows the ensemble-averaged anomalous wind profile (in arrows [m/s]) calculated from zonal (u) and vertical (w) wind (times 6000 for scaling) differences between *AtlCB* and *CTRL* runs, and the zonal wind anomalies (in shaded color) from *AtlCB* comparing to *CTRL*, while (b) shows the *CTRL* ensemble-averaged wind profile, and (c) shows the *AtlCB* wind profile.

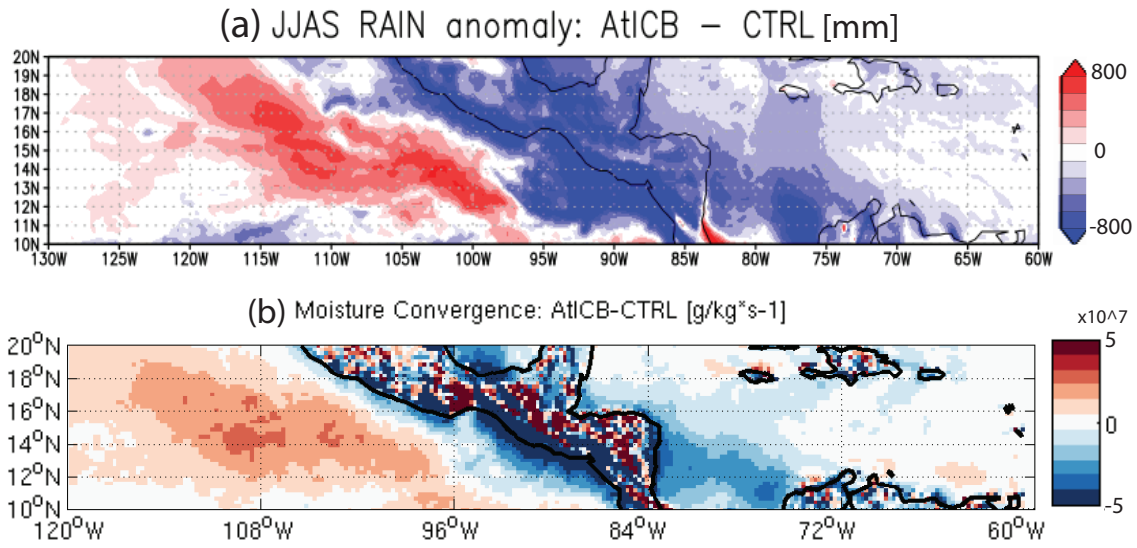


Figure 2.7. JJAS accumulated precipitation (a) and seasonal-mean vertical-integrated (1000hPa to 500hPa) moisture convergence (b) differences between *AtlCB* and *CTRL*. Red colors in (a) indicate more precipitation in *AtlCB* than *CTRL*. While red colors in (b) indicate anomalous moisture convergence, blue colors indicate anomalous moisture divergence.

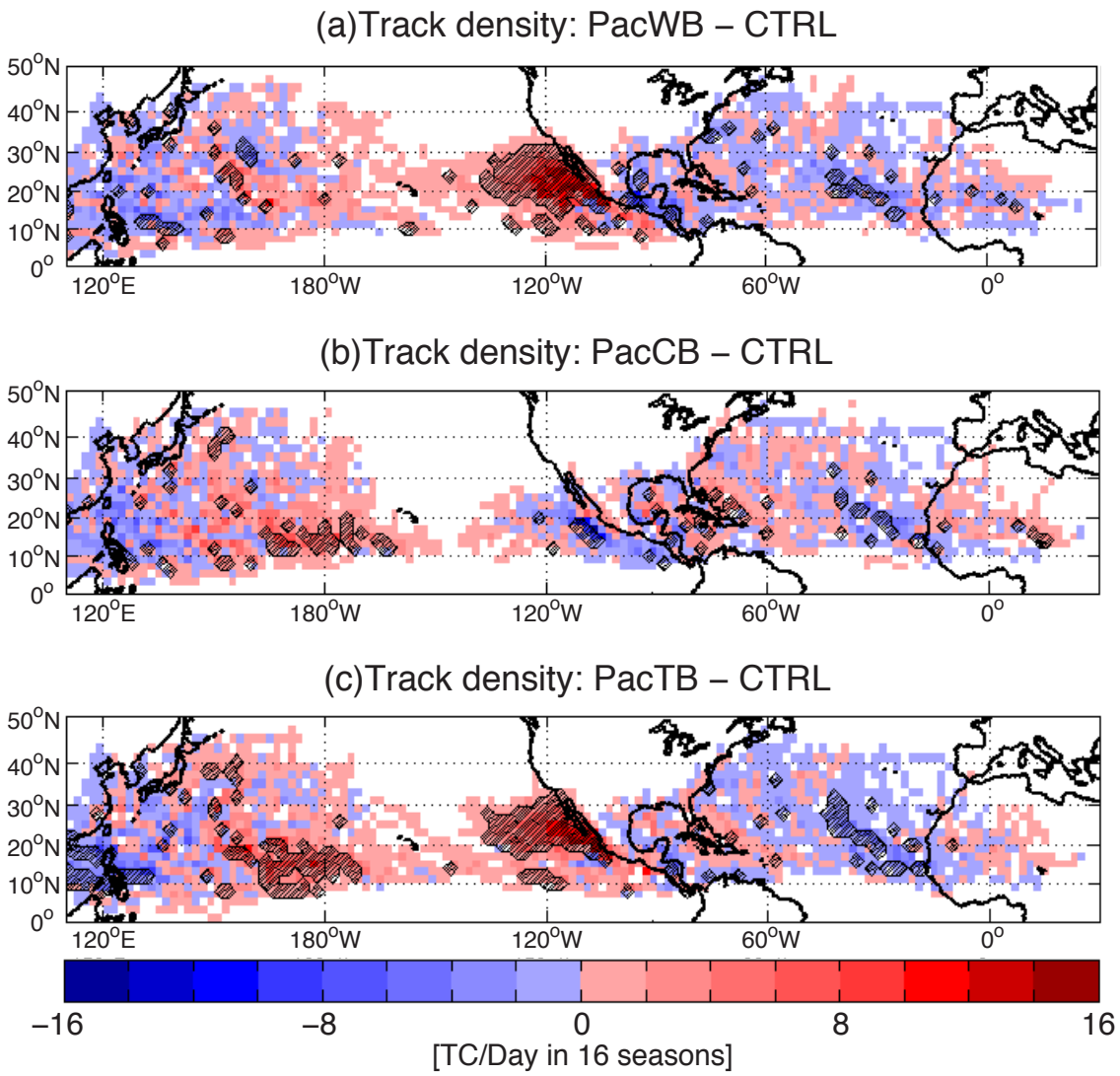


Figure 2.8. Same as Figure 2.2, but results from Pacific bias runs instead of Atlantic bias runs are shown. The colorbar is identical to that in Figure 2.2.

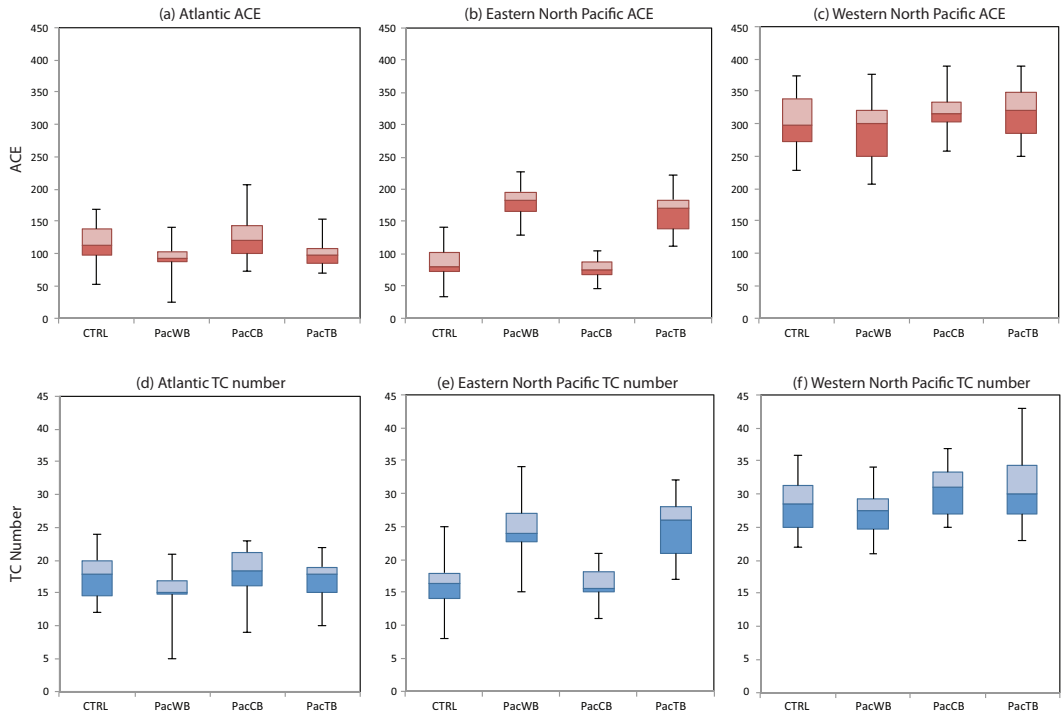


Figure 2.9. Same as Figure 2.3, but results from Pacific bias runs instead of Atlantic bias runs are shown.

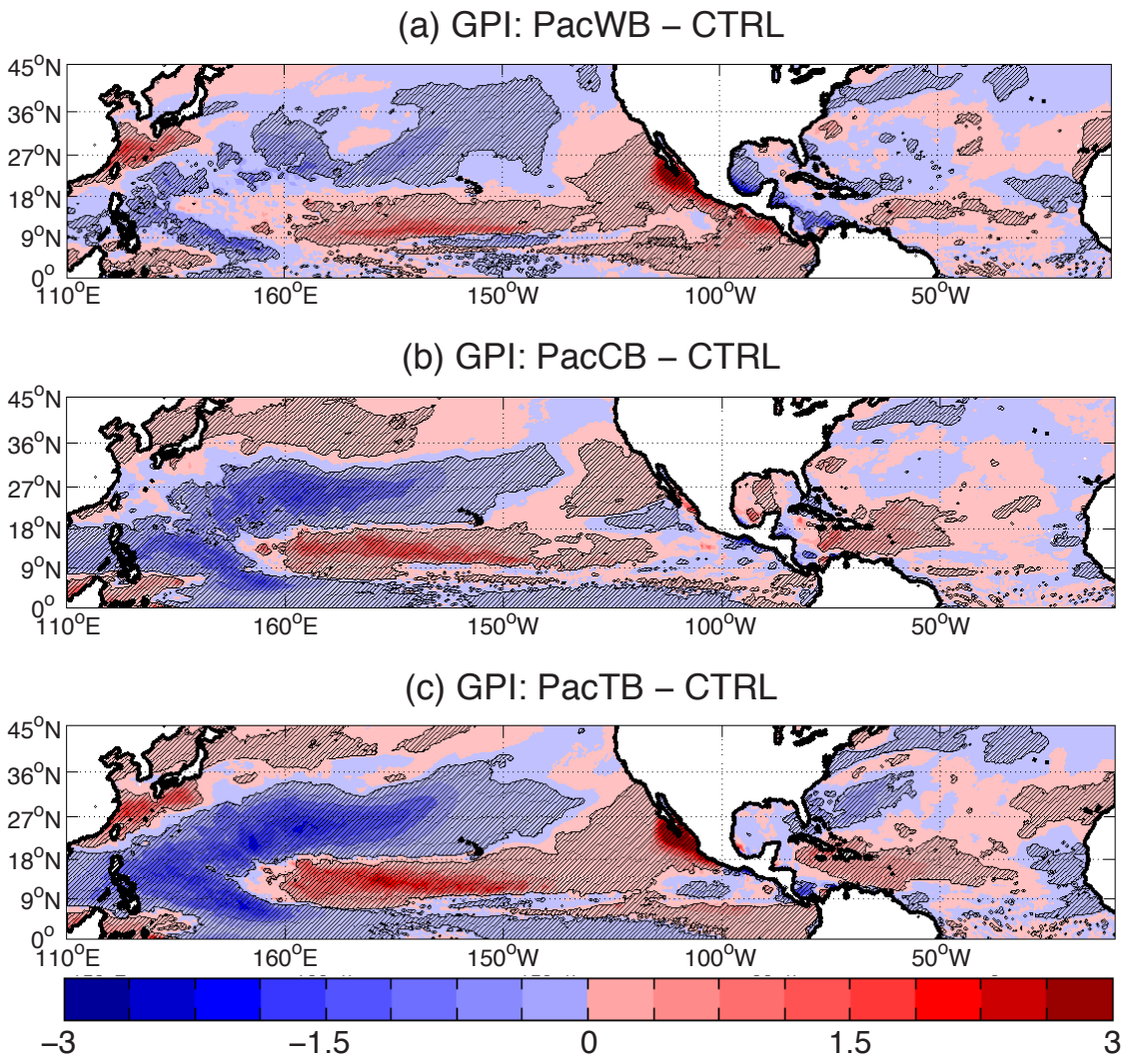


Figure 2.10. Same as Figure 2.4, but results from Pacific bias runs instead of Atlantic bias runs are shown.

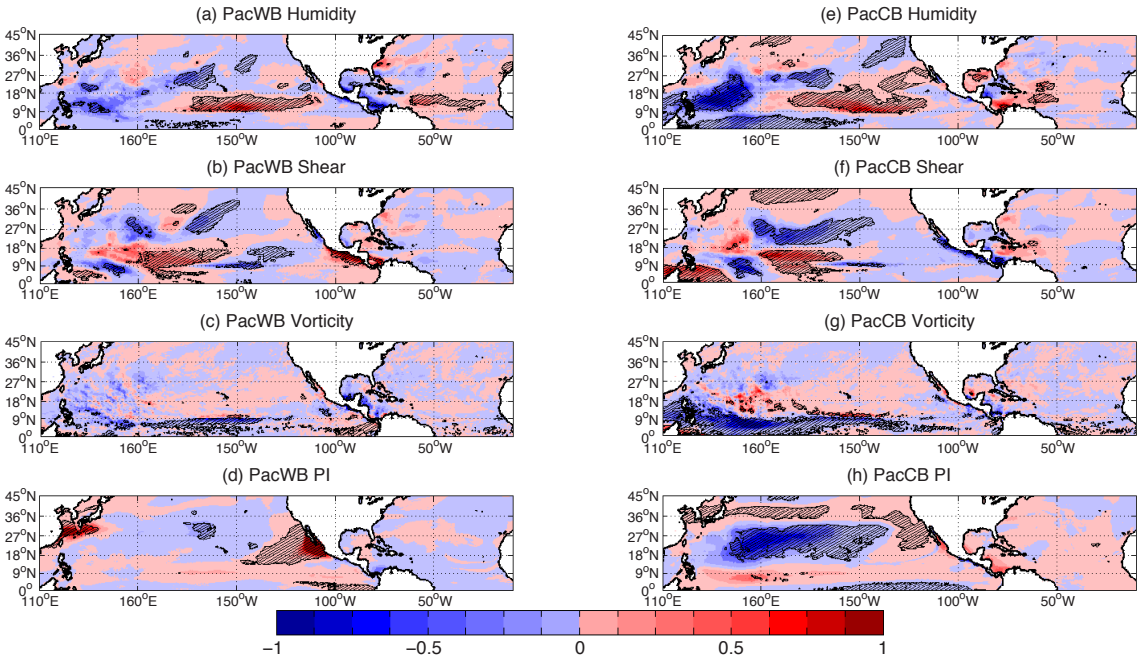


Figure 2.11. Similar to Figure 2.5, but with results from Pacific warm bias runs showing on left panels, and those from Pacific cold bias runs showing on right panels.

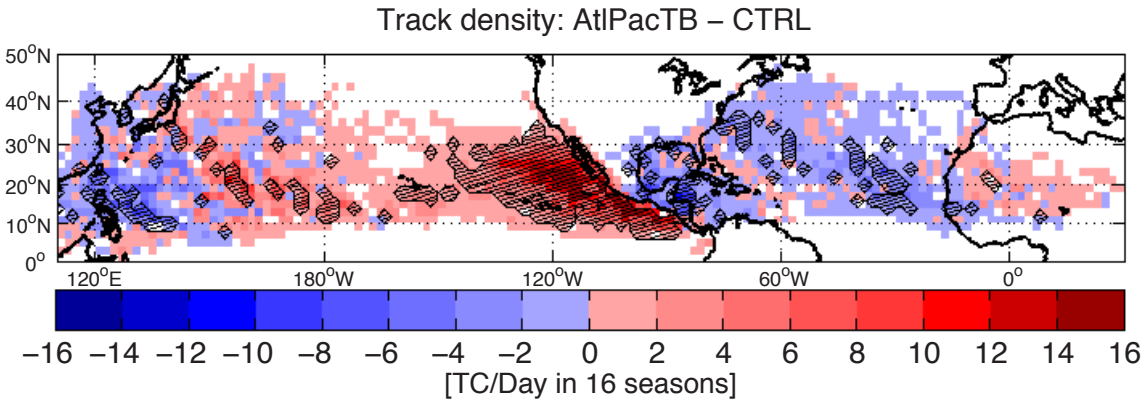


Figure 2.12. Similar to Figure 2.2, showing the differences between track density ensemble means of Atlantic and Pacific total bias (*AtlPacTB*) runs, and that of control (*CTRL*) runs.

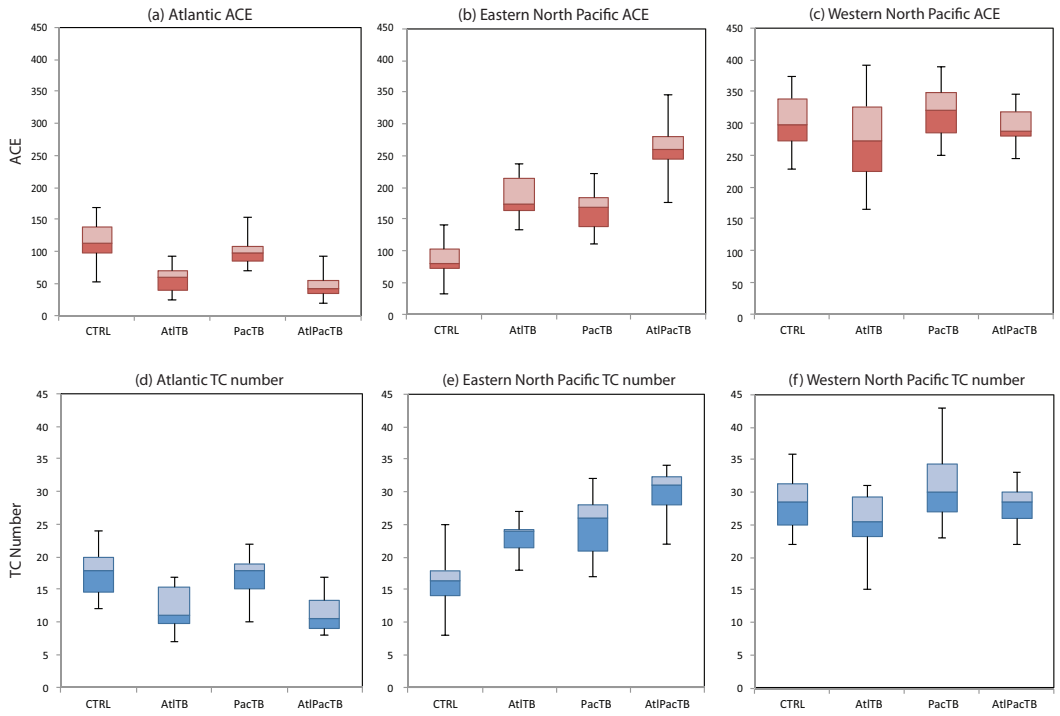


Figure 2.13. Same as Figure 2.3, but results from Atlantic total bias (*AtlTB*), Pacific total bias (*PacTB*), and combined Atlantic and Pacific total bias (*AtlPacTB*) runs instead of Atlantic bias runs are shown.

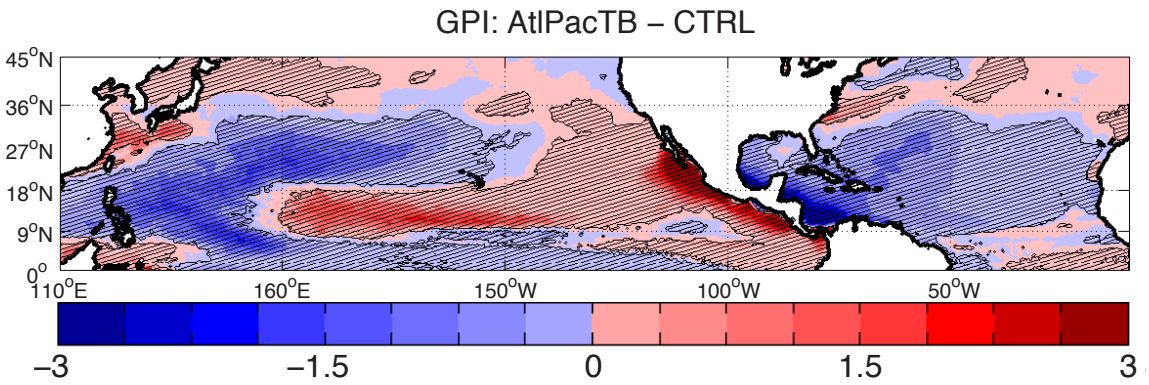


Figure 2.14. Similar to Figure 2.4, showing the differences between GPI ensemble means of combined Atlantic and Pacific bias (*AtlPacTB*) runs and that of control (*CTRL*) runs.

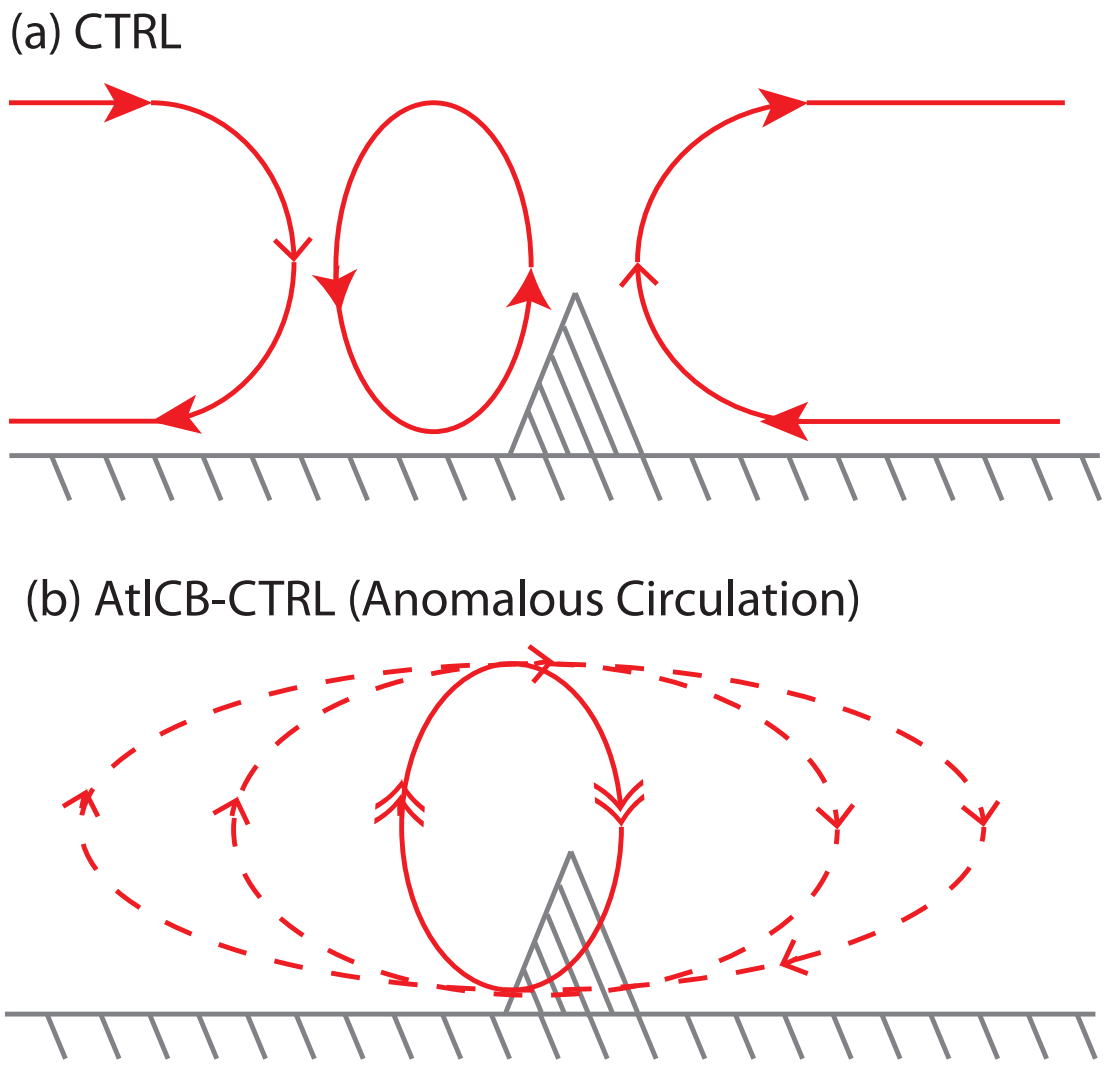


Figure 2.15. The mechanism of remote influence of the Atlantic cold bias *(AtlCB)* on ENP TCs.

| SST bias | Experiment Name |
|---|---|
| Control (without bias) | CTRL |
| Atlantic warm bias | AtlWB |
| Atlantic cold bias | AtlCB |
| Atlantic total bias | AtlTB |
| Pacific warm bias | PacWB |
| Pacific cold bias | PacCB |
| Pacific total bias | PacTB |
| Atlantic and Pacific total bias | AtlPacTB |

Table 2.1. Experiment names for control and bias runs, and the associated SST biases that included in the SST forcings for each experiment.

| | CTRL | AtlWB | AtlCB | AtlTB |
|---|---|---|---|---|
| **Atlantic ACE** | 116 | 128 | 42 [-64%] | 57 [-51%] |
| **ENP ACE** | 87 | 81 | 220 [153%] | 185 [113%] |
| **WNP ACE** | 302 | 295 | 285 | 278 |
| **Atlantic number of TCs** | 18 | 20 | 9 [-50%] | 12 [-33%] |
| **ENP number of TCs** | 16 | 16 | 26 [63%] | 23 [44%] |
| **WNP number of TCs** | 28 | 27 | 28 | 25 |

Table 2.2. Ensemble means (from 16 ensemble members each) of ACE and the number of TCs from control (*CTRL*) and Atlantic bias (*AtlWB*, *AtlCB*, and *AtlTB*) runs in both real number and percentage difference from *CTRL* (only shown if the difference from *CTRL* is significant at the 5% level).

| | CTRL | PacWB | PacCB | PacTB |
|---|---|---|---|---|
| **Atlantic ACE** | 116 | 92 [-21%] | 125 | 100 |
| **ENP ACE** | 87 | 181 [108%] | 75 | 166 [91%] |
| **WNP ACE** | 302 | 292 | 314 | 317 |
| **Atlantic number of TCs** | 18 | 15 | 18 | 17 |
| **ENP number of TCs** | 16 | 25 [56%] | 16 | 25 [56%] |
| **WNP number of TCs** | 28 | 27 | 31 | 31 |

Table 2.3. Identical to Table 2.2, but showing the results for control and Pacific bias (*PacWB*, *PacCB*, and *PacTB*) runs.

| | CTRL | AtlTB | PacTB | AtlPacTB |
|---|---|---|---|---|
| **Atlantic ACE** | 116 | 57 [-51%] | 100 | 47 [-59%] |
| **ENP ACE** | 87 | 185 [113%] | 166 [91%] | 260 [199%] |
| **WNP ACE** | 302 | 278 | 317 | 297 |
| **Atlantic number of TCs** | 18 | 12 [-33%] | 17 | 11 [-39%] |
| **ENP number of TCs** | 16 | 23 [44%] | 25 [56%] | 30 [88%] |
| **WNP number of TCs** | 28 | 25 | 31 | 28 |

Table 2.4. Identical to Table 2.2, but showing the results for control, Atlantic total bias (*AtlTB*), Pacific total bias (*PacTB*), and combined Atlantic and Pacific total bias (*AtlPacTB*) runs.

# CHAPTER III

# UNCERTAINTY AND FEASIBILITY OF DYNAMICAL DOWNSCALING FOR TROPICAL CYCLONE PREDICTION AT SEASONAL-TO-DECADAL TIME SCALES

## 3.1. Introduction and Objectives

With the advancement of computing technology and improvement of weather and climate models, dynamical models have recently demonstrated increased potential for predicting TC activity at seasonal or longer timescales, especially in the Atlantic basin (Zhao et al. 2010; Chen and Lin 2013). Different from short-term synoptic prediction of TCs that can rely on persisted SSTs, seasonal or longer-timescale TC prediction requires accurate knowledge of future SST information. Therefore, the most desirable approach to make seasonal or longer-timescale TC prediction is to use coupled climate models where SST variation and TC activity can be predicted simultaneously in one system. However, such an approach, known as tier-one forecast (Palmer et al. 2004; Saha et al. 2006; Zhu and Shukla, 2013), has proven to be challenging because current generation climate models have severe biases and systematic errors in presenting tropical SSTs, which can have a major impact on TC simulations and forecast skills, as shown and discussed in the previous Chapter. To overcome these biases, flux adjustment has been used in coupled climate model seasonal TC forecast (i.e., Vecchi et al. 2014). Given that climate model biases are likely to persist for decades (Ritcher 2015) and high computational cost puts hard constraints on the use of TC-resolving coupled climate models for seasonal TC predictions, tier-one climate prediction is suggested not to be a practical approach at this stage (Zhu and Shukla, 2013). Despite of the above problems, tier-one approach is being utilized by some

operational centers (Palmer et al. 2004; Saha et al. 2006), and has demonstrated some successes for some specific studies (e.g., Zhu and Shukla, 2013).

An alternative to the tier-one forecast is the tier-two forecast approach in which seasonal or longer-timescale SST forecasts are first performed by low-resolution coupled climate models, and then forecasted SST anomalies, after being bias corrected, are superimposed onto the observed SST climatology to force a TC-permitting or TC-resolving atmosphere-only model to make TC forecasts. Since SST biases have been removed by using the observed SST climatology, the tier-two forecast approach is free of SST bias influence. However, its disadvantages include 1) coupled ocean-atmosphere feedback is not included in the TC forecast and 2) forecasted SST anomalies at long lead times can contain large uncertainties. Therefore, the tier-two approach may be problematic in some regions such as the Indian Ocean, where the local air-sea feedback has a strong impact on SST (Zhu and Shukla, 2013). In the tier-two approach, either a high-resolution global atmosphere model or a regional atmosphere model can be used in the second stage of the approach. Advantages of using a regional model are to allow higher resolution to better resolve TCs and larger ensemble to better estimate forecast uncertainties. Disadvantages include new uncertainties associated with lateral boundary conditions required for the regional modeling approach. This regional model tier-two forecast approach is also known as dynamical downscaling approach (Barnston et al. 2010). Through this approach, since atmospheric-only models are used, one is able to separate the impact of SST forcing uncertainty from the uncertainty due to atmospheric internal variability as well as the lateral boundary conditions on model forecast skills.

In this Chapter, we examine the uncertainty and feasibility of the dynamical downscaling (tier-two) approach for seasonal or longer-timescale TC forecast in the global tropics. We will

use a WRF-based TC-permitting TCM for TC prediction and use SST anomalies derived from Community Earth System Model (CESM) Decadal Prediction Large Ensemble (DP-LE). The objectives of the study are to address the following scientific questions: 1) What is the feasibility of using a WRF-based TC-permitting TCM forced by SST anomalies from CESM-DP-LE for seasonal or longer-timescale TC forecast in the global tropics? 2) How do errors in the predicted SST affect model forecast skills? 3) How much influence can lateral boundary condition uncertainties have on model forecast skills? 4) What is the relative importance of the impact from atmospheric internal variability (initial conditions) on TC forecast skills, comparing to the impact from SST forcings when generating ensemble members?

The Chapter is organized as follows: Section 2 introduces the model and the data we utilized (including CEM-SP-LE), as well as the designs of all simulations. Section 3 demonstrates the results of seasonal TC simulations comparing the impact of uncertainty from SST forcings, lateral boundary conditions, and internal variability. The last section discusses the implications and uncertainties of the results as well as possible future works.

### 3.2. Model Description and Experimental Designs

As mentioned above, we examine the regional model two-tier forecast approach, in which a WRF-based TC-permitting TCM is used for TC prediction and SST anomalies derived from CESM-DP-LE are used to force the TCM. In the following, we give a brief description of CESM-DP-LE, TCM and other datasets used in our analysis.

*3.2.1 CESM-DP-LE*

CESM-DP-LE was carried out by NCAR (Yeager et al. 2018). It is a 40-member ensemble of decadal prediction simulations generated by CESM version 1.1. The atmospheric component of the model is the Community Atmospheric Model version 5 (CAM5) (Hurrell et al. 2013), with 1° horizontal resolution and 30 vertical levels; the ocean component is the Parallel Ocean Program version 2 (POP2) (Danabasoglu et al. 2012), with 1° horizontal resolution and 60 vertical levels; the sea ice component is the Los Alamos National Laboratory Community Ice Code version 4 (LANL-CICE4) (Hunke and Lipscomb 2008); the land component is the Community Land Model version 4 (CLM4) (Lawrence et al. 2011). The CESM-DP-LE simulations were initialized on every November 1$^{st}$ from 1954 to 2015, each of which was integrated forward for about 10 years (122 months). The radiative forcings (such as greenhouse gases and aerosols) are historical forcings from 1954 to 2005 and projected forcings after 2006, respectively, in the simulations. Moreover, while the atmospheric and land models were initialized with one of the members from CESM-LE (Kay et al. 2015), the initial conditions used in ocean and sea ice models were generated by the coupled ocean-sea ice (FOSI) configuration of CESM, which was forced at the surface with a blended wind field (CORE*, defined in Yeager et al. 2018). Due to the full field initialization (as opposed to anomaly initialization), all the predicted variables need to be "drift adjusted" by removing the lead-time–dependent model climatology. In our study, we used the "drift adjusted" daily mean SST anomalies and added them onto the observed SST climatology to generate a full SST field, which were then used to force the TCM for TC prediction.

As discussed in Yeager et al. (2018), one of the scientific objectives of CESM-DP-LE is to investigate the impact of both external (radiative) forcing and ocean initialization on hindcast

skill. Yeager et al. (2018) compared the CESM-DP-LE to CESM-LE – an uninitialized complementary set of large ensemble simulations generated by the same model and radiative forcings (Kay et al. 2015), and showed an enhancement in skill caused by initialization, suggesting a role of ocean memory in decadal climate prediction (Smith et al 2010). The CESM-DP-LE was also compared to the persistence forecasts to show the improvement in skill contributed by the external forcing. The results show that CESM-DP-LE has high skill in predicting SST and upper ocean heat content from seasonal to decadal timescales, contributed from both initialization and external forcing, especially in the Atlantic basin (Yeager et al. 2018). They reasoned that the enhanced forecast skill was associated with the ocean memory related to Atlantic Meridional Overturning Circulation (AMOC) (Figure 1 and 2 in Yeager et al. 2018).

However, all the skill analyses shown in Yeager et al. (2018) were based on annual mean. To better demonstrate the SST forecast skills during the Northern Hemisphere TC season, we computed the forecast skill of season-mean SST within the months during which TCs are most active. Figure 3.1 shows the correlation coefficients of the TC season-mean (MJJASON) SST anomalies (SSTA) between CESM-DP-LE and observation (CFSR) during 1979 to 2009, which correspond to verification at lead time 6 to 12 months. The regions with correlation coefficients that pass the 95% student t-test are hatched. High correlation appears in Atlantic, consisting with the high forecast skill of annual mean SSTA shown in the region (Yeager et al. 2018). Moreover, reasonably high skills are seen in the WNP and tropical Pacific regions, suggesting the potential of downscaling CESM-DP-LE for TC predictions at lead time longer than 6 months. The correlation in the ENP, however, shows a much lower value (comparing to that in the Atlantic and WNP during the TC season, or to the correlation of the annual mean SSTs in ENP shown in Yeager et al. (2018)), indicating relatively low skills in predicting SSTA in ENP

during the TC season 6-month in advance. The same correlation map between the observed and CESM-DP-LE predicted SSTAs at lead time of 18- to 24- months shows much lower values (not shown), especially in the equatorial Pacific region, indicating a sharp decrease in forecast skill of TC season SSTAs 1.5-to-2 years in advance. Similar results are shown for the annual-mean Nino3 SST forecast skill (Figure 9 in Yeager et al. 2018), in which a significant decrease in the skill is observed from lead time 1 to 2 years. Given the relative skillful forecast of TC seasonal SSTA by CESM-DP-LE in lead time 6 to 12 months, it is of interest to examine whether the predicted SST anomalies are useful for tier-two TC forecast at these time scales. We note that this forecast time scale is longer than the typical seasonal climate forecast time scale that is on the order of 6 months.

### *3.2.2 WRF-Based TCM*

The same TCM configuration of WRF (as in Chapter 2), with 27km horizontal resolution and 32 vertical layers, covering a domain extending from 30°S to 50°N around the globe, was utilized to carry out TC forecasts. As discussed in Chapter 2, the TCM developed by Patricola et al. (2016) and used in Chapter 2 has some major systematic errors and biases that can strongly influence TC simulations. These include an overestimation of the rainfall and the associated mid-level vertical motions in Africa and Amazon region. To reduce these errors and biases, a new set of physical parameterizations was used to improve simulation of the tropical circulation and TCs (see Fu, 2018). The sensitivity of these parameterizations of the TCM (hereafter referred to as TCM version 2 or simply TCM2) was tested over both the Atlantic and Pacific regions, and improvements in the simulations of TC-related environmental conditions were shown in detail by Fu (2018).

Of particular note is the improvement of the simulated large-scale circulations and basin-wide tropical cyclone activity made by using the new parameterizations in the ENP. Here, we show some of the results demonstrating the fidelity of the improved TCM in reproducing TC variability in the global tropics. Figure 3.2 (by Fu, personal communication) shows TCM2 simulated 10-member ensemble of TC numbers, ACE, and hurricane numbers in the Atlantic, given the "perfect" (observed) SST from Environmental Prediction (NCEP) Climate Forecast System Reanalysis (CFSR, Saha et al., 2010) (1990 to 2010) and the Climate Forecast System version 2 (CFSv2, Saha et al., 2014) (2011 onwards). High skills of the model in simulating seasonal Atlantic TC activity is demonstrated, with the correlation between simulation (ensemble-averaged) and observation (IBTrACS, Knapp et al., 2010) of 0.68, 0.60, and 0.65 for TC number, ACE, and hurricane number, respectively. Correlation coefficients of comparable values to the Atlantic are also shown in both ENP (Fu, 2018) and WNP (Fu, personal communication), with the value for WNP ACE as high as 0.81 (not shown). When comparing to other TC-permitting models (e.g., Chen and Lin 2013), TCM2 shows particularly high skills in simulating basin-wide TC activity in Pacific (especially WNP), as previously published models (e.g., Chen and Lin 2013) typically show much higher skills in Atlantic than in Pacific. Therefore, TCM2 is a suitable modeling tool for the purpose of downscaling TCs in the global tropics.

### *3.2.3 Experimental Design*

As shown in Vecchi et al. (2014), dynamical model-based seasonal TC forecasts have demonstrated remarkable skills in predicting certain aggregate measures of TC activity up to 6 months in advance. However, model forecast skill for lead time longer than 6 months remains

quite low, presumably because of the low skill in forecasting SST anomalies at the long lead time. In this study, we explore uncertainty and feasibility of TC forecast at lead time longer than 6 months by taking the advantage of the large ensemble of decadal SST forecasts from CESM-DP-LE that initializes forecasts every November 1st from 1954 to 2015 as described above. We conducted ensembles of hindcast runs (Table 3.1) for two ENSO events (1997/98 and 2015/16), in which the daily CESM-DP-LE SST anomalies (DP SSTA) with a 6- to 12- month lead time (corresponding to May to November) were used to force TCM2. We choose this prediction period because 1) it corresponds to the Northern Hemisphere TC season and 2) CESM-DP-LE shows much higher skill score during TC season in this period than in longer lead times, as discussed in section 2.1.

#### *3.2.3.1 Two Cases: 1997/1998 and 2015/2016*

ENSO is one of the strongest climate modes that influence tropical TC activity (Tang and Neelin 2004; Gray 1984a,b). The TC-season (May to November) mean of both observation and CESM-DP-LE (6- to 12- month lead) calculated Niño3.4 regional-averaged SSTA are shown in figure 3.3, with a correlation coefficient of about 0.55, which is comparable to the annual value of lead year 1 (Figure 9 in Yeager et al. 2018), but much higher than other decadal prediction dataset such as CESM-LE (~0.25) (Kay et al. 2015) and CCSM4-DP (~0.3) (Yeager et al. 2012). Several strong El Niño events can be identified in the time series: 1982/83, 1987/88, 1997/98, and 2015/16. Note that the TC season does not correspond to the months for calculating Niño index (November to the following January) when ENSO peaks, so the magnitudes and interannual variability of the time series shown in Figure 3.3 are different from Niño3.4 index. For example, 1982/83 is known as one of the strongest El Niño events based on the Niño index,

but the value of the observed TC season Niño3.4 SSTA is shown to be weaker than the 1987/88 event, which is a weaker event than the one in 1982/83. The CESM-DP-LE successfully reproduced the peaks of 1987/88, 1997/98, and 2015/16 events, but the strength was overestimated in 1987 and underestimated in 1997 and 2015. For the corresponding La Niña events, CESM-DP-LE underestimates (absolute) the strength in 1988 but overestimates the strength of the 1997 and 2016 events. Moreover, since TCM2 was validated for the period 1990 to 2016, the two ENSO events in 1997/98 and 2015/16 were utilized as two extreme ENSO cases to investigate the feasibility of dynamical downscaling using TCM2, as these events are known as the two strongest El Niños in the observed record. As will be discussed below, although CESM-DP-LE correctly predicted the occurrence of these two events, it has considerable errors in predicting the pattern and magnitudes of SSTA. One of our objectives is to examine the extent to which the uncertainty in predicted SST can influence the TC forecast skills of TCM2.

#### *3.2.3.2 SSTA Representations During the Two Cases*

Figure 3.4 and 3.5 compare the observed seasonal-mean (May to November) SSTA in 1997, 1998 and 2015, 2016 to those of persisted (*PSST*) and CESM-DP-LE predicted (*DPm*). The observed SST, which is referred to as *CTRL* because it is used to force TCM2 in *CTRL*, is derived from NCEP Climate Forecast System Reanalysis (CFSR) (Saha et al. 2010) for 1997 and 1998, and Climate Forecast System Version 2 (CRSv2) (Saha et al. 2014) for 2015 and 2016, respectively. The persisted SSTA, *PSST*, which is used as a baseline to measure model predictive skill of TC season SSTA, is the October monthly mean observed SSTA, which is the month before CESM-DP-LE were initialized in November 1. The predicted SSTA, *DPm*, is the 10-member ensemble-mean SSTA derived from CESM-DP-LE averaged over lead time 6 – 12

months (i.e., from May to November). As can be seen, *PSST* in the tropical Pacific regions is completely out of sign with *CTRL*, but is in better agreement with the *CTRL* in mid-latitudes, especially in 1997. Note that in 2015 the *PSST* patterns are similar to the observed (*CTRL*) in the northern hemisphere, but with weaker magnitudes. The better agreement between persisted and observed SSTAs in 2015 is due to the long lasting anomalous warming in the northeast Pacific from 2013 to 2015 (Bond et al. 2015; Zaba and Rudnick, 2016), combined with the El Niño condition in the previous (2014) year. The CESM-DP-LE captures the El Niño and La Niña related SSTAs in the equatorial Pacific and pattern correlation between the observed and predicted season mean SSTAs are 0.57 for 1997 and 0.49 for 1998. However, it is clear that CESM-DP-LE underestimates the equatorial warming in 1997, but overestimates the westward extension of the warming. In contrast, the equatorial cooling in 1998 is overestimated by CESM-DP-LE. Moreover, both the observation and CESM-DP-LE show weak warm anomalies in the Atlantic MDR region for both 1997 and 1998. Similar relation between the observed (*CTRL*) and the predicted (*DPm*) SSTA are shown in 2015 and 2016, with CEMS-DP-LE underestimating the equatorial warming during the 2015 warm event, but overestimating the cooling during the 2016 cold event, respectively (Figure 3.5). The pattern correlations between observed and predicted SSTAs are 0.56 for 2015 and 0.25 for 2016. These results suggest a systematic bias in the predicted SSTA related ENSO that can reach to an amplitude of up to ~1°C. In the following subsection, we describe a set of numerical experiments designed to assess the impact of these SST errors on tier-two forecast skill of TCs using TCM2, relative to the impact due to uncertainties in atmospheric internal variability and lateral boundary conditions.

#### *3.2.3.3 Experiment Description*

To answer the questions stated in the introduction section, we conducted several sets of numerical experiments for the two ENSO cases (1997 warm and 1998 cold event, and 2015 warm and 2016 cold events) (Table 3.1). For each event, we carried out an ensemble of 10 TC-season runs for a given SST forcing, including observed SST (*CTRL*), persisted SST (*PSST*), predicted SST (*DPm*) and climatological SST (*CSST*) (Table 3.1). Within each of these ensembles, ensemble members differ only in atmospheric initiations by altering the start dates of the simulations, while SST forcing remains the same. These experiments are designed to examine the extent to which predicted SST errors impact on TC prediction. Specifically, the *CTRL* simulations were forced with the SST, lateral boundary conditions, and the atmospheric initial conditions from the reanalysis (i.e., CFSR for 1997/1998, and CFSv2 for 2015/2016, as noted before). The *PSST, DPm*, and *CSST* experiments are the same as *CTRL*, except persisted, predicted and climatological SSTs were used for *PSST, DPm and CSST*, respectively. By comparing these three sets of downscaling experiments (forced with persisted, predicted and climatological SST) to the *CTRL* experiment, we intend to determine how errors in predicted SSTs can affect TCM forecast skills on seasonal TCs.

In addition to the above, we performed another ensemble of TCM2 forecast runs, which is similar to the *DPm* ensemble except that each member has identical atmospheric initial condition and lateral boundary condition, but its SST forcing is derived from an individual ensemble member of CESM-DP-LE. We refer this ensemble as *DPs* experiment. By comparing *DPm* (CESM-DP-LE ensemble mean SSTA) to *DPs* (CESM-DP-LE individual member SSTA) experiments, we intend to assess the relative importance of the impact from atmospheric internal variability and uncertainties in SST forcing on prediction of seasonal TC activity.

Last but not least, to quantify the influence of lateral boundary condition uncertainty on TCM2 forecast skill, we carried out an additional ensemble of runs. This ensemble, which is referred to as *BC* experiments, is similar to *DPs* except that the lateral boundary conditions of the El Niño year (1997 and 2015) are switched with the following La Niña year (1998 and 2016). Together with the *CSST* ensemble, these ensembles of runs allow us to examine the impact of uncertainties in the lateral boundary conditions on TC prediction using the tier-two TCM2 approach.

## 3.3. Results

### *3.3.1 TCM2's Potential TC Forecast Skill*

The *CTRL* ensemble, where observed SST and lateral boundary conditions are used, can be used to evaluate the potential TC forecast skill of TCM2. Figure 3.6 and 3.7 compare the observed and TCM-simulated ACE anomalies for 1997/8 and 2015/6 ENSO events, respectively, while Figure 3.8 and 3.9 compare the anomalies of observed and TCM-simulated TC numbers. Among the three TC active regions in the Northern Hemisphere, TCM2 performs the best in ENP, where signs for both ACE and TC number anomalies are correctly simulated by TCM2 for both 1997/8 and 2015/6 cases. However, the amplitude of the simulated anomalies is generally weaker than those of the observed, particularly in 1997 both ACE and TC number are significantly underestimated by the model. In the Atlantic, given the perfect SSTs, TCM2 also simulates the correct ACE and TC number anomalies during 1997 and 2015 El Niño, but gives the wrong sign anomalies of ACE and TC number during 1998 La Niña. In the WNP basin, TCM2 simulates ACE values well, but not TC numbers. Overall, with perfect SST forcing and lateral boundary conditions, TCM2 demonstrates some useful skills in hindcasting ACE and TC

number anomalies in Atlantic, ENP, and WNP, with correct signs in most of the regions for the two major ENSO TC seasons in 1997/1998 and 2015/2016. However, the amplitudes of the anomalies are generally underestimated compared to the observed values.

Besides the basin-averaged TC indexes, TCM2 also shows skill in capturing spatial pattern difference of TC track density between El Niño and La Niña (see Fu, 2018). For the two ESNO cases in this study, ensemble mean TC track density difference between El Niño and La Niño shows an eastward shift in the WNP and a westward shift in track density in the ENP to the central Pacific, particularly for the 1997/1998 event (Figure 3.10a), consistent with observation (see Figure 3.13 in Fu, 2018). These shifts in TC track density are less clear in the 2015/6 case (Figure 3.11a), possibly because the 2015 El Niño is an "uncanonical" event with large-scale anomalous warming in the northeastern Pacific persisted from 2013 to mid-2016 (Bond et al. 2015; Zaba and Rudnick, 2016). Given the possible impact from extratropics to TCs (Zhang and Wang, 2016) and the TCM2's northern boundary at 50°N where the maximum anomalies of SST (and minimum anomalies of SLP) in extratopical Pacific occurred in 2015, some of the extratropical influence on TCs may not be accurately represented by TCM2. The observation does suggest a record-high TC season (2015) in the Central Pacific (NOAA Tropical Weather Summary, 2016).

Thus, even with some biases, both multi-decadal hindcast runs (discussed in section 2.2) and the specific ENSO event runs (discussed above in this section) reasonably simulate the seasonal TC variability (quantified by ACE, TC number, and track density pattern) when forced with control SST. In other words, the new-parameterized TCM2 show high potential forecast skills in predicting seasonal TC variability when accurate SST is given.

*3.3.2 Impact of Predicted SST Errors on TC Hindcast*

SST forcing has been considered as one of the most important factors for predicting seasonal TC activity (e.g., Chen and Lin 2013; Zhao et al. 2010). By comparing results of observed (*CTRL*), persisted (*PSST*), predicted (*DPm*), and climatological SST (*CSST*) forced runs, we attempt to quantify the impact of errors in predicted SST on TCM2's skills on seasonal TC forecast.

***3.3.2.1 Model Skills with Predicted SST***

Using ACE and TC count as a metric of TC forecast skill, TCM2 generally shows higher skill in seasonal forecast when forced with the observed SSTA in *CTRL* or predicted ensemble-mean SSTA in *DPm*, comparing to the persisted SSTA in *PSST* (Figure 3.6, 3.7, 3.8, and 3.9). In particular, *PSST* experiment fails to simulate the observed ACE or TC count in the ENP, presumably because the persisted SSTAs have very different structures to the observed SSTAs during the selected ENSO events (please refer to section 2.3.2). Both anomalous ACE and TC count are in opposite sign to the observed values for most of the simulations, with the exception of 2015, when the persisted SSTA gives a reasonable representation of the observed SSTA (Figure 3.5a and b). In contrast, *DPm* experiments show good skills in predicting seasonal TC variation in the ENP during these ENSO events, with both the correct signs of ACE and TC count anomalies and similar magnitudes to those in *CTRL* and observation for most of the simulation years.

Similar results are found in the WNP: The ACE and the number of TC anomalies in *DPm* are generally closer to those in *CTRL* than in *PSST*, except that for 2016 *DPm* failed to beat *PSST*. However, this relative high score in ACE does not necessarily indicate high skills in

forecasting 2016 TC activity using the persisted SSTA. For example, the TC track density difference between 2015 and 2016 in *PSST* (Figure 3.11b) shows a pattern that is completely out of sign to the pattern in *CTRL* (Figure 3.11a) in the Pacific. One reason for the inconsistency in skills represented by the ACE and track density is related to the fact that ACE is an aggregated TC measure over a large spatial domain, which tends to remove any spatial TC variation within a TC active region. On the other hand, TC track density maps reveal spatial occurrence of TCs. It is conceivable that even for similar ACE values, TC track density distributions can be quite different.

El Niño-La Nina TC track density differences for various ensemble experiments are shown in Figure 3.10 and 3.11 for 1997/8 and 2015/6 ENSO event, respectively. It is evident that the patterns in *DPm* are more similar to those in *CTRL*, while the patterns in *PSST* tend to out of sign with those in *CTRL*, particularly in the Pacific (Figure 3.10b and Figure 3.11b). This again suggests that *DPm* is more skillful in capturing seasonal TC variability than *PSST*, indicating the potential value of using predicted SSTA in seasonal TC forecast. However, one interesting failure in *DPm* is in capturing the eastward shift of TCs in WNP (Figure 3.10c) as shown in *CTRL* (Figure 3.10a). One possible reason for this failure may be attributed to the fact that the predicted SSTA used in *DPm* underestimates the warm anomalies and the W-E SST gradient change along the equatorial Pacific, which may be critical in driving the shift of TC tracks during El Niño and La Niña events (as discussed in Chapter 2 Section 3.2). Wang and Chan (2002) also suggested that the occurrences of the W-E shift depend on the strength of ENSO events. A way to better understand this model failure in predicting TC track shift in *DPm* is through future work in analyzing GPI and large-scale atmospheric circulation changes.

#### *3.3.2.2 Insensitivity of ACE to Errors in Predicted SSTA*

Even though the predicted SSTA errors are large in *PSST* and *DPm*, no significant differences in Atlantic ACE are shown in 1997 from different experiments (Figure 3.6a). Previous studies suggest ENSO-related warm (cold) SSTA in the tropical Eastern Pacific can remotely suppress (strengthen) TC activity in Atlantic. With the weaker predicted SSTA in both the equatorial eastern Pacific and Atlantic MDR compared to observed SSTA, the simulated Atlantic ACE in *DPm* is surprisingly not that different from the value in *CTRL*. In fact, even the ACE value in the *PSST* is not significantly different from the value in CTRL for both 1997 and 2015 El Niño. All the simulated ACE anomalies, including those in *CTRL*, are significantly weaker than the observed ACE anomalies. A part of reason for the muted ACE response to SSTA may be related to the insufficient model resolutions that do not resolve TCs, giving rise to weaker ACE variation. The insensitivity of ACE to SSTA differences raises a question of whether ACE is a useful measure of model predictive skill. Another possible reason is that in 1997 and 2015, ENSO and AMM are both in their positive phase (Figure 3.4 and 3.5). Patricola et al. (2014) shows that this combination of SSTAs can cause a cancellation effect of the remote influence of El Niño and local influence of AMM on Atlantic TCs, and thus reducing dependence of TCs on SSTA. Similar arguments seem to be applicable to explain the ACE response during La Nina events in 1998 and 2016, which are interestingly much stronger in *DPm*. In contrast to the El Niño cases, the predicted cold SSTAs in equatorial Pacific are exaggerated considerably, which can contribute to a large increase in Atlantic ACE value. Additionally, in 1998 and 2016 La Niña in the Pacific concurred with positive phase AMM, the hincasted Atlantic ACE values show more significant differences among different experiments. *DPm* runs in both two years (1998 and 2016) generated larger ACE values in the Atlantic region than *CTRL*

(Figure 3.6d and 3.7d), which even agree better to the observed ACE values than *CTRL*. However, these large ACE values are likely attributed to the exaggerated cold SSTA in the equatorial Pacific and warm SSTA in the Atlantic MDR by CESM-DP-LE, both of which can contribute to overestimations of Atlantic MDR warm anomalies and ENP cold anomalies. Both of these overestimations can increase the Atlantic TC activity (Figure 3.4d and f for 1998; Figure 3.5d and f for 2016). Therefore, using ACE as sole metric to gauge seasonal TC activity may not give a complete measure of model forecast skills and quantification of the uncertainty of SST forcings.

### *3.3.3 Uncertainty from Lateral Boundary Conditions*

Uncertainties in lateral boundary conditions can also influence regional model TC forecast skills. To investigate the impact from the lateral boundary conditions, we conducted two pairs of simulations: (1) *DPs* and *BC*, and (2) *CTRL* and *CSST*, as discussed in Section 2. *DPs* and *BC* simulations were generated by using the same SST forcings and initial conditions, but different lateral boundary conditions. On the other hand, the only difference between *CTRL* and *CSST* is the SST forcing; in the latter the SST is set to the observed climatological annual cycle value without any SSTA added. With the channel configuration of the model, it is important to test whether the energy transport through the lateral boundaries of the model domain will have significant impact in the region of our interest. In other words, we would like to better understand if the uncertainties from the lateral boundaries can be neglected when TCM2 is used as a tool to forecast seasonal TC activity.

#### *3.3.3.1 ACE, TC Counts, and Track Density Anomalies*

The results (ACE, TC counts, and track density) from *BC* simulations are significantly different from *DPs*, suggesting a significant impact on simulated TC variations from the lateral boundary conditions, at least during these four years with El Niño and La Niña conditions. These differences in the simulated TC activity are most pronounce in the ENP region, especially in the 2015/2016 ENSO event, with the anomalies in track density, ACE, and TC numbers all showing opposite signs between *BC* and *DPs* simulations (Figure 3.11d and e; Figure 3.7b and e; Figure 3.9b and e). Similar differences are shown between *CSST* and *CTRL*, where again ensemble means of ENP ACE and TC numbers between the two ensembles show opposite signs in 2015/2016 (Figure 3.7b and e; Figure 3.9b and e). While the track density anomalies between 2015 and 2016 in *CSST* show no significant positive or negative sign in ENP (Figure 3.11f), it is significantly different from the *CTRL* track density anomalies, which shows overall negative anomalies in ENP (Figure 3.11a). Differences between *DPs* and *BC*, as well as *CTRL* and *CSST*, can also be seen in 1997/1998 cases (Figure 3.6b and e; Figure 3.8b and e), but the differences in the track density anomalies (Figure 3.10) are not as significant as 2015/2016.

#### *3.3.3.2 GPI Analysis of DPs and BC*

To better understand how the TC-related environments can change with different lateral boundary conditions, we performed GPI analysis (as described in Chapter 2) for *DPs* and *BC* runs, in which the TC activity shows large responses to changes in lateral boundary conditions. The significant differences between GPIs in the two ensembles (Figure 3.12) and the corresponding contributions from different terms (Figure 3.13 to 3.16) suggest that there are changes in large-scale atmospheric circulation due to differences in the boundary conditions,

especially in 1997 and 1998. Nevertheless, although the GPI differences between *DPs* and *BC* are overall more pronounce in 1997 and 1998 (Figure 3.12a and b), very large differences are shown in 2015 and 2016 in the (coastal) ENP (Figure 3.12c and d), which are consistent with the large changes in track density (Figure 3.11d and e), ACE (Figure 3.7b and e), and TC count (Figure 3.9b and e) anomalies between *DPs* and *BC* runs. We further investigate which environmental variables are driving these significant changes in TC activity.

In both 1997 and 1998, the humidity, shear, and PI term all contribute to changes from *DPs* to *BC* in mid-latitudes (Figure 3.13 and 3.14). On the contrary, the contribution from vorticity is largest in the tropics, including MDR in both Pacific and Atlantic basins. However, humidity and shear terms also contribute to changes in GPI in the tropics. Therefore, for the 1997 and 1998 case, swapping the boundary conditions between the two years generates changes in TC-related environment from mid-latitudes all the way to the tropics.

In 2015 and 2016, even with record-high warming in the northeast Pacific (Bond et al. 2015; Zaba and Rudnick, 2016) and SSTA in Niño regions comparable to that of 1997, the contributions from all the variables are relatively small (Figure 3.15 and 3.16) compared to 1997 and 1998. (Note that the colorbar range for all the term contribution plots is identical.) However, the contribution from vorticity term shows significant changes in the ENP MDR region, consistent with the large and significant changes in ACE, number of TCs, and track density differences. It is possible that the large anomalies (both in atmosphere and in SST) in northern mid-latitudes in 2015 can generate large inconsistency at the lateral boundary when switching lateral boundary conditions with 2016.

#### *3.3.3.3 Heat Transport Analysis*

Previous studies (e.g. Kang et al. 2008) show that the position of the ITCZ and the associated Hadley Cells in the tropical atmosphere can be influenced by cross-equatorial heat transport, which is a part of meridional heat transport of the atmosphere. It is possible that the meridional heat transports at the northern and southern boundary of the model are different between the El Niño and La Niña years, which can then influence the position of the ITCZ and thus cause TCs to change even though the SST forcing remains the same. To explore this possibility, we calculated the moist static energy transport using the 6-hourly data of NCEP-DOE Reanalysis 2 (NCEP2) (Kanamitsu et al. 2002). The NCEP2 dataset was utilized due to its long enough data period (1979 to 2018), which covers all four year (1997, 1998, 2015, and 2016) of our simulations. The moist static energy transport can be calculated as follows:

$$AHT = \int_0^{2\pi} d\lambda \int_{Pt}^{Ps} \frac{avHcos\psi}{g} dp,$$

where $H \equiv C_{pa} \equiv C_{pa}T + l_v q + gz$ represents the moist static energy. $C_{pa}$ and $l_v$ are specific heat capacity of dry air and latent heat of evaporation, respectively. q and z are the specific humidity and geopotential height, whereas the v in the main equation represents the meridional velocity.

The impact of lateral boundary conditions on TCs is suggested by the differences in meridional moist static energy transport between El Niño and La Niña years, especially between 2015 and 2016 (Figure 3.17). The values of the moist static energy transport in the reanalysis show a large change from 2015 to 2016 at both the southern (30°S) and northern boundaries (50°N) of TCM. However, even though 2015 was known to be the year of anomalous warming in the northern mid-latitude Pacific, the transport in 2016 shows a much larger overall value, especially in the southern hemisphere. On the other hand, the meridional moist static energy

transport values in 1997 and 1998, even though also showing some differences, are much closer comparing to 2015 and 2016. This seems to be consistent with the much larger impact of switching boundary conditions on simulated TCs in 2015 and 2016. Moreover, the standard deviation (or the value spread) of the moist static energy transport for the four simulation years (1997, 1998, 2015, and 2016) and climatology (1979 to 2017) also indicates large variability at the latitudes of the TCM boundaries, especially at the southern boundary, suggesting the southern lateral boundary of the TCM might have a stronger impact on TC simulations than the northern boundary. It suggests that cautions should be exercised when using lateral boundary conditions for simulating and predicting TCs.

A similar set of simulations testing the impact of lateral boundary conditions in TCM has been performed using climatological boundary conditions instead of those of the particular (1997, 1998, 2015, and 2016) simulation years (Fu, personal communication, 2017). The result suggests that the model climatology of ACE and TC number is changed, but the interannual variability of basin-wide TC activity is not significantly changed. Therefore, it is possible that the impact of lateral boundary conditions on the TC activity in our simulations is due to the large inconsistency between the SST forcings and the lateral boundary conditions, since the SSTA and boundary condition variability are pronounced during these El Niño and La Niña years. The fact that the impact of the lateral boundary conditions on simulated TCs is much larger in *BC* compared to *CSST*, and in 2015/16 case compared to 1997/98 case, suggests possible strong influences of lateral boundary conditions on TC simulations.

*3.3.4 Uncertainty from Atmospheric Internal Variability (Initial Conditions)*

Comparison between *DPm* (CESM-DP-LE ensemble-mean SST forcing) and *DPs* (individual ensemble member SST) simulations allows us to investigate the relative importance of the uncertainty from atmospheric internal variability and from forecasted SSTs in generating ensemble forecast of seasonal TC activity. The results suggest that in terms of ACE and TC number the effects of both uncertainties are about equal in all ocean basins (Figure 3.6, 3.7, 3.8, and 3.9). Moreover, the spatial patterns of track density difference between El Niño and La Niña years also show very high similarity between the *DPs* and *DPm* runs (Figure 3.10c and d; Figure 3.11c and d). This suggests that the overall model forecast skill of seasonal TC activity is insensitive to whether one perturbs atmospheric initial conditions or uses individual ensemble member of predicted SST from CESM-DP-LE. However, *DPs* shows generally larger ensemble spreads than *DPm*, especially during the El Niño years (1998 and 2016) when the predicted SSTA are weaker. This suggests that uncertainties in SST forecast may contribute more to uncertainties in TC forecast than atmospheric internal variability. In summary, in tier-two seasonal TC forecast, it may be more desirable to use individual ensemble member of predicted SST from a low-resolution global forecast system, as it gives a large sample of TC forecast uncertainties.

**3.4. Summary and Future Work**

While the results show some potential skill of TC prediction at lead time from 6 to 12 months using CESM-DP-LE predicted SSTA to force TCM2, this study raises more questions than answers, and further analyses are required to address these questions. For example, despite large differences between observed, persisted, and CESM-DP-LE predicted SSTAs, simulated

ACE shows remarkable insensitivity in some simulation years and regions. If these results can be confirmed by future studies that carry over a longer verification period, then it raises a question about whether aggregated TC metrics, such as ACE and TC count, are adequate measure of model predictive skill of seasonal or longer time scale TC variability.

One reason for the insensitivity may be related to the use of area average in deriving these metrics, which tend to remove any spatial TC variation within a TC active region. For example, it is well known that TCs in WNP tend to shift zonally during ENSO, while retaining their total number (Wang and Chan, 2002). A similar shift has recently been reported in the ENP by Fu et al. (2017). Therefore, a more useful measure for TC predictability should take into consideration the changes in TC spatial variation, such as TC track density that shows more sensitivity to difference in SSTA patterns. For instance, the track density response to El Niño show opposite patterns between *CTRL* and *PSST*. In addition, the eastward TC track shift during El Niño is captured by *CTRL*, but not by DP. However, horizontal resolutions of current generation climate models are insufficient to resolve or permit TCs, which makes it impractical to accurately track TCs in these models. Therefore, other metrics should be developed and used (rather than using ACE alone) when quantifying predictability of seasonal TCs. One approach is cluster analysis that divides TCs tracks into different groups, allowing spatial variations of TC tracks (e.g., Camargo et al. 2007; Camargo et al. 2008; Corporal-Lodangco et al. 2014).

Furthermore, both GPI and meridional moist static energy transport analyses indicate that mid-latitude atmospheric conditions at 50°N and 30°S may strongly influence simulated TC activity, suggesting that tropical SSTs may not be the only dominant predictor of TC activity. However, whether this conjecture is correct or not requires further numerical experiments over a

longer verification period, as the present study is based on only two ENSO events, i.e., 1997/8 and 2015/6 event, whose sample size is too small to draw any definitive conclusion.

Another notable result from this study that is worth further investigating is that uncertainties in TC forecasts is more affected by uncertainties in forecasted SST than by atmospheric internal variability. This finding suggests that in tier-two TC forecast approach, it is more desirable to using individual member of ensemble SST forecasts than using ensemble-mean SST, as the former allows a better sampling of uncertainties in SST forecast.

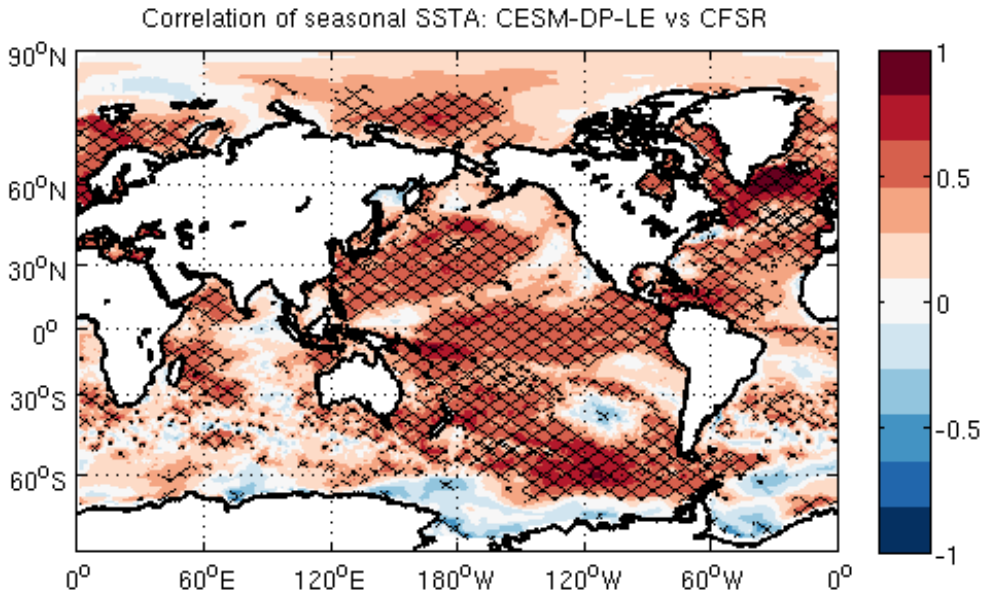


Figure 3.1. Anomaly correlation coefficient of seasonal mean (MJJASON) SST anomalies derived from CESM-DP-LE (averaged over lead time 6 to 12 months) and the observation (CFSR).

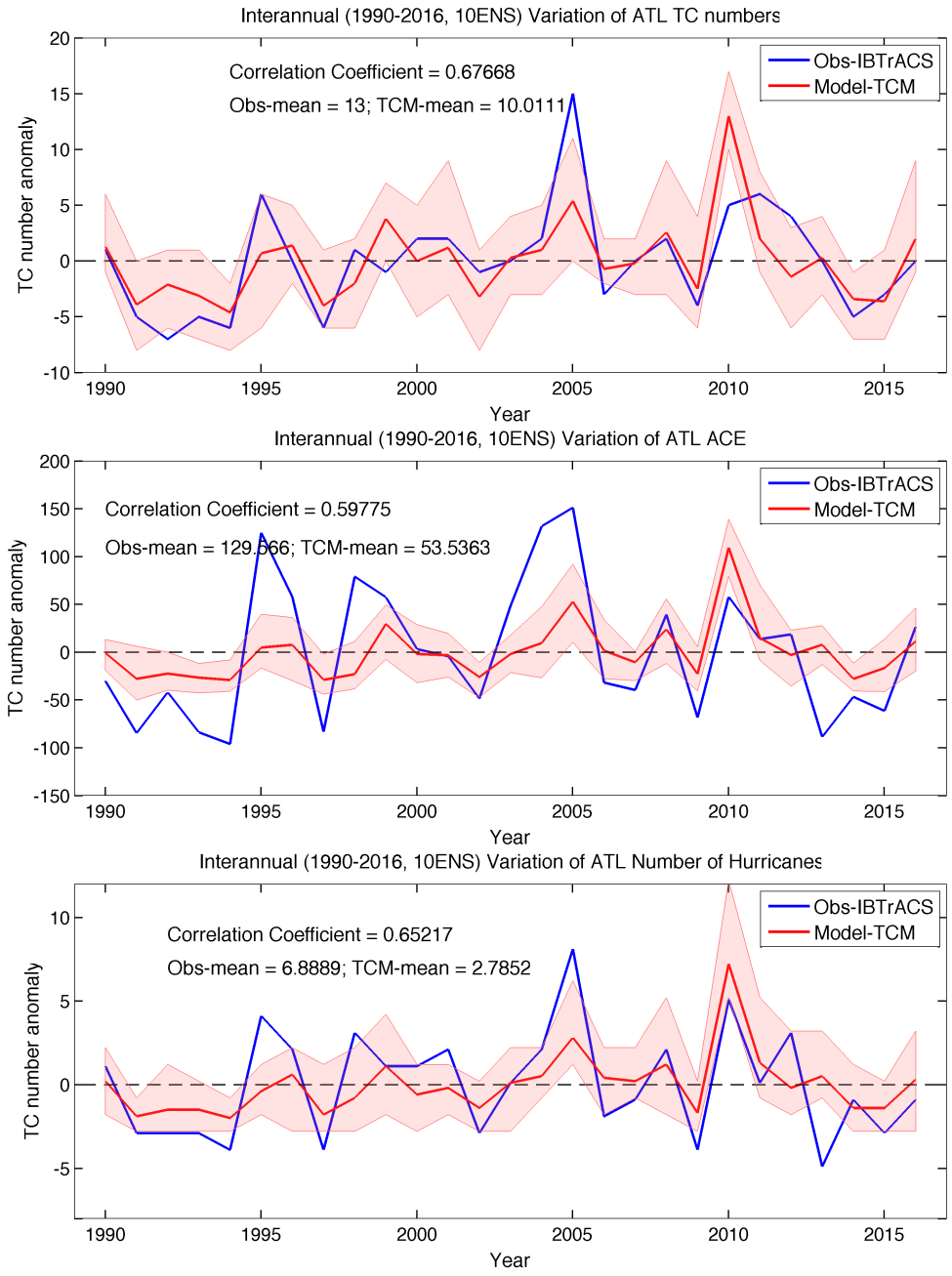


Figure 3.2. Anomalies of number of TCs, ACE, and number of hurricanes in Atlantic. Blue lines show the observational values from IBTrACS, and red lines show the ensemble-mean values from 10-member ensemble runs generated by improved TCM.

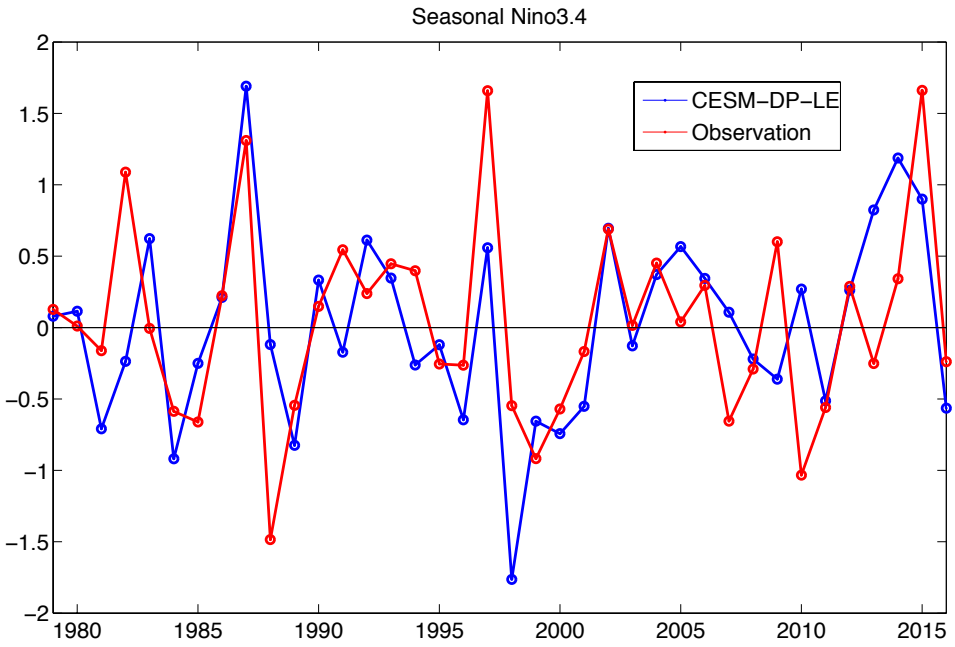


Figure 3.3. Seasonal-mean Niño3.4 region-averaged SST anomalies.

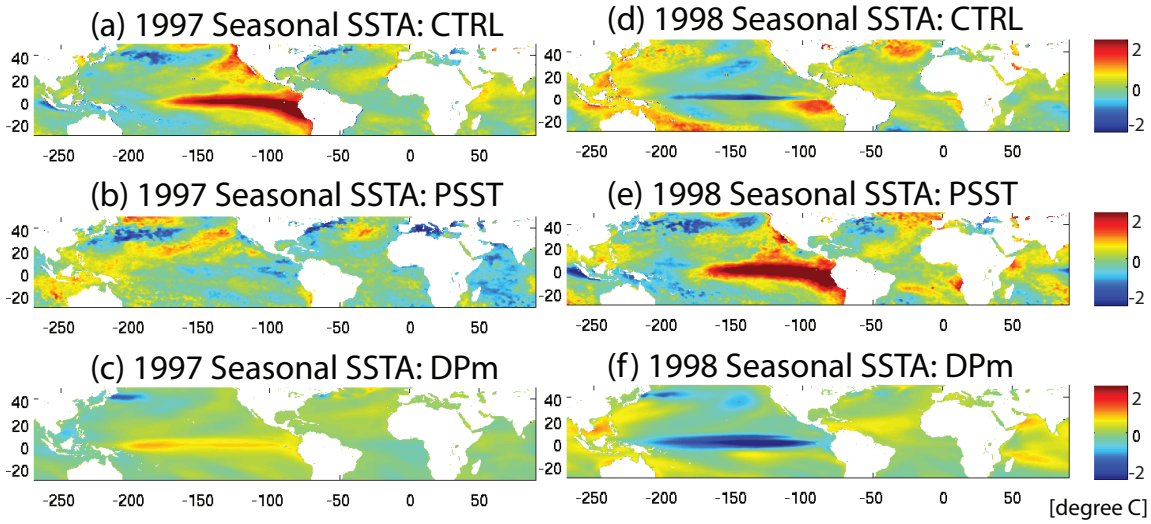


Figure 3.4. Observed (*CTRL*), Persisted (*PSST*), and CESM-DP-LE predicted (*DPm*) seasonal SSTA in 1997 and 1998.

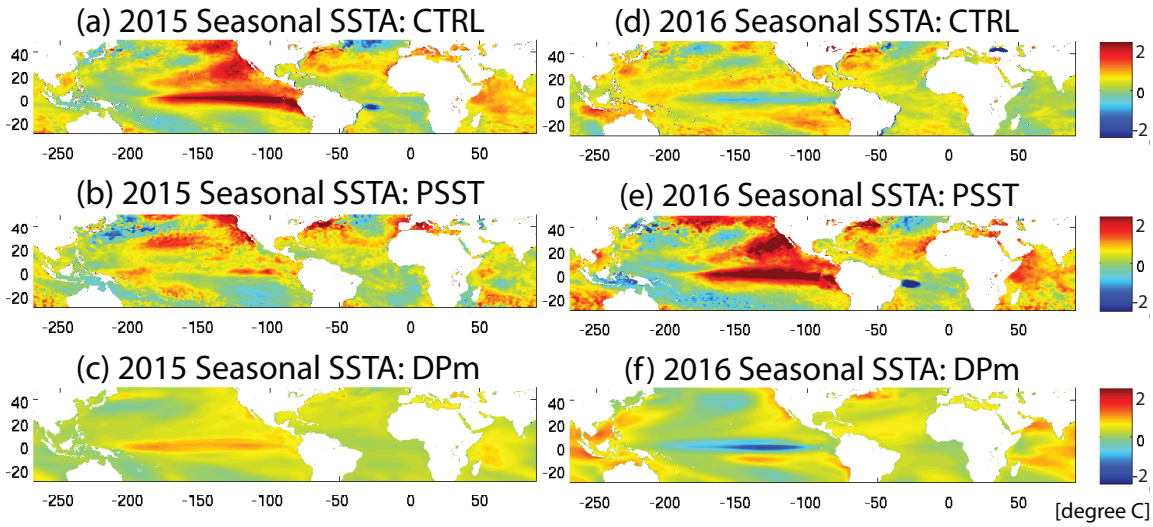


Figure 3.5. Observed (*CTRL*), Persisted (*PSST*), and CESM-DP-LE predicted (*DPm*) seasonal SSTA in 2015 and 2016.

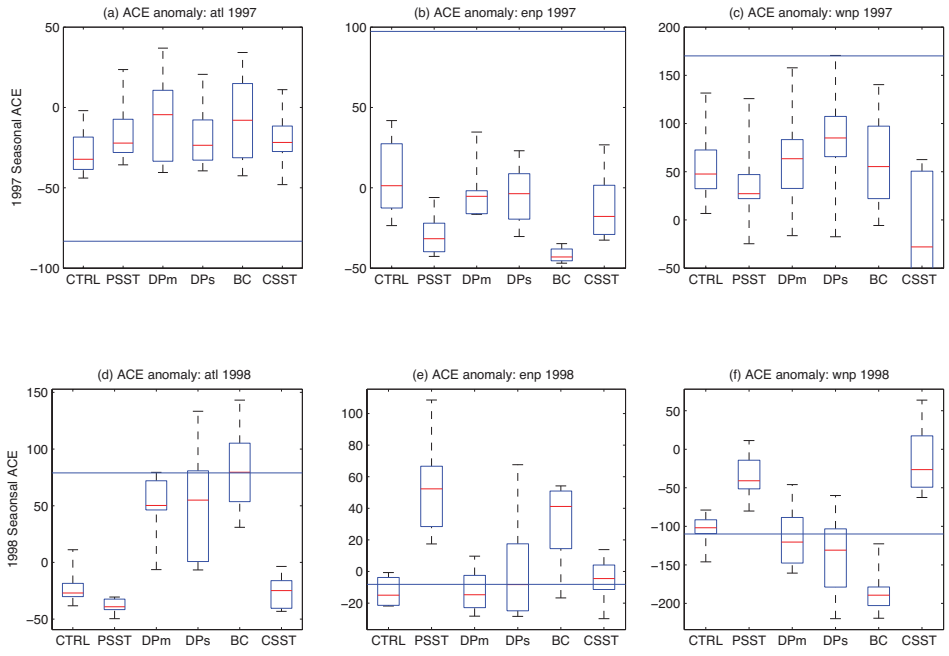


Figure 3.6. ACE anomalies in different (Atlantic, Eastern North Pacific, and Western North Pacific) ocean basins for all experiments (1997 and 1998). Horizontal lines show the observed values calculated from IBTrACS.

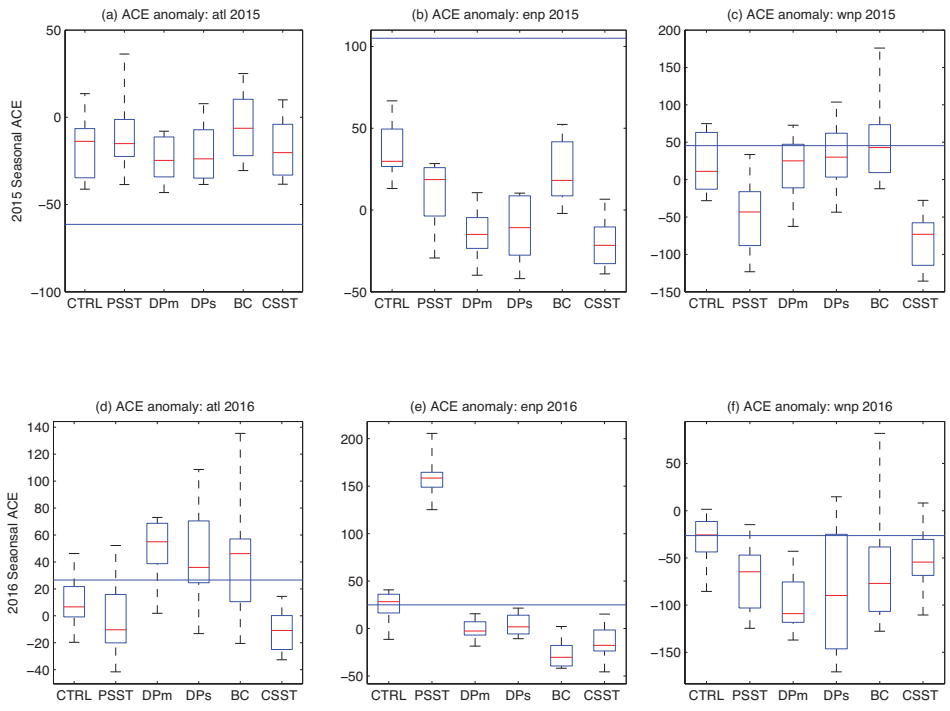


Figure 3.7. ACE anomalies in different (Atlantic, Eastern North Pacific, and Western North Pacific) ocean basins for all experiments (2015 and 2016). Horizontal lines show the observed values calculated from IBTrACS.

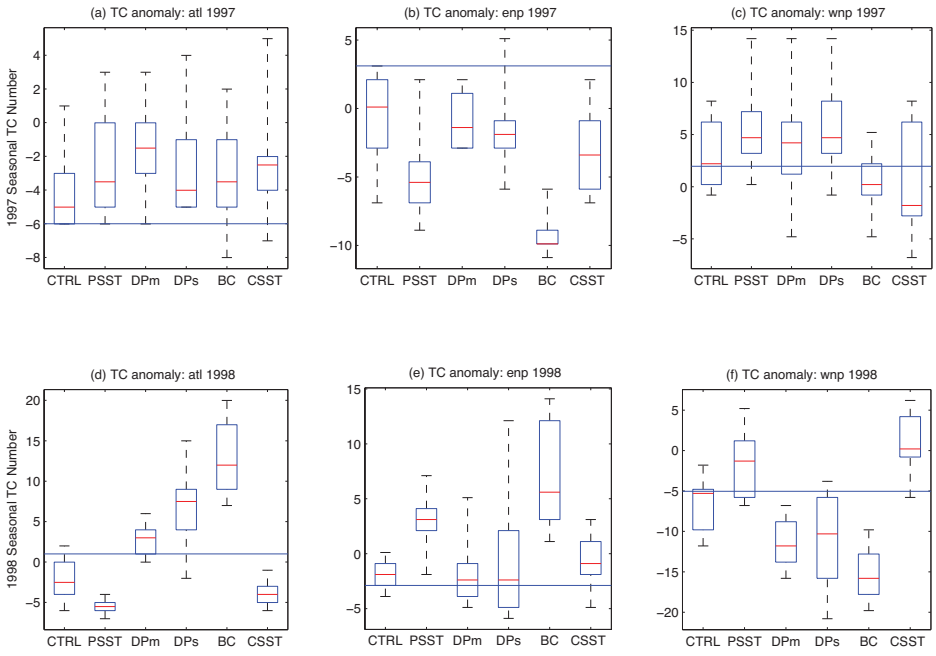


Figure 3.8. Anomalies of TC number in different (Atlantic, Eastern North Pacific, and Western North Pacific) ocean basins for all experiments (1997 and 1998). Horizontal lines show the observed values calculated from IBTrACS.

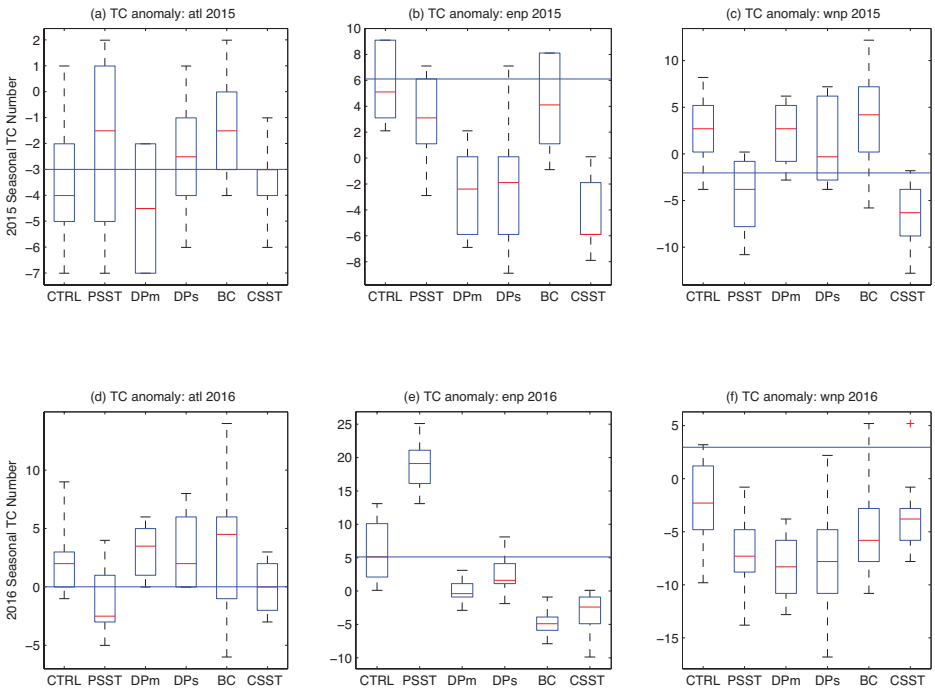


Figure 3.9. Anomalies of TC number in different (Atlantic, Eastern North Pacific, and Western North Pacific) ocean basins for all experiments (2015 and 2016). Horizontal lines show the observed values calculated from IBTrACS.

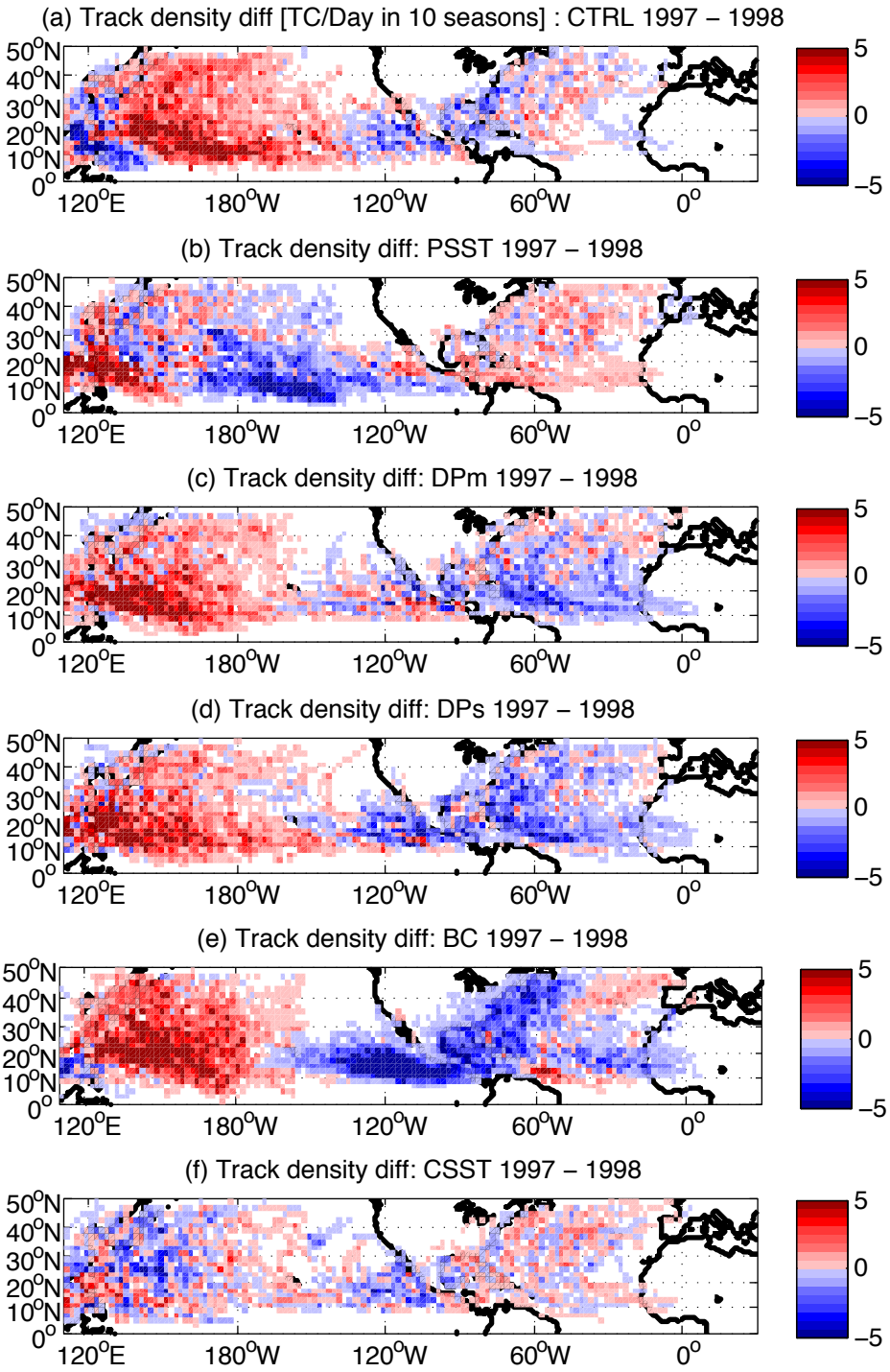


Figure 3.10. Track density differences between El Niño (1997) and La Niña (1998) years for all six (*CTRL*, *PSST*, *DPm*, *DPs*, *BC*, and *CSST*) experiments.

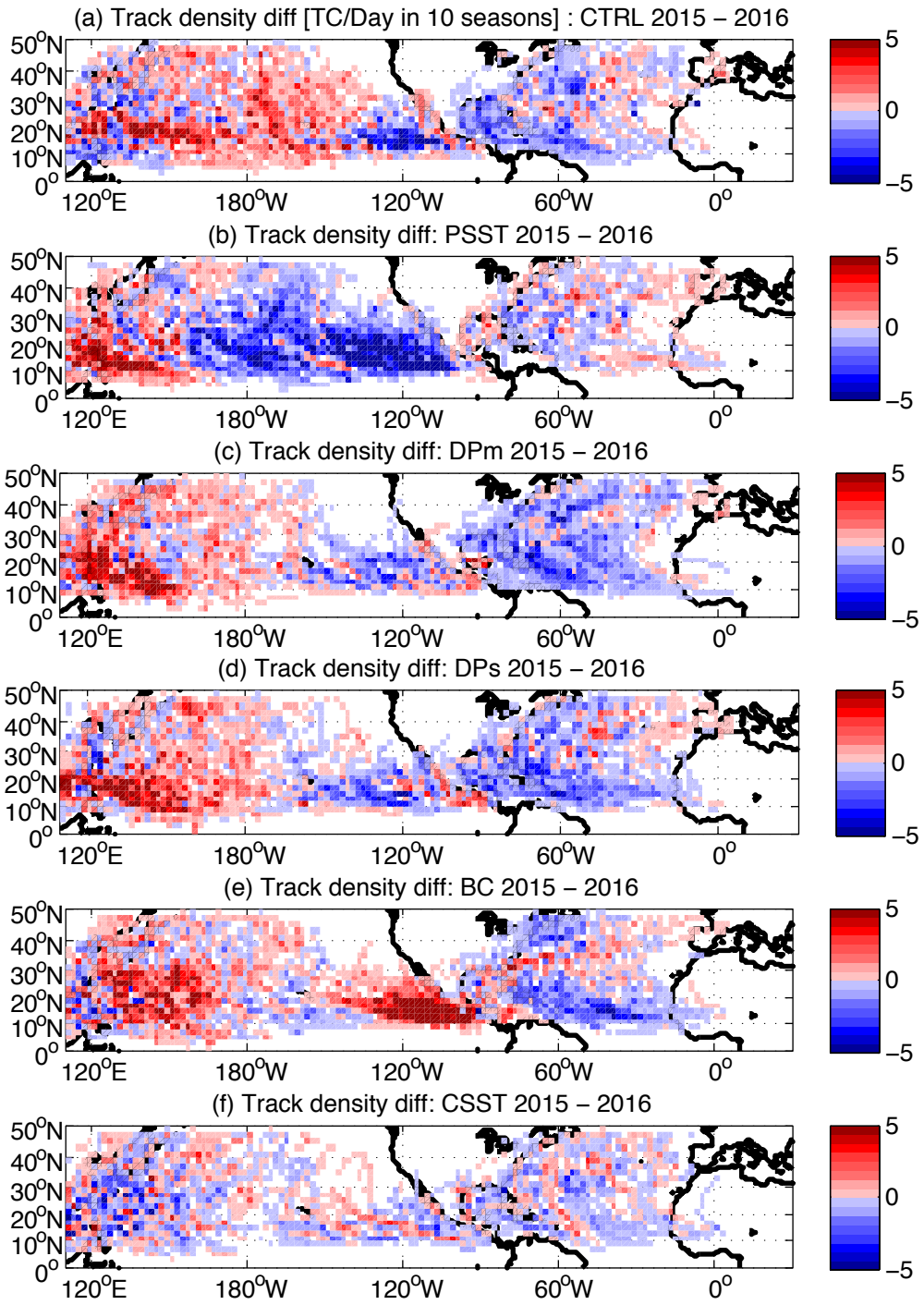


Figure 3.11. Track density differences between El Niño (2015) and La Niña (2016) years for all six (*CTRL*, *PSST*, *DPm*, *DPs*, *BC*, and *CSST*) experiments.

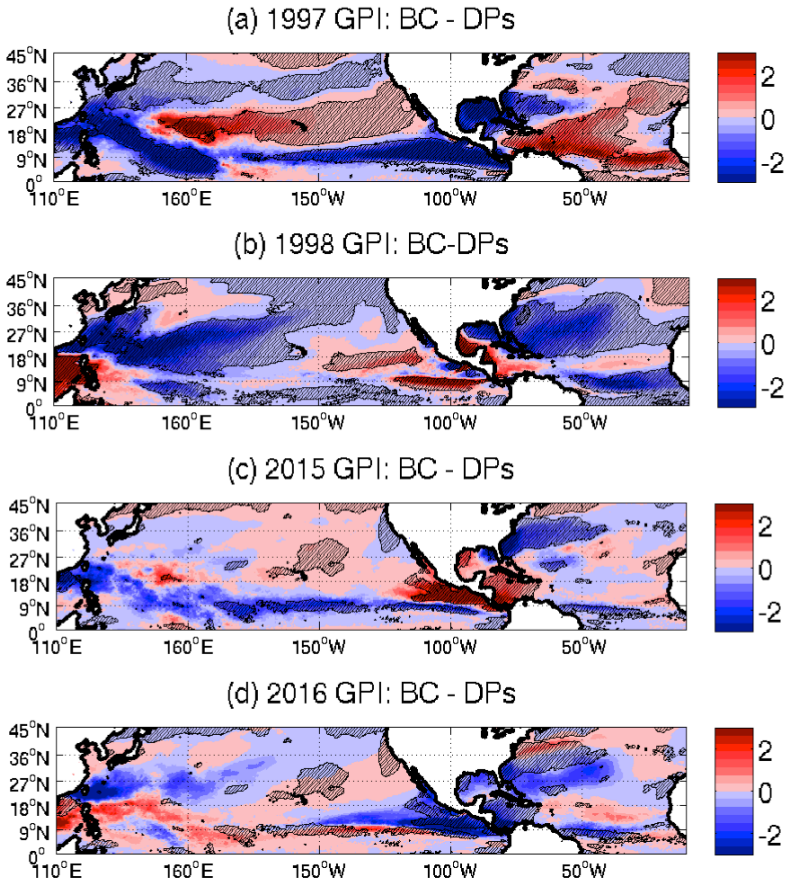


Figure 3.12. GPI differences between *BC* and *DPs* runs for the four simulation years.

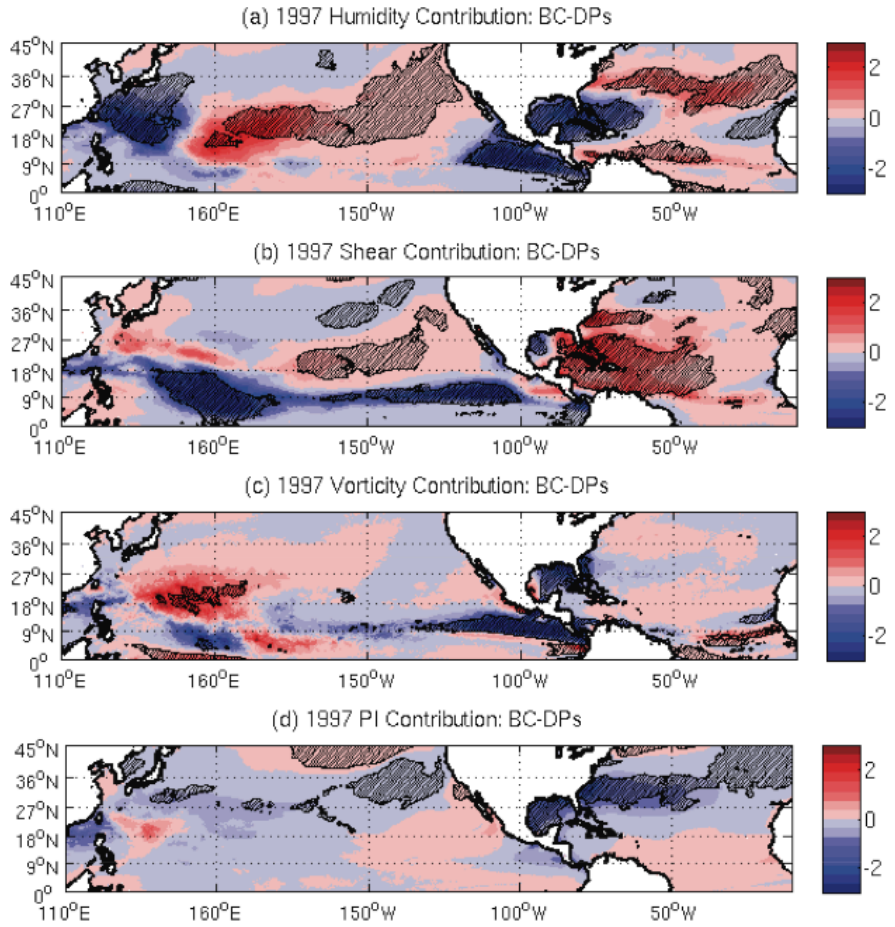


Figure 3.13. Term contributions on GPI differences (*BC* comparing to *DPs*) for 1997.

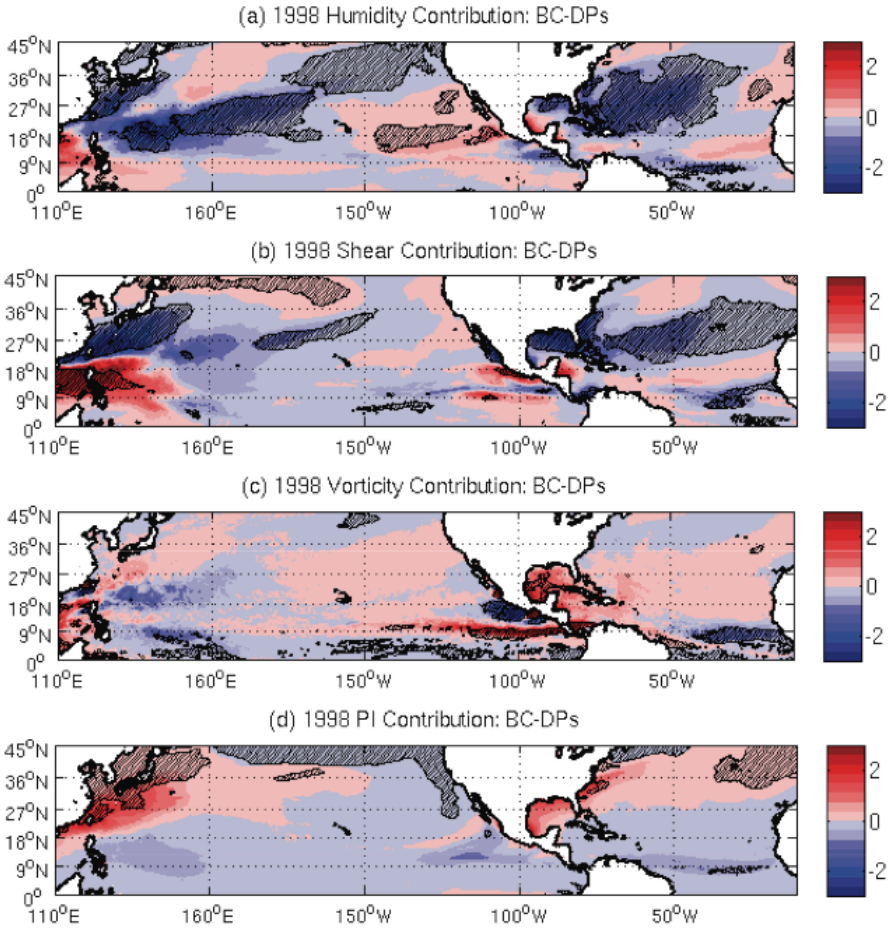


Figure 3.14. Term contributions on GPI differences (*BC* comparing to *DPs*) for 1998.

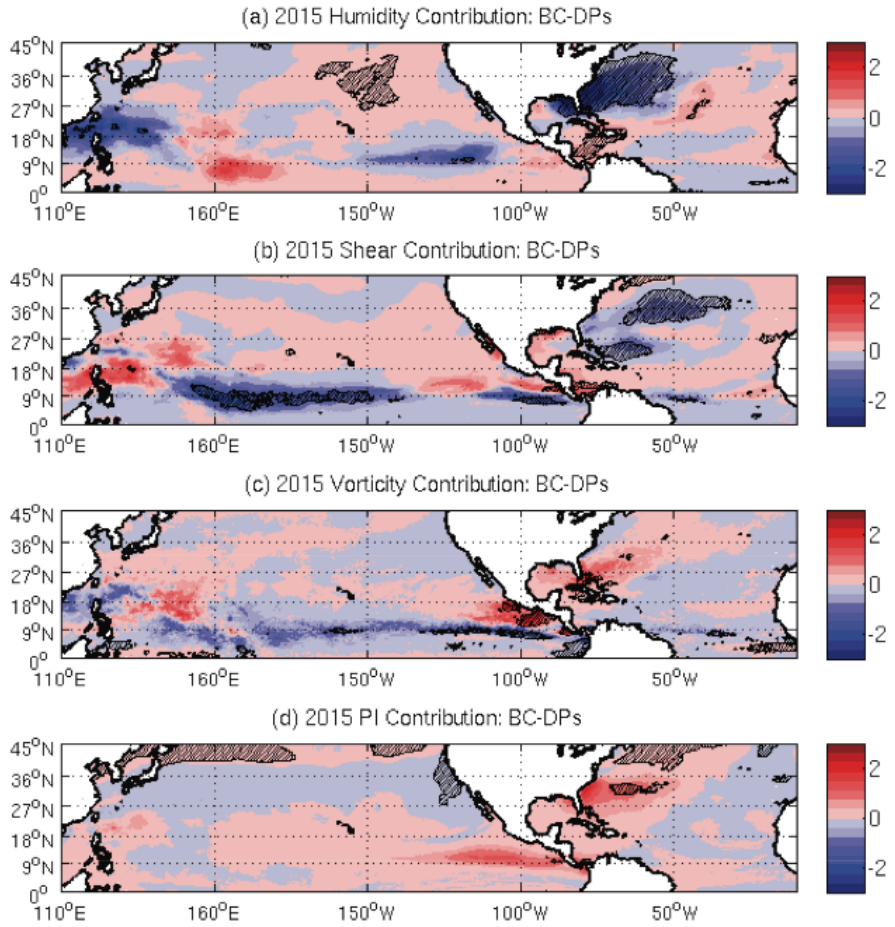


Figure 3.15. Term contributions on GPI differences (*BC* comparing to *DPs*) for 2015.

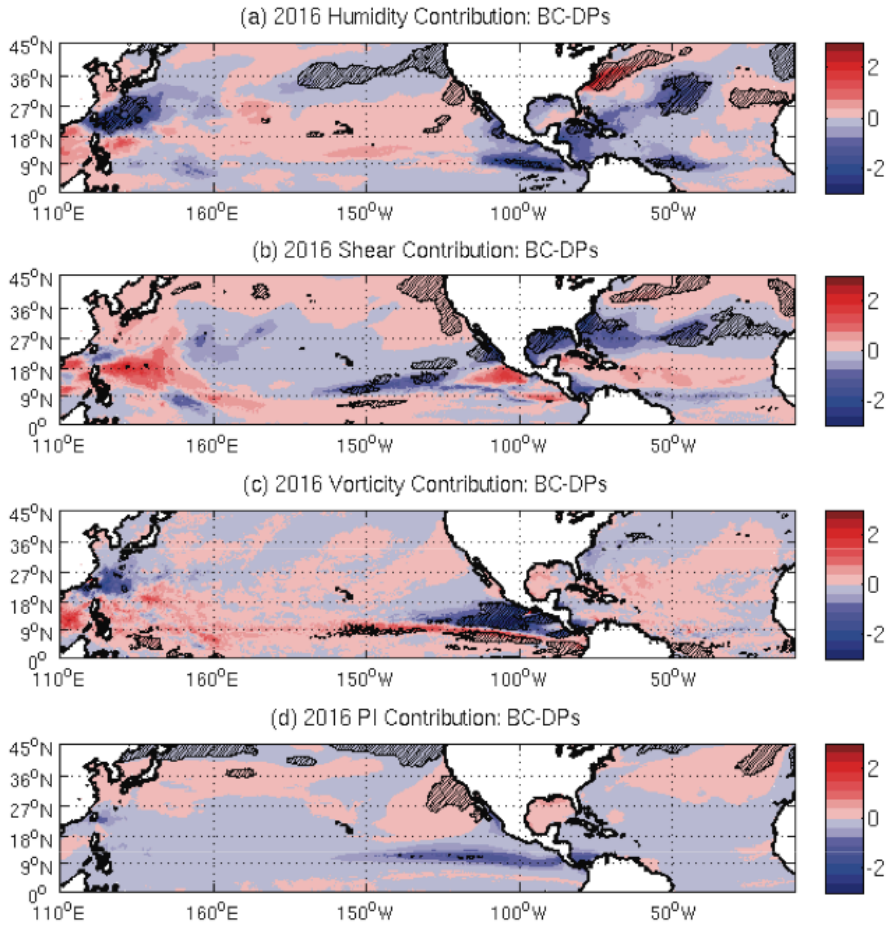


Figure 3.16. Term contributions on GPI differences (*BC* comparing to *DPs*) for 2016.

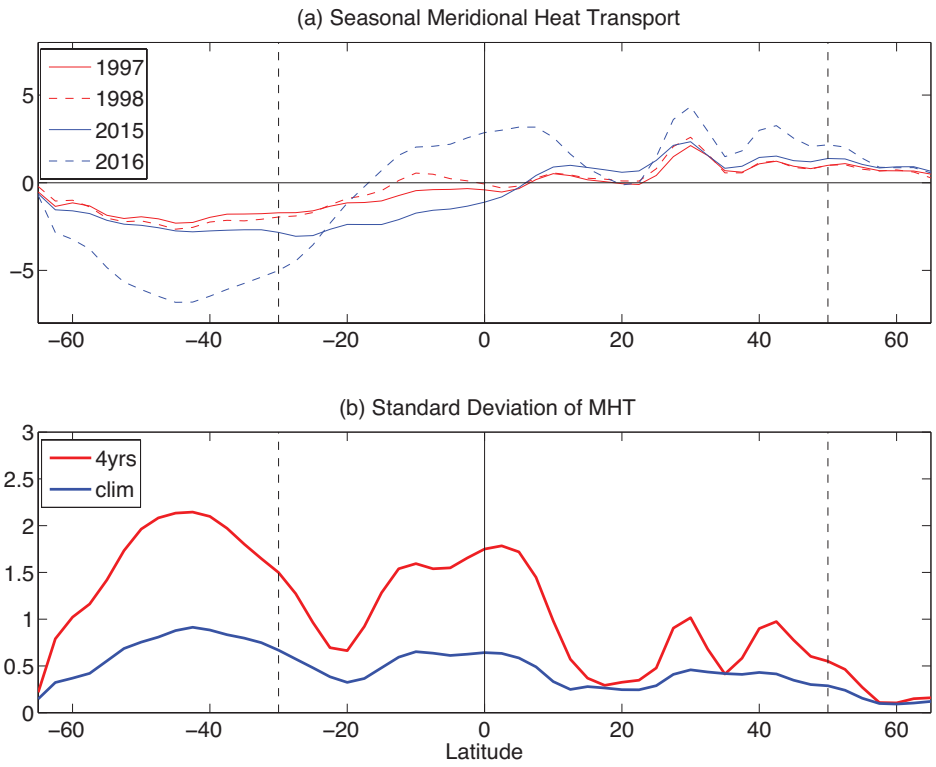


Figure 3.17. Seasonal (JJASON)-mean (a) meridional heat transport (MHT) and (b) its standard deviation calculated from NCEP2. (a) shows the MHT for four different years, and (b) shows the standard deviation of the 4 years in red, and of climatology (1979 to 2017) in blue.

| Experiment (10 members each) | SSTA forcing (all added onto observed climatology) | Lateral boundary conditions (BCs) | Atmospheric initial conditions (ICs) |
|---|---|---|---|
| ***CTRL*** | CFSR (1997/1998) & CFSv2 (2015/2016) | CFSR & CFSv2 | Different ICs |
| ***PSST*** | The Oct monthly mean SSTA from the previous year (eg., for 1997 simulations, PSST is based on Oct 1996 SSTA) | Same as *CTRL* | Same as *CTRL* |
| ***CSST*** | Climatological annual cycle from CFSR/CFSv2 (no SST anomalies) | Same as *CTRL* | Same as *CTRL* |
| ***DPm*** | CESM-DP 10-member-averaged SSTA | Same as *CTRL* | Same as *CTRL* |
| ***DPs*** | CESM-DP 10 ensemble members' SSTAs | Same as *CTRL* | Same ICs |
| ***BC*** | Same as *DPs* | Switching 1997 lateral BCs with those of 1998 (and switching 2015 with 2016) | Same as *DPs* |

Table 3.1. List of experiments and associated SST forcing, lateral boundary conditions, and initial conditions.

# CHAPTER IV

# EXPLORING LONG-TERM PREDICTABILITY OF TROPICAL CYCLONES USING CESM DECADAL PREDICTION LARGE ENSEMBLE (CESM-DP-LE)

## 4.1. Introduction and Objectives

Studies have shown that variability of North Atlantic TCs is substantial on decadal timescales (Smith et al. 2010). Since 1970s, a relationship between SST and Atlantic TC activity has been established through observations (Emanuel 2005; Emanuel et al. 2008; Webster et al. 2005). In particular, a "shift" to more active tropical cyclone period occurred in the mid-1990s (Goldenberg et al. 2001; Klotzbach 2006; Vecchi et al. 2013), coincided with a change in phase of the Atlantic multidecadal oscillation (AMO) (Goldenberg et al. 2001; Zhang and Delworth 2006). However, the dominant causes of this increased TC activity in the Atlantic still remain as an open scientific problem (Wang and Wu 2013). While some studies relate the upswing of the TC activity to a local change in the Atlantic basin (Holland 2007, Wu and Wang 2008; Wu et al. 2010), some studies attribute the change in TC to the ongoing global warming (e.g., Emanuel 2005; Webster et al. 2005), and other suggest a dominant contribution from the warm phase of AMO (e.g., Zhang and Delworth 2006; Kossin and Vimont 2007). Because of the uncertainty in our understanding of the underlying mechanism, it is still unclear whether the increase in predictability skills in environmental variability in the Atlantic on intermediate timescales (multiyear to decadal), such as AMO, can directly contribute to better predictions in Atlantic TC activity.

As mentioned above, a few studies linked the twentieth century AMO to decadal variability of Atlantic hurricane activity (Klotzbach and Gray 2008; Wang et al. 2012; Zhang and

Delworth 2006). During the warm phase of the AMO, studies suggest a northward shift in the ITCZ location, which can induce anomalous rising near the Atlantic MDR (e.g., Zhang and Delworth 2006). This change in vertical motion can further suppress the vertical shear in the region, and thus increase the TC formations in Atlantic. Moreover, the prospects of predicting decadal change in the north Atlantic surface temperature and the associated AMO variability have been demonstrated using coupled climate models. The predictability appears to be derived from the long-term ocean memory associated with the Atlantic Meridional Overturning Circulation (AMOC) (Latif 2006; Yeager and Robson 2017). Nevertheless, the model forecast of tropical Atlantic temperature variability that is arguably most important for Atlantic TC variability is shown to be less skillful on decadal time scales than that in the extratropical Atlantic. It is, therefore, of interests to further examine the prospective of predicting Atlantic TC activity on multiyear to decadal timescales, given the current climate models' skill in simulating and predicting AMO-related surface temperature fluctuations (e.g., Vecchi et al. 2013).

The NCAR CESM decadal prediction large ensemble (CEMS-DP-LE) has recently been shown to be skillful in predicting AMO-related SST on multiyear-to-decadal timescales (Yeager et al. 2018). Decadal SST forecast skills are particularly high and impressible in the North Atlantic, but relatively low in tropical Pacific SSTs. In other words, the model is capable of predicting AMO-related decadal SST variation in the North Atlantic, but is incapable of predicting the SST variability in Pacific caused by the remote influence of the AMO. Given that Atlantic TCs can be influenced by both local Atlantic SST condition and remote condition in the Pacific, it is uncertain if the skillful prediction of decadal SST variation in Northern Atlantic alone by CESM-DP-LE can be translated to useful skills in predicting decadal TC variability in the North Atlantic. Besides, the representations of TC-related environmental variables in

CESM-DP-LE have not been fully investigated, leaving a gap in our understanding of the potential value of CESM-DP-LE in decadal TC forecast in the Atlantic. Furthermore, few previous studies examine the predictability of TC activity through TC-related environment variables other than SST (e.g., Zhang and Delworth 2006; Bruyère et al. 2012). To explore potential value of using CESM-DP-LE in Atlantic TC forecast on decadal timescales, in this Chapter we analyze TC-related environmental changes on multiyear to decadal timescales using observed and CESM-DP-LE datasets. The results of this study can give a first assessment of the potential skill of the CESM-DP-LE in predicting TC environment condition variations on multiyear to decadal timescales, which can be used for decadal TC forecast in the Atlantic.

The Chapter is organized as follows: Section 2 introduces the data we utilized, as well as justifies the use of GPI (please refer to Chapter 2) to quantify the TC predictability using CESM-DP-LE. Section 3 demonstrates the representations of TC-related environment conditions through examining CESM-DP-LE-based GPI on multiyear to decadal timescales. The last section summarizes the implications and uncertainties of the results.

## 4.2. Data and Research Method

### *4.2.1 CESM-DP-LE*

The same 10 ensemble members from the CESM-DP-LE dataset (as we used in Chapter 3) is utilized, but at longer lead times from lead year (or LY) 2 to 10 and with a longer simulation period from 1964 to 2017, in order to focus on multiyear to decadal timescales. CESM-DP-LE shows high fidelities in representing SST, surface air temperature, and precipitation on multiyear to decadal timescales, as recently shown by Yeager et al. (2018). In particular, the SST prediction skill of the model is higher on seasonal-to-interannual timescales

(3-12 months) in all ocean basins. On longer (pendatal to decadal) timescales, the skill of CESM-DP-LE in predicting SST is shown to be significantly reduced in the Tropical Pacific, but is remarkably high in both the North Atlantic and WNP basins.

By comparing to uninitialized CESM-LE (Kay et al. 2015), Yeager et al (2018) is able to attribute the high SST skill of CESM-DP-LE in the north Atlantic, especially the subpolar region (Figure 2i to l in Yeager et al. 2018), to the ocean initialization. With the remarkably high skill in predicting the subpolar north Atlantic SST and relatively low but positive SST skill in both eastern subtropical and tropical Atlantic regions, Yeager et al. (2018) suggest that the CESM-DP-LE is capable of predicting AMO-like SST multi-years in advance. However, as SST condition in ENP is known to be an important factor controlling TCs in both Pacific and Atlantic basins (e.g., Tang and Neelin 2004; Gray 1984a,b) and the SST skill of CESM-DP-LE is particularly low in ENP, it is not clear how the high skill of CESM-DP-LE in the North Atlantic and other parts of Pacific can translate into useful skills in predicting TC activity on multiyear-to-decadal timescales. Therefore, in this Chapter, we will address this question by examine the skill of the model in predicting TC environment condition changes on multiyear to decadal TC predictability by comparing predicted TC Genesis Potential Index (GPI) to observed GPI.

### *4.2.2 Genesis Potential Index*

GPI has been widely used as a proxy to quantitatively infer TC activity from low-resolution climate models, in which the resolutions are not high enough to explicitly simulate TCs. GPI has been examined and utilized to quantify TC activity on different timescales from intraseasonal (Camargo et al. 2009) and seasonal (Camargo et al. 2007a; Yokoi et al. 2009) to future climate change (Vecchi and Soden 2007b) and even to paleoclimate timescales (Korty et

al. 2012ab). GPI has been shown to be a suitable proxy to explore the impact of large-scale environmental changes on TCs in climate models, especially in the Atlantic region (e.g., Bruyère et al. 2012; Camargo 2013; Patricola et al. 2014). The advantages of using GPI to quantify TC activity on longer (than interannual) timescales are: (1) No specific threshold is used when calculating GPI (comparing to the studies that were based on certain thresholds for TC formation such as Gray 1979, and statistical models that were tuned under a given climate), therefore can be used under various climate conditions; (2) GPI has been examined by many previous studies under various climate conditions, and shown to represent TC activity well (e.g. Vecchi and Soden 2007b). In this Chapter, we adopt this approach and examine the TC environmental favorability by computing and comparing GPIs and the related terms using reanalysis and CESM-DP-LE datasets. A total of 4860 TC seasons (54 simulation years by 10 ensemble member by 9 lead years) GPI (Emanuel and Nolan, 2004) was calculated based on CESM-DP-LE. The CESM-DP-LE variables used in GPI calculation are monthly mean of absolute vorticity at 850 hPa (from u and v), relative humidity at 600 hPa, potential intensity (from SST, sea-level pressure, and atmospheric temperature and specific humidity profiles), and vertical wind shear between 850 and 200 hPa (from u and v).

The monthly NCEP reanalysis dataset (Kalnay et al. 1996) was used to compute the "observed" GPI due to its long record length (from 1948 to now). The observed GPI is then used to validate the predicted GPI. Additionally, since only anomaly fields were obtained from CESM-DP-LE (after removing model drift), the climatology fields derived from NCEP were used to generate full field variables by adding the two together, which were used to compute the predicted GPI from CESM-DP-LE. The representation of NCEP-based GPI terms has been quantified by previous studies (Camargo 2013; Bruyère et al. 2012). In particular, Bruyère et al.

(2012) show a high correlation between 5-year running mean of Atlantic TC counts and NCEP-based potential intensity and shear in an extended MDR region during the TC season (ASO) for the period of 1960 to 2009. However, almost no correlation is shown between the NCEP-based GPI variability in Gulf of Mexico and the Atlantic TC counts, even though the Gulf of Mexico produces about 20% of the Atlantic TCs, and has the highest GPI values in the Northern Atlantic. To better capture the relationship between GPI (and the associated terms) and the basin-wide TC activity in the Atlantic, we consider only the conventional MDR (e.g., Gray 1984a,b; Elsner et al. 2006; Klotzbach 2011) and exclude the Gulf of Mexico region when compute area-averaged values.

## 4.3. Results

### *4.3.1 Evaluating Skills of CESM-DP-LE in Predicting Decadal Changes of TC Environment Condition*

To evaluate the skill of CESM-DP-LE in predicting TC environment condition changes on multiyear-to-decadal timescales, we focus on the peak TC months from August to October and consider this period as the season of interest (Bruyère et al. 2012; Camargo 2013). The area of interest is the North Tropical Atlantic from 0 to 30°N, as CESM-DP-LE shows considerable skill in the North Atlantic. We also evaluated the CESM-DP-LE skills in the Pacific basin and found low scores, especially in the WNP. Therefore, in this Chapter, we focus on evaluating GPI-based forecast skills in Atlantic using predicted anomalies from CESM-DP-LE on multiyear to decadal time scales. Because the focus is on decadal prediction, a 5-year running mean was applied to most of our analyses.

#### *4.3.1.1 GPI from CESM-DP-LE*

Figure 4.1 show the spatial patters of anomaly correlation coefficients between NCEP- and CESM-DP-LE-based GPI, after applying a 5-year-running-means to both time series at each grid point in the Atlantic region. Positive correlation is clearly observed in the Atlantic MDR (yellow-squared region) for all lead years. Figure 4.2 shows similar anomaly correlation maps to those of Figure 4.1, except that 5-year running mean was not applied to the GPI time series, and thus the anomaly correlation also includes the interannual variability. A comparison between Figure 4.1 and 4.2 shows clearly that CESM-DP-LE is more skillful in predicting multiyear-to-decadal observed GPI variability than interannual variability, although even without the 5-year running mean, there are significant anomaly correlations between observed and predicted GPI within the Atlantic MDR region at all lead years. It suggests that CESM-DP-LE is quite skillful in predicting GPI variability on internal-to-decadal timescales.

Consistent with the SST forecast skill shown in Yeager et al. (2018), the CESM-DP-LE predictive skill on GPI does not significantly decrease with lead years longer than interannual timescale (i.e., longer than lead year 1). In other words, GPI correlation skills calculated at shorter lead years do not outperform those calculated from longer lead years in CESM-DP-LE, at least for lead year 2 to 10. Moreover, no robust correlation skills are found in the Gulf of Mexico, even after applying the 5-year running mean filter to the GPI time series (Figure 4.1). This indicates that CESM-DP-LE forecast skill of GPI is limited to the Atlantic MDR. As such, we exclude the Gulf region when computing Atlantic area-mean GPI time series in the following analyses.

#### *4.3.1.2 Diagnosing GPI Terms*

As descripted in previous chapters and the methodology section, GPI consists of four terms: vorticity, humidity, potential intensity, and shear terms. To further investigate the representation of each term (associated with different TC-related variables) in CESM-DP-LE, correlation coefficients were also calculated for the four terms from NCEP and CESM-DP-LE (Figure 4.3 to 4.10).

Figure 4.3 and 4.4 shows the correlations of the vorticity terms variability in CESM-DP-LE and NCEP, with and without 5-year running mean, respectively. In most part of the Atlantic MDR, the anomaly correlation of vorticity term variability between CESM-DP-LE and NCEP has positive values. The Atlantic MDR is just north of the Atlantic ITCZ where anticyclonic vorticity dominates because of the trade winds converging into the ITCZ from the North tend to rotate clockwise. When the ITCZ shifts north-south in response to AMO-like SST variation, it will generate vorticity anomalies in the Atlantic MDR, which in turn contribute to GPI variability. The results shown in Figure 4.3 and 4.4 suggest that CESM-DP-LE is capable of predicting low-level vorticity (850 hPa) changes in the Atlantic MDR at lead time of 2 – 10 years. Similar arguments apply to the positive anomaly correlation of vertical wind shear in the region (Figure 4.9 and 10). The low-level convergent flow and upper-level divergent flow in the vicinity of the ITCZ create a strong vertical wind shear regime. As the ITCZ shifts north-south in response to AMO-like SST variation, the vertical wind shear regime also shifts. The fact that the anomaly correlation of wind shear term is mostly positive over the Atlantic MDR suggests that CESM-DP-LE is skillful in predicting vertical wind shear variability in the Atlantic MDR at lead time of 2 – 10 years. Therefore, we argue that a significant portion of the skillful forecast of GPI by CESM-DP-LE in the Atlantic MDR may come from the ability of CESM-DP-LE to

forecast north-south shift of the ITCZ on multiyear-to-decadal time scales, which affects both the vorticity and vertical wind shear in the Atlantic MDR.

The other significant contribution to the skillful forecast of GPI by CESM-DP-LE comes from potential intensity (maxPI) variability, which is primarily linked to the local SST variability. Figure 4.7 and 4.8 show very high positive anomaly correlation values of maxPI variability with and without the 5-year running mean. This finding is consistent with the results of highly skillful decadal SST forecast in the North Atlantic shown by Yeager et al (2018). Therefore, CESM-DP-LE shows skills in predicting environmental vorticity, vertical wind shear and maxPI changes in the Atlantic MDR at lead time of 2 – 10 years, all of which contribute positively to the skillful forecast of GPI.

In contrast, CESM-DP-LE failed to predict humidity-induced GPI variability in the Atlantic MDR. Figure 4.5 and 4.6 show predominantly negative anomaly correlation coefficients in much of the MDR with and without the 5-year running mean. It indicates that CESM-DP-LE is not capable of predicting mid-level (600 hPa) humidity in the Atlantic MDR on multiyear-to-decadal time scales. This negative skill of predicting humidity-induced GPI contributes negatively to the GPI skill score. However, it should be noted that previous studies indicated a relatively weak relationship between TC activity and humidity derived from NCEP in the Atlantic (e.g., Bruyère et al. 2012). Therefore, the poor skill of CESM-DP-LE in predicting mid-level humidity may not have a strong influence on the overall GPI forecast skill of CESM-DP-LE. As previous studies shown, the maxPI and wind shear are the two most important factors in determining TC activity in the Atlantic region (e.g., Bruyère et al. 2012; Camargo 2013; Vecchi et al. 2013). The skillful forecast of these two terms in GPI by CESM-DP-LE

indicates potential high skills of CESM-DP-LE in predicting basin-wide TC activity in the Atlantic, at least during the simulation period of 1964 to 2017.

### *4.3.2 MDR GPI and TC Time Series Analysis*

#### ***4.3.2.1 MDR GPI Time Series***

In this study we define the main development region (MDR) of TCs in the Atlantic to be from 10° to 20°N and from 60°W to 15°W, and use the ASO as TC season average to derive an MDR GPI time series, as Bruyère et al. (2012) show that such a GPI time series explain a large portion of the variance of annual TC frequency in the Atlantic. In the following, we will use this GPI time series to further examine CESM-DP-LE's skill on predicting Atlantic TC activity during the period of 1964 to 2017. To focus on multiyear-to-decadal time scales, 5-year running mean smoothing was applied to all the time series (as in Vecchi et al. 2013), and all the time series (including GPI and associated terms, as well as observed annual TC frequencies) were normalized by maximum values.

Figure 4.11a compares the observed annual TC frequency to the NCEP-based and CESM-DP-LE-predicted MDR GPI time series. Note that for each given year, there are 10 ensemble members of CESM-DP-LE and 9 forecasts at different lead year 2 to 10, which give rise to a total of 90 forecasted GPI values. The predicted MDR GPI shown in Figure 4.11a is the average of the 90 values, which includes 10-member mean and 9 lead year average. Figure 4.11b shows the ensemble mean of predicted MDR GPI values averaged over different lead year groups. There is clearly a close relationship between the annual TC frequency and the MDR GPI: correlation coefficients between TC frequency and NCEP-based MDR GPI and between TC frequency and CESM-DP-LE-predicted MDR GPI are 0.38 and 0.87 (all above 99%

significant level), respectively. Note that the correlation between the observed TC frequency and CESM-DP-LE-predicted MDR GPI has even higher value than that between observed TC frequency and NCEP-based MDR GPI. Moreover, the correlation between NCEP-based and CESM-DP-LE-predicted MDR GPI is at 0.51. Of particular interest is the decadal shift in the mid-1990s when the Atlantic TC frequency experienced a sharp increase. The NCEP-based MDR GPI well captures this sharp increase, albeit with about 1 year of delay. CESM-DP-LE predicted GPI also shows a sharp increase in the mid-1990s, agreeing with the observed decadal shift in the Atlantic TC frequency, but the phase delay is further increased compared to NCEP. However, both the NCEP-based and CESM-DP-LE-predicted GPIs fail to capture the peak in early 2000s, and CESM-DP-LE also fails to predict the decrease in TC activity after 2010. In addition, both GPIs fail to track the Atlantic TC activity before 1970s.

When separating CESM-DP-LE predicted GPI by different lead year groups, no significant change is observed in terms of the overall correlation values between the GPI and TC frequency (Figure 4.11b) and the correlation coefficients change from 0.85, 0.84, to 0.85 from lead year group 2-6, 4-8, to 6-10. However, there is a clear improvement in predicting the phase of the decadal shift when using the GPI at shorter lead year group (2-6). Interestingly, this improvement does not behave linearly as there is no improvement in phase prediction when comparing the predicted GPIs at lead year group 4-8 and 6-10.

#### *4.3.2.2 Decomposition of GPI*

As in section 3.1.2, we investigated the GPI-related predictability from four different large-scale environmental variables: vorticity, vertical wind shear, maxPI, and humidity, and the results are shown in Figure 4.12. Consistent with previous studies (e.g., Zhang and Delworth

2006; Bruyère et al. 2012), the shear- and maxPI-term variability derived from NCEP represent very well the variability of Atlantic TC frequency, with correlation coefficients (with TC number) of 0.86 and 0.91 for shear and potential intensity, respectively (Figure 4.12a and d). The CESM-DP-LE-predicted wind shear and potential intensity terms also well predict the variability of TCs, with correlation coefficients (with observed TC number) of 0.90 and 0.84 (Figure 4.12a and d). The large-scale vorticity variability also shows a good relationship with the observed TC frequency, with a correlation coefficient of 0.83 for CESM-DP-LE.

However, the relationship between mid-level humidity and the observed TC frequency is quite different between CESM-DP-LE and NCEP. While the humidity variability from NCEP has almost no correlation with the observed TC frequency, consistent with previous studies, such as Bruyère et al. 2012, the CESM-DP-LE-predicted humidity variability shows a remarkably good relationship with the TC frequency and the correlation between the two is 0.85. Therefore, there is a large discrepancy between NCEP reanalyzed and CESM-DP-LE predicted mid-level humidity variability on multiyear-to-decadal time scales. This discrepancy is likely a key contributor to the higher correlation between the observed TC frequency and CESM-DP-LE-predicted MDR GPI (0.87) than between observed TC frequency and NCEP-based MDR GPI (0.38).

It is worth noting that although all four contributing environment variables to GPI derived from CESM-DP-LE show high correlations with the observed TC frequency, none of them can reproduce the peak in TC frequency during middle 2000s. One possible reason for this discrepancy is that the TC frequency peak in middle 2000s is a part of atmospheric internal variability, which cannot be predicted by CESM-DP-LE. Nevertheless, the fact that all four contributing environment variables to GPI in CESM-DP-LE show high correlations with

multiyear-to-decadal changes in Atlantic TC frequency offers a potential capability for developing a decadal Atlantic TC prediction through either statistical or dynamical downscaling of CESM-DP-LE.

### 4.4. Summary and Discussion

The results of this study suggest potential skill of CESM-DP-LE in predicting TC-related environmental changes on multiyear-to-decadal timescales for lead year 2 to 10 in the Atlantic MDR. In particular, CESM-DP-LE shows high fidelity in predicting the decadal shift in the mid 1990s that marked a sharp increase in Atlantic TC activity. While previous studies have demonstrated useful skill in predicting Atlantic TC activity on different timescales using SST and vertical wind shear variability, our results suggest that all four contributing environmental variables (potential intensity, shear, humidity, and vorticity) to GPI are highly correlated with the observed TC frequency from 1964 to 2017, and thus can all contribute positively to CESM-DP-LE TC prediction at multiyear-to-decadal time scales. Of particular interest is the finding that CESM-DP-LE predicted mid-level humidity changes shows a high correlation with the TC frequency on multiyear-to-decadal time scales, which is in sharp contrast to NCEP-based mid-level humidity that shows no correlation with the TC frequency. The latter is consistent with Bruyère et al. (2012) who show that NCEP-based mid-level humidity has no skill in representing Atlantic TC frequency variability during the period from 1960s to 2000s. This discrepancy between NCEP and CESM-DP-LE may be blamed for the higher correlation between CESM-DP-LE predicted humidity and the observed TC frequency than between NCEP-based humidity and TC frequency.

The high skill of CESM-DP-LE in predicting TC environmental condition changes on multiyear-to-decadal time scales appears mainly related to its high fidelity in predicting low-frequency SST variability in the North Atlantic. Figure 4.13 shows a linear regression of pentadal global SST anomalies onto the pentadal Atlantic MDR GPI time series during the period of 1964 to 2017 using NCEP reanalysis (Figure 4.13a) and CESM-DP-LE data (Figure 4.13b), respectively. While the NCEP regression map shows an AMO-like SST pattern in the Atlantic and a PDO-like pattern in the Pacific, the CESM-DP-LE regression map show a warming pattern everywhere in the global ocean with highest amplitude in the North Atlantic. The only area that the two patterns shares in common is the North Atlantic and Northwestern Pacific. In the tropical Pacific, the two patterns have opposite sign. Therefore, it appears that the agreement between NCEP and CESM-DP-LE is largely attributed to the skillful forecast of AMO-like SST variability in the North Atlantic by CESM-DP-LE. The tropical Pacific SST plays a secondary role in influencing TC variability on multiyear-to-decadal time scales.

There are current debates on whether the AMO-like SST in the North Atlantic is an internal variability of the coupled ocean-atmosphere system or an externally forced response. CESM-DP-LE includes both of these components. To separate these two factors, one can compare CESM-DP-LE to a large ensemble of uninitialized CESM runs, as shown Yeager et al. (2018). As a future work, we plan to carry out similar analysis on the uninitialized CESM large-ensemble (CESM-LE, Kay et al. 2015) and compare the results to those shown in this study. Such a comparison can shed light on whether ocean memory plays a critical role for the skillful forecast of the Atlantic TC environmental condition changes on multiyear-to-decadal time scales by CESM-DP-LE.

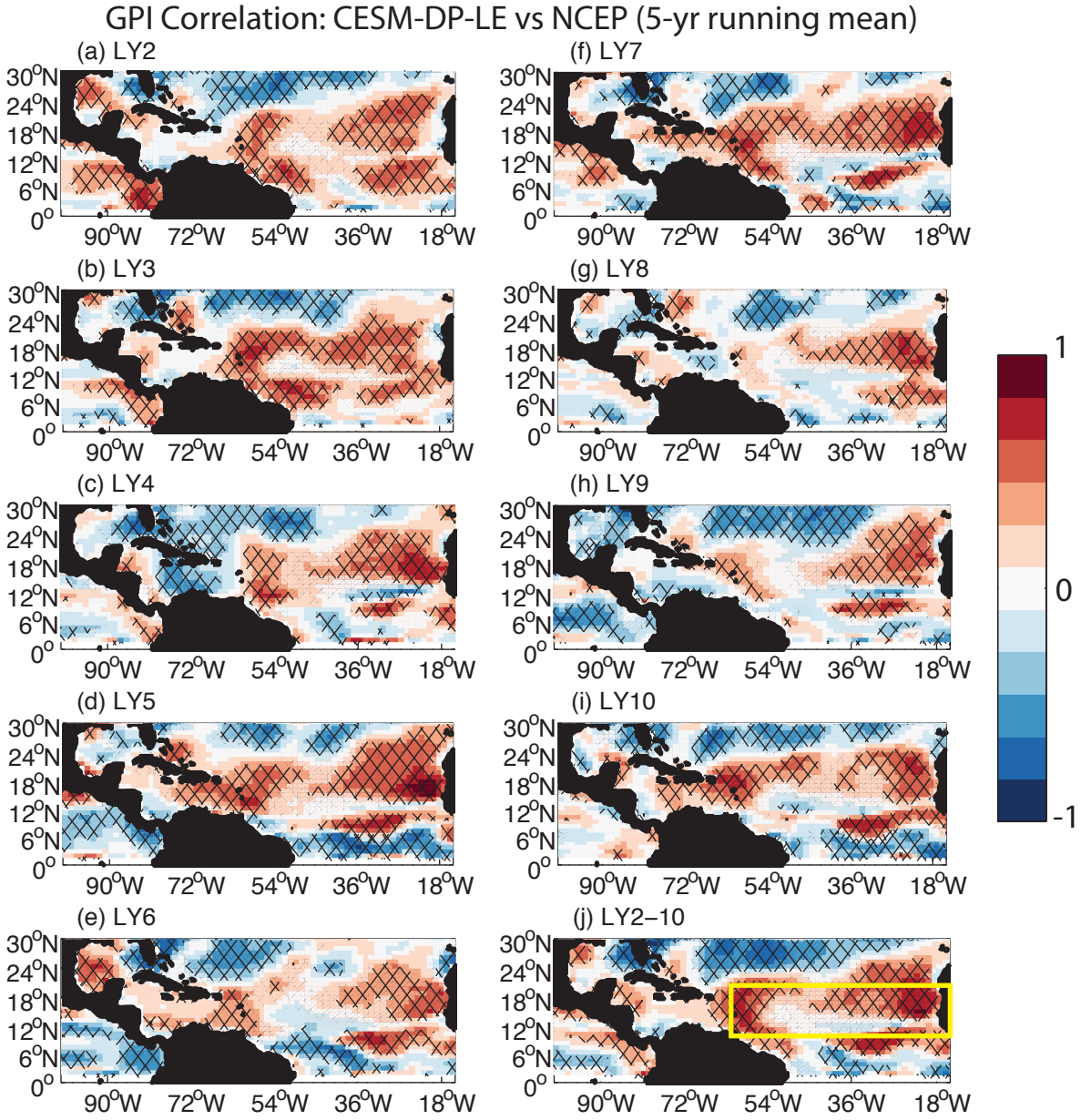


Figure 4.1. Correlation coefficients of 5-year running mean GPI calculated from CESM-DP-LE and NCEP. Each figure showing results for different lead years from CESM-DP-LE, while (j) demonstrating the results of lead year 2 to 10 mean. The yellow box in (j) shows the region of conventional Atlantic MDR. All the regions with values passed the 95% student t-test are hatched.

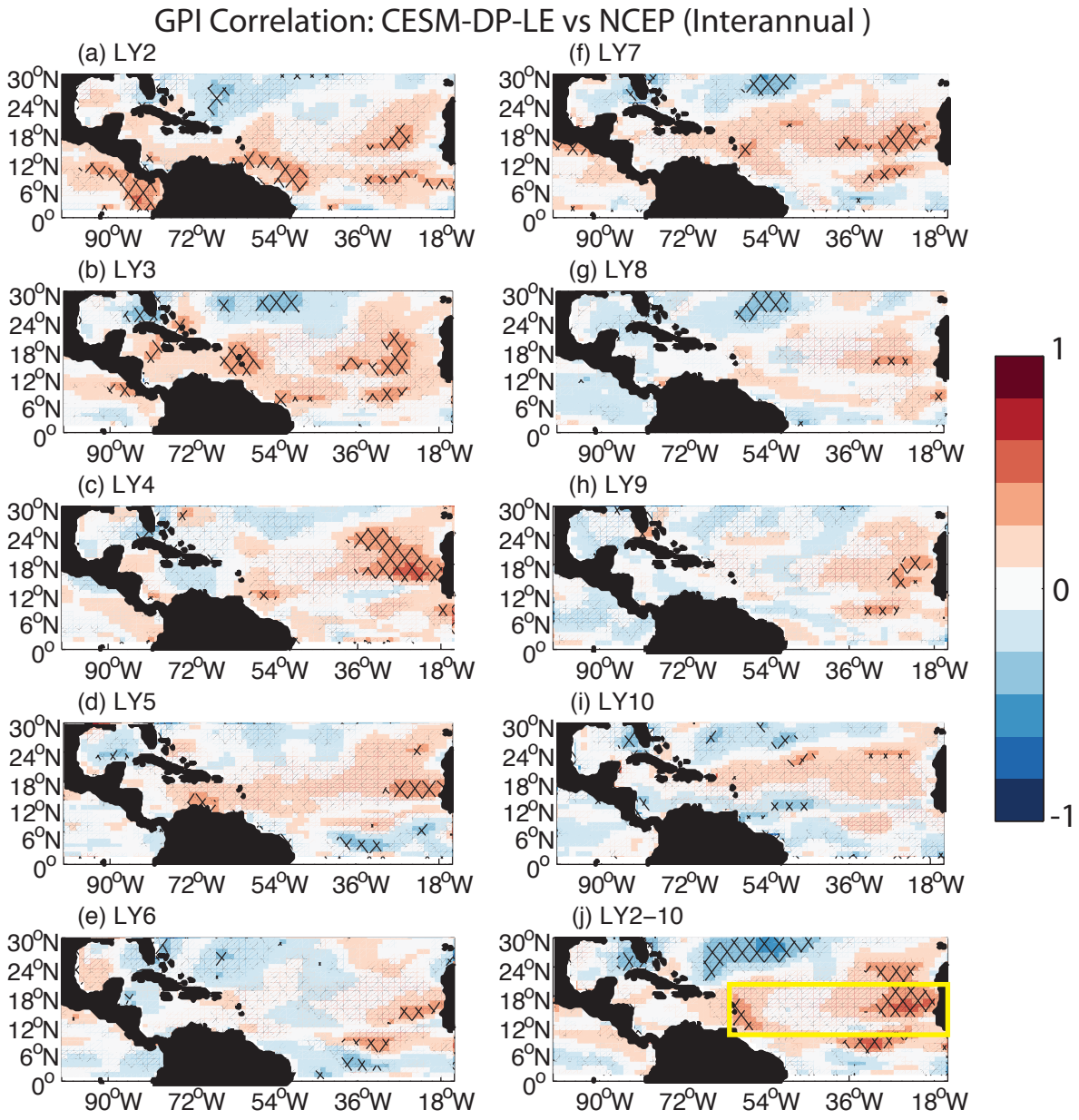


Figure 4.2. Identical to figure 4.1, but for results of interannual values instead of 5-year running means.

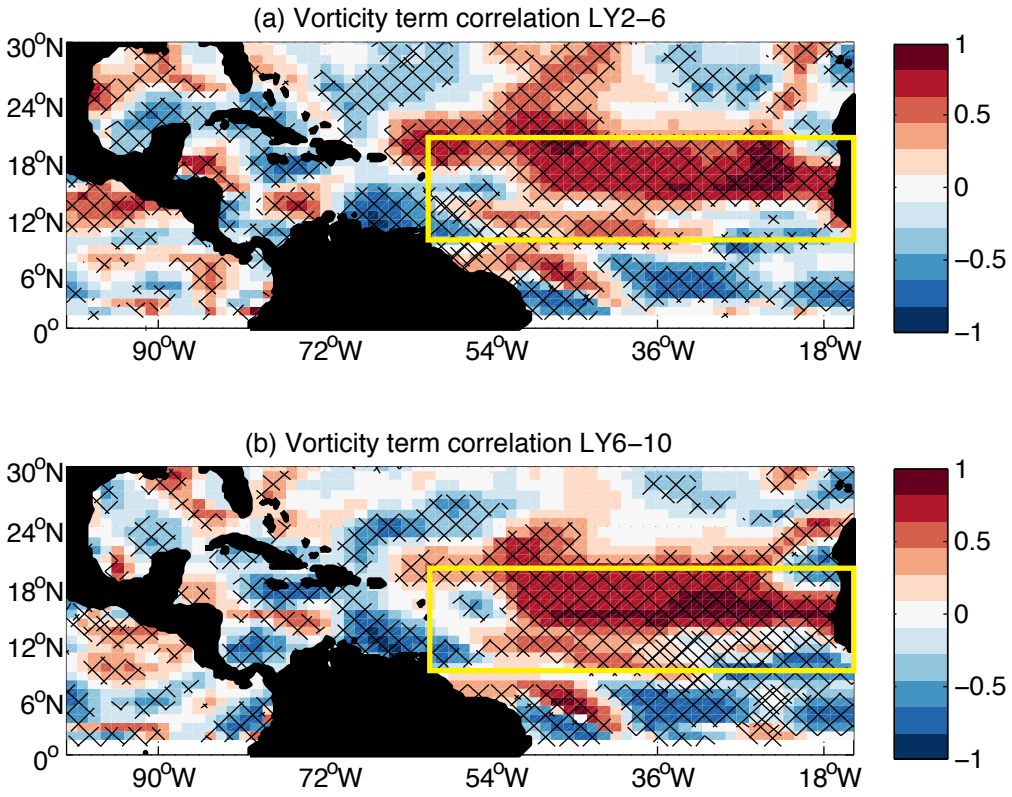


Figure 4.3. Correlation coefficients of 5-year running mean vorticity terms calculated from CESM-DP-LE and NCEP. The yellow box shows the region of conventional Atlantic MDR, and all the regions with values passed the 95% student t-test are hatched.

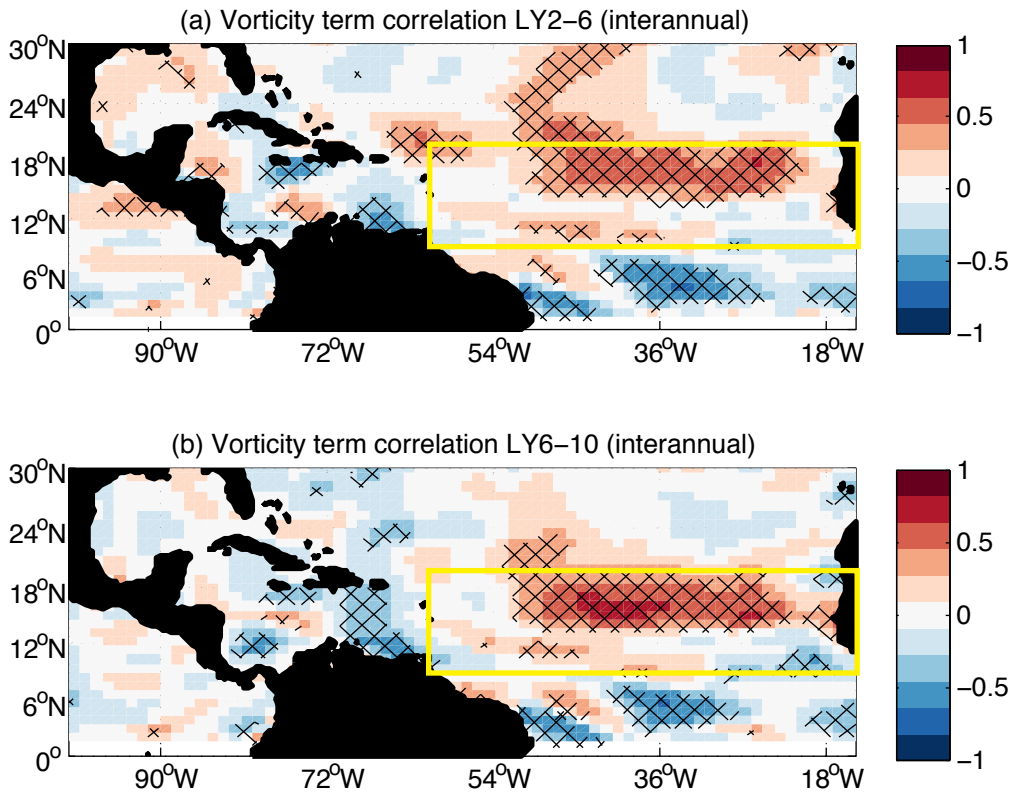


Figure 4.4. Same as figure 4.3, but showing results for interannual values instead of 5-year running means.

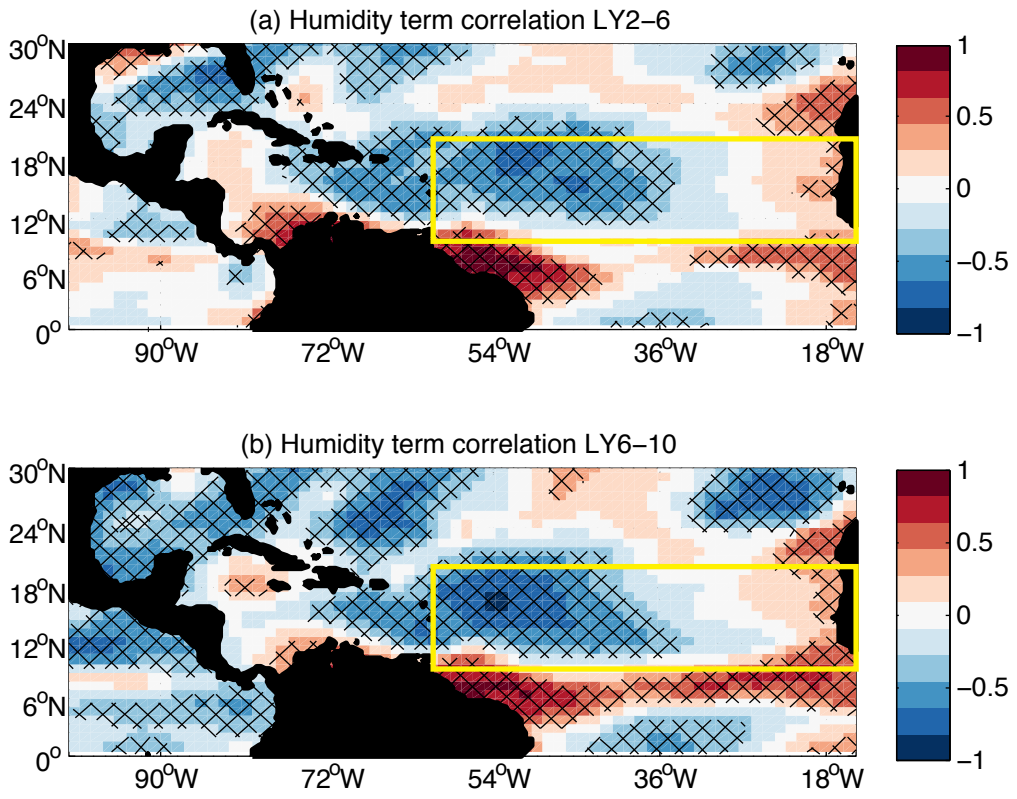


Figure 4.5. Correlation coefficients of 5-year running mean humidity terms calculated from CESM-DP-LE and NCEP. The yellow box shows the region of conventional Atlantic MDR, and all the regions with values passed the 95% student t-test are hatched.

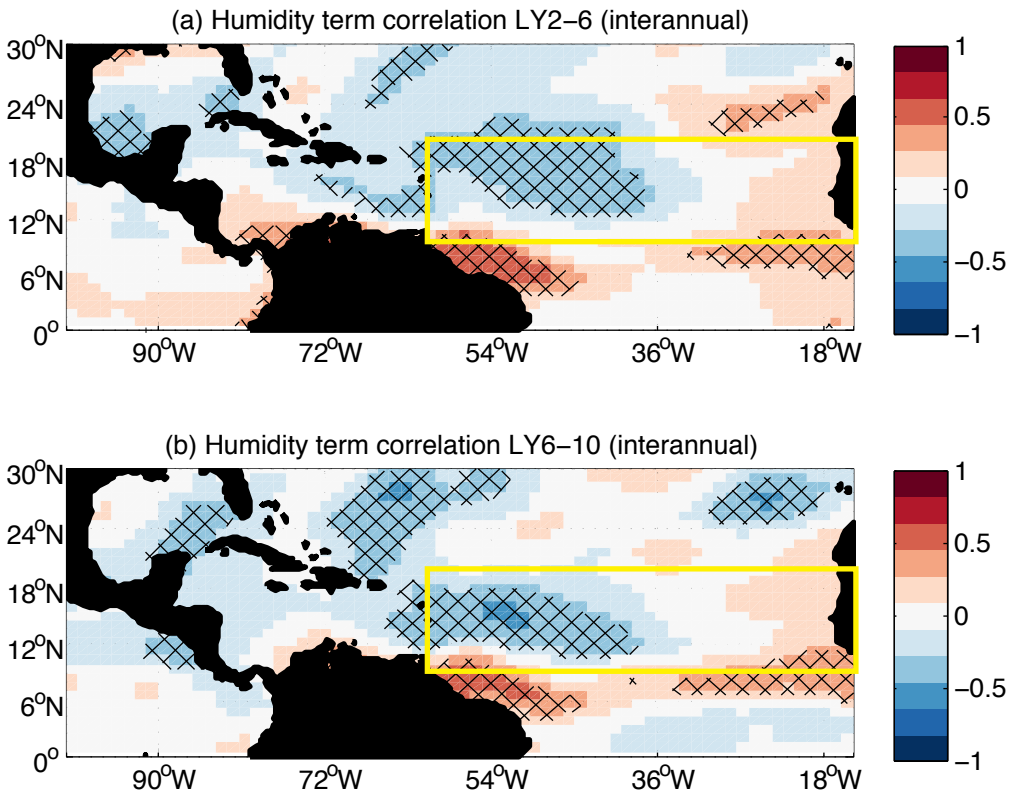


Figure 4.6. Same as figure 4.5, but showing results for interannual values instead of 5-year running means.

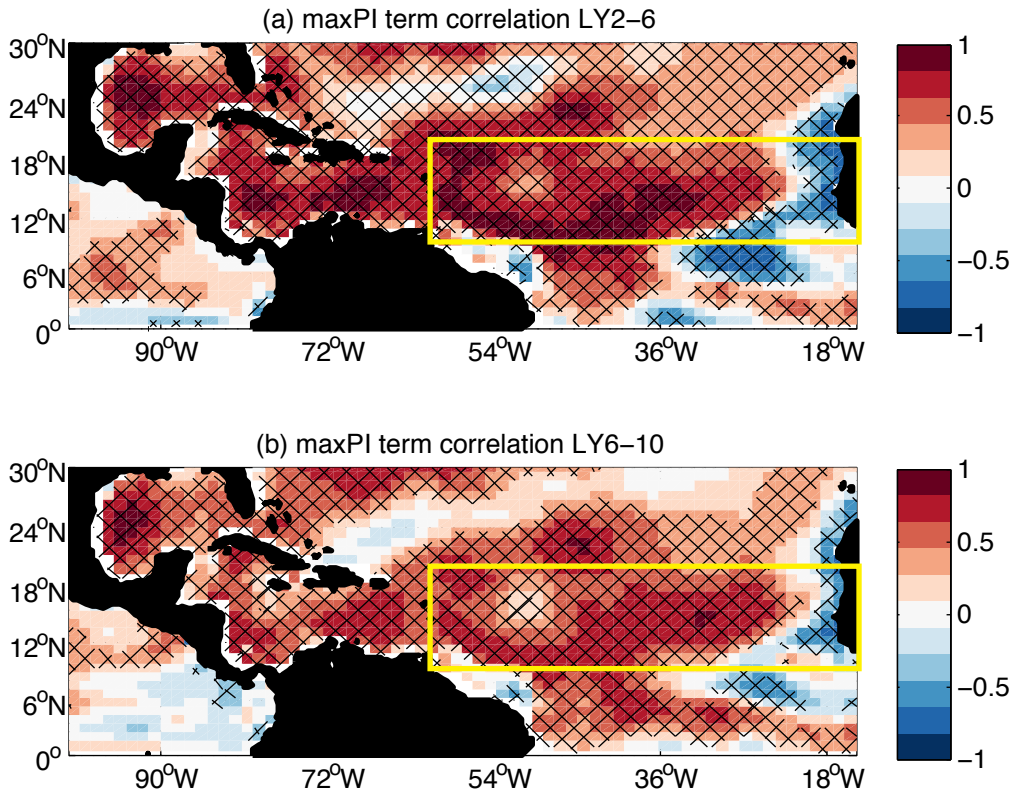


Figure 4.7. Correlation coefficients of 5-year running-mean maximum potential intensity (maxPI) terms calculated from CESM-DP-LE and NCEP. The yellow box shows the region of conventional Atlantic MDR, and all the regions with values passed the 95% student t-test are hatched.

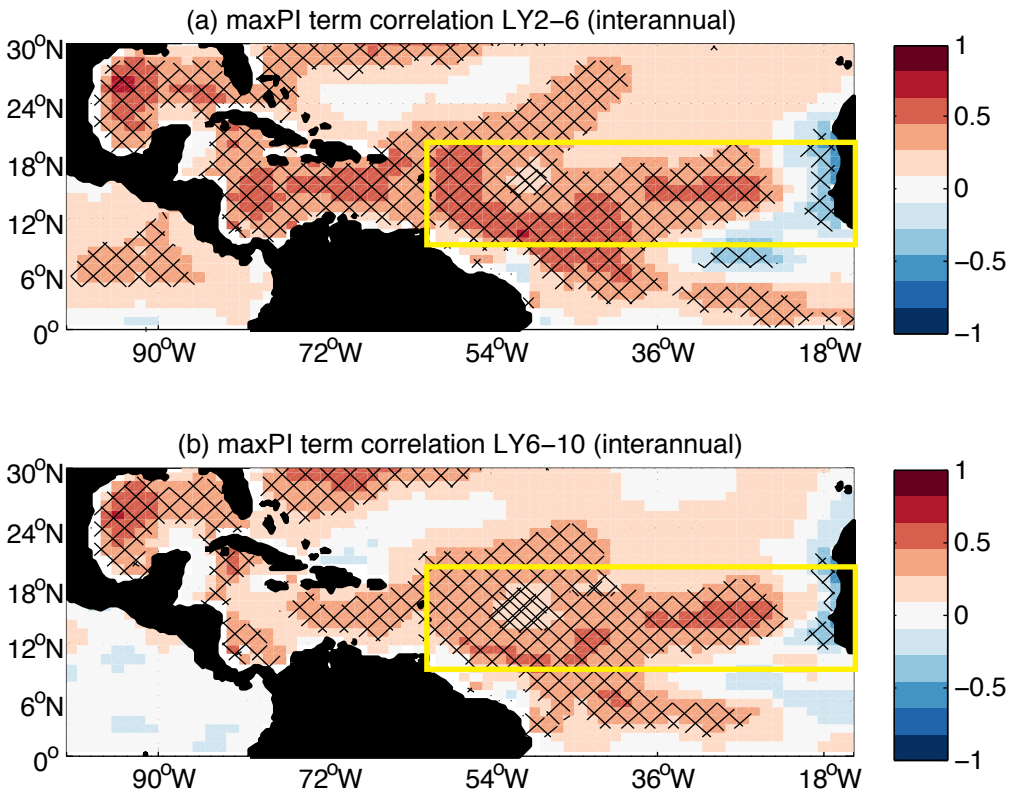


Figure 4.8. Same as figure 4.7, but showing results for interannual values instead of 5-year running means.

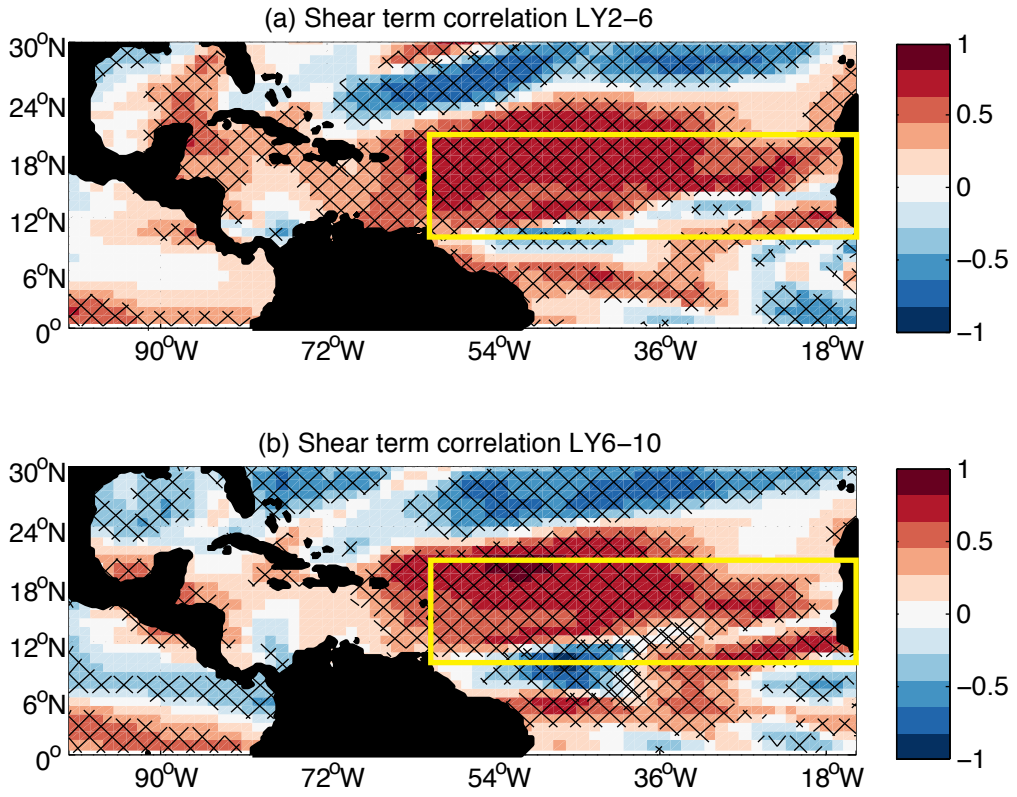


Figure 4.9. Correlation coefficients of 5-year running mean shear terms calculated from CESM-DP-LE and NCEP. The yellow box shows the region of conventional Atlantic MDR, and all the regions with values passed the 95% student t-test are hatched.

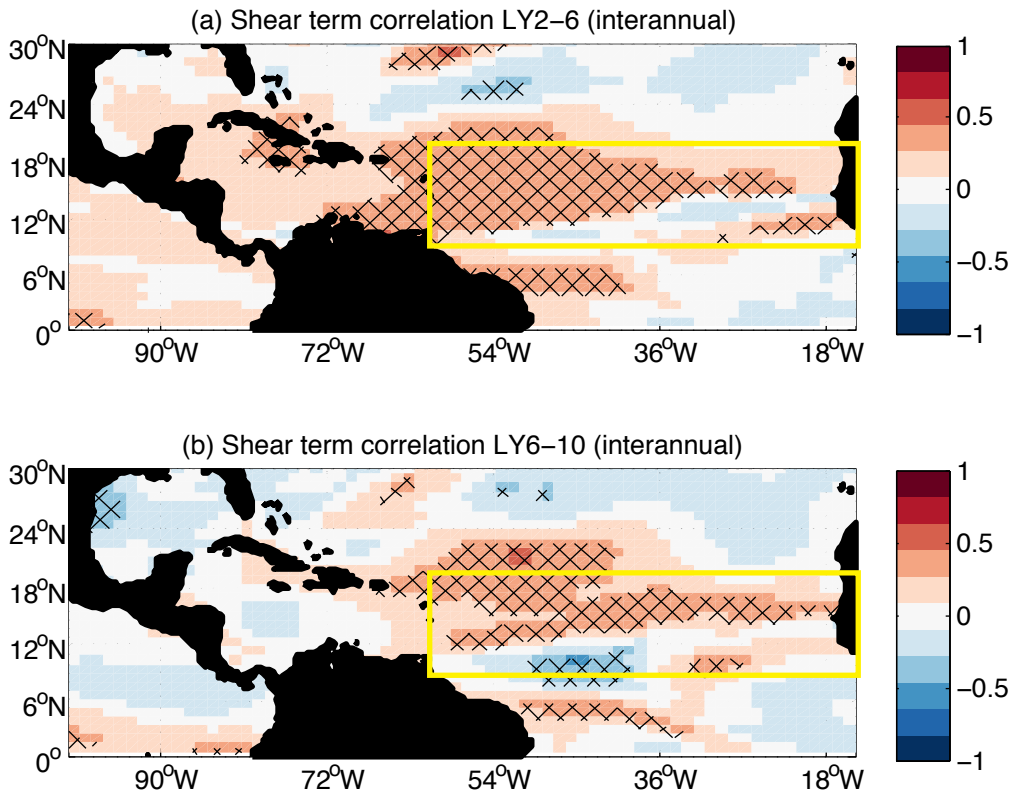


Figure 4.10. Same as figure 4.9, but showing results for interannual values instead of 5-year running means.

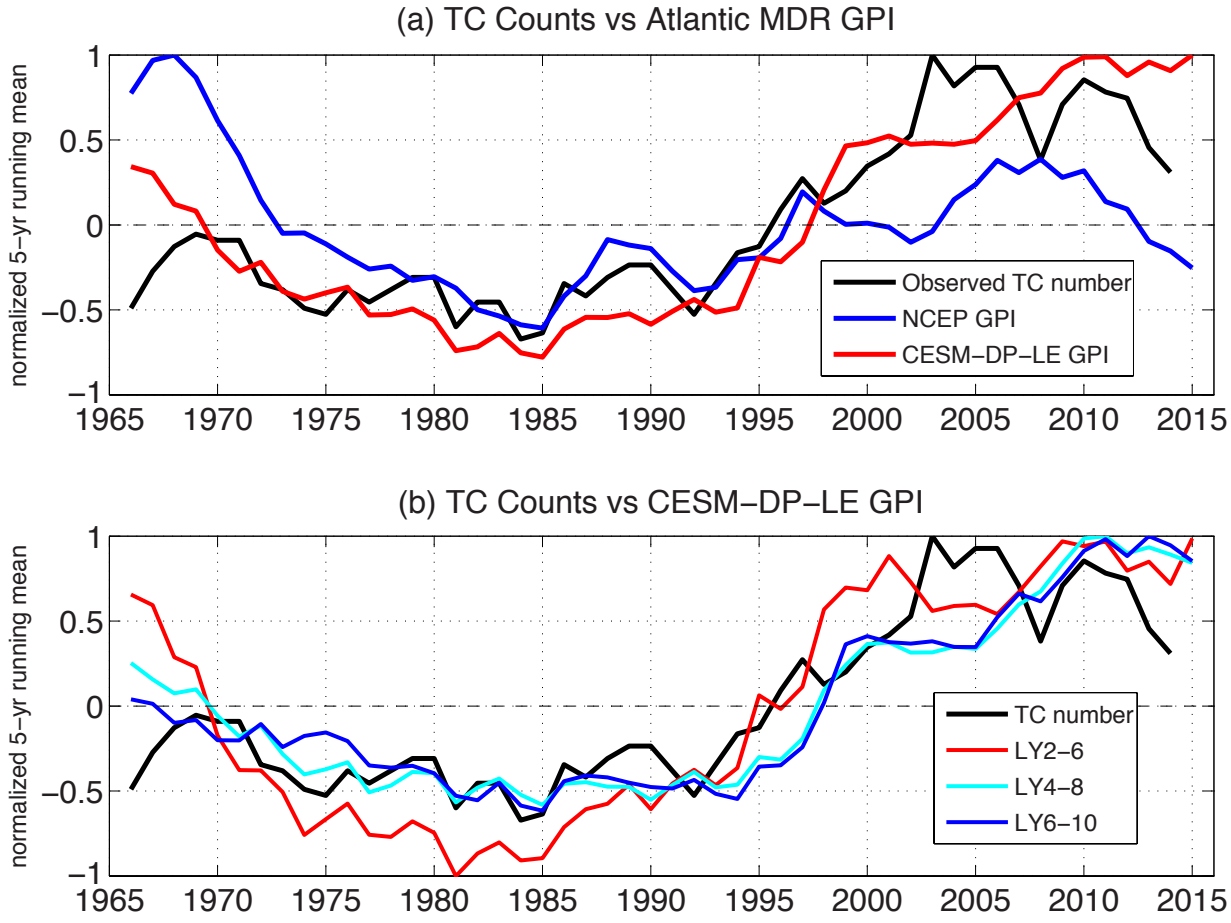


Figure 4.11: Normalized time series of 5-year running mean HURDAT2 TC counts and Atlantic MDR GPI .alculated from CESM-DP-LE and NCEP. (a) shows the 5-year running mean of observed (HURDAT2) TC counts in black, NCEP-based MDR GPI in blue, and CESM-DP-LE-based GPI in red. (b) shows the 5-year running mean TC number in black, and different color lines showing 5-year running GPI from different lead years in CESM-DP-LE.

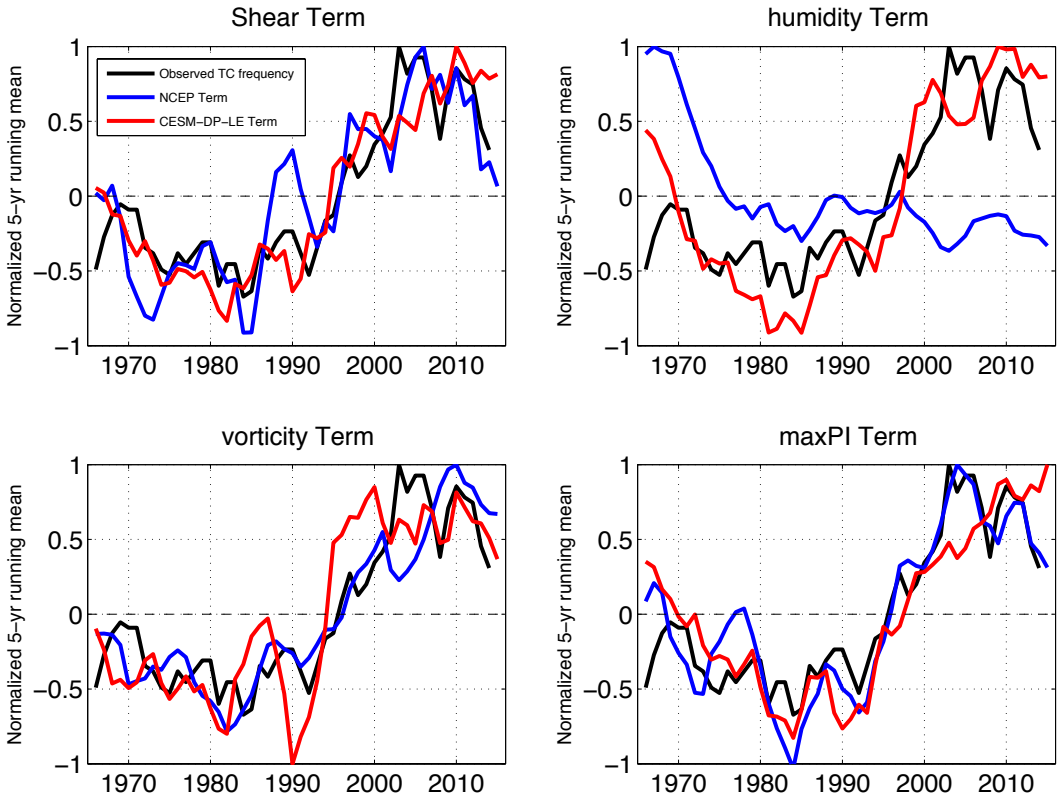


Figure 4.12. Normalized 5-year running mean time series of TC counts (in black) and each term ((a)shear, (b) humidity, (c) vorticity, and (d) potential intensity terms) in GPI calculated from NCEP (in blue) as well as CESM-DP-LE (in red).

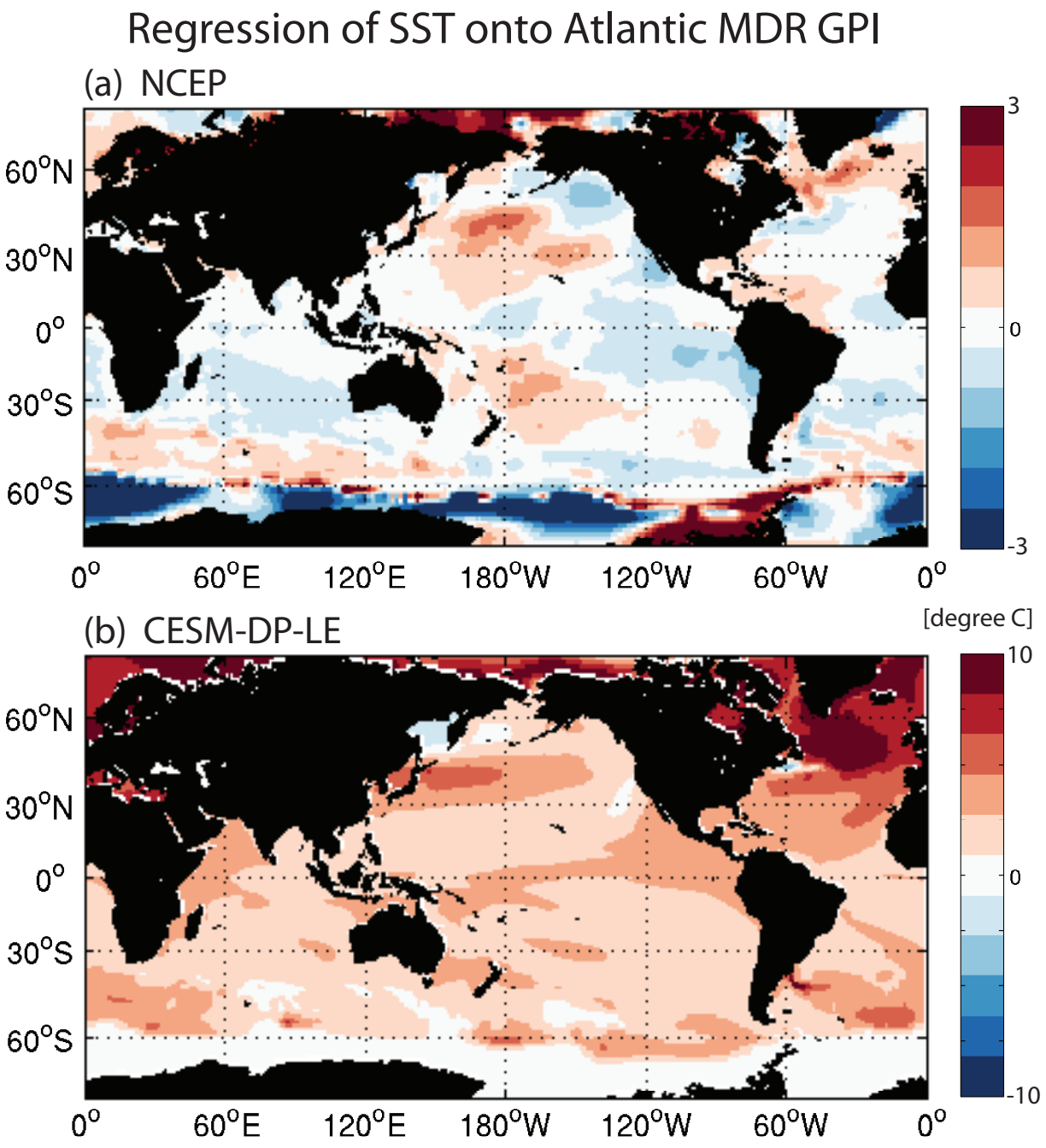


Figure 4.13. Regression coefficients of 5-year running mean global SST onto 5-year running mean Atlantic MDR GPI time series. Results from both NCEP (a) and CESM-DP-LE (b) are shown.

# CHAPTER V

# CONCLUSIONS AND FUTURE WORK

The impacts of SST forcings, including biases and prediction errors, and TC-related environmental variables on TC simulations and prediction on seasonal-to-decadal timescales were examined in this dissertation through three interrelated research streams. First, by separating the tropical SST biases common to current generation climate models by region and by sign, we performed a large number of ensembles of simulations using a TC-permitting tropical-channel WRF model. The relative importance of the impact of SST biases in different ocean basins on seasonal-to-interannual TC simulations and the underlying dynamics were investigated by comparing these ensembles of simulations. Second, the same model (with improved parameterizations) was forced with the predicted SST anomalies from CESM Decadal Prediction Large Ensemble (DP-LE) to examine the feasibility of seasonal-to-longer time scales TC forecast in the global tropics. Utilizing different SST forcings and boundary and initial conditions, the relative importance of the impact from uncertainties of atmospheric internal variability, SST forcings, and the lateral boundary conditions on TC forecast skill was explored. Third, we analyzed the predictability of TC-related environmental variables from CESM-DP-LE to investigate the potential predictability of TCs on multiyear to decadal timescales. GPI and its associated terms were used to quantify multiyear-to-decadal TC potential predictability in the Atlantic. The main conclusions of the three studies are summarized as follows.

## 5.1 Conclusions

The results from ensembles of TC-permitting tropical-channel WRF simulations suggest that tropical SST biases in climate models can induce significant influences on TC simulations both locally in and remote from tropical Atlantic and Pacific basins. The simulations suggest an underrepresentation in Atlantic TC activity caused by the Atlantic cold bias alone, and an overrepresentation in ENP TC activity due to the Atlantic cold bias and Pacific warm bias jointly. While the local impact of SST biases on TC activity is generally induced by changes in local atmospheric conditions conducive to TC genesis and development, the remote impact of the Atlantic bias on the ENP TCs appears to be related to changes in the regional circulation over the Central America, where topographic effect plays an important role. Moreover, an eastward shift in WNP TCs was generated by the Pacific SST biases, even though basin-wide TC activity indicators change insignificantly. The results of Chapter II point to the importance of considering SST bias effects on simulated TC activity in climate model studies and highlight key regions where reducing SST biases could potentially improve TC representation in climate models.

With improved parameterizations, in Chapter III we used a modified tropical-channel WRF, which shows potential skill in predicting TC at lead-time from 6-to-12 months using predicted SST anomalies from CESM-DP-LE. However, even with significantly differences among observed, persisted, and predicted SST anomalies, the simulated ACE values and TC counts show no significant differences in certain simulation years and ocean basins, raising a question whether the aggregated metrics, such as ACE and TC counts, are useful measures of model predictive skills, since the area averaging used in these metrics tends to remove any spatial variation of TCs. Nevertheless, due to low horizontal resolutions of current generation

climate models, TCs cannot be accurately tracked. Therefore, metrics other than ACE or TC count alone should be developed to examine seasonal TC predictability. In addition, significant impact from the lateral boundaries of the tropical-channel WRF on the simulated TCs were suggested by both GPI and moist static energy transport analyses, indicating that tropical SSTs may not necessarily be the only dominant factor for TC predictability.

Furthermore, by investigating TC-related environmental condition changes from a long (1964 to 2017) decadal prediction experiments, our results suggest high potential skills of CESM-DP-LE in predicting Atlantic TCs on lead year 2 to 10. The GPI decomposition analysis suggests that all four large-scale environmental variables, including potential intensity, shear, humidity, and vorticity, contribute the high skill of CESM-DP-LE in the Atlantic, with correlation higher than 0.8 between the 5-year running mean seasonal TC count and predicted Atlantic MDR GPI. In particular, the mid-level humidity predicted by CESM-DP-LE shows much better skill in predicting Atlantic TC frequency than that of NCEP. The results of Chapter IV give an assessment of the potential skill of the CESM-DP-LE in predicting TC variations on multiyear to decadal timescales, and suggest a potential value in downscaling CESM-DP-LE for decadal TC prediction in the Atlantic.

### 5.2 Future Work

Even though the impact of the Atlantic SST biases on both Atlantic and Pacific TC activity and the underlying mechanisms were investigated in Chapter II, the impact of Pacific biases was not fully examined in our study. For example, unlike the warm bias in the southeastern Atlantic, the Pacific warm bias contains two parts, one in the northern and the other in the southern tropics, raising the question whether one of the warm biases has the dominant

influence over the other one. In addition, the impact of tropical SST biases on the TC activity in the Indian Ocean, which is also known as a region strongly influenced by TCs, was not discussed in Chapter II, since the ensemble size (16 members) was not large enough, and the number of TCs generated in that region is small, both of which leads to insufficient sample size to test statistically significance of the results in the Indian Ocean. Therefore, more simulations with larger ensemble size should be performed in future studies to quantify the impact in the Indian Ocean.

While the results in Chapter III show potential skills of dynamical downscaling CESM-DP-LE for seasonal TC prediction, the study raises more questions than answers, pointing to the need of future studies for further understanding the mechanisms and the relative importance of the impact of lateral boundary conditions, SST forcings, and atmospheric internal variability on TCM simulation of seasonal TC activity. For example, a set of sensitivity experiments is needed to investigate the impact of locations of the lateral boundaries on TCs. Moreover, increasing the verification period of the TCM prediction simulations is also needed. It is clear from the analysis presented in Chapter III that examining only two ENSO events is not sufficient to generate robust results for evaluating model skills. Furthermore, the impact of SSTs, boundary conditions, and internal variability (initial conditions) should be better investigated by quantifying the changes in large-scale circulations and the TC-related atmospheric conditions.

Finally, to better examine the multi-year to decadal Atlantic TC predicting skill in CESM-DP-LE, further analysis needs to be performed to demonstrate the relationship between the TC-related environmental variables in MDR and the large-scale variability in CESM-DP-LE. In particular, the dominant factor for the high predictability should be investigated. It is of interests to examine whether the high predictability in CESM-DP-LE can be attribute to the high

predictability in AMO-related features, presumably contributed by the ocean initialization. On possible approach is to quantify the representation of TC-related terms and GPI in CESM-LE – an uninitialized complementary set of large ensemble simulations. Since large improvement in predicting AMO-related SST patterns were demonstrated for CESM-DP-LE comparing to CESM-LE, the increased skill is argued to be caused by the initialization (Yeager et al. 2018). By comparing the results of Chapter IV to a similar analysis on CESM-LE, we can potentially examine the influence of ocean memory on TC predictability on longer timescales.

# REFERENCES


Barnston, A. G., Li, S., Mason, S. J., DeWitt, D. G., Goddard, L., & Gong, X. (2010). Verification of the first 11 years of IRI's seasonal climate forecasts. Journal of Applied Meteorology and Climatology, 49, 493–520.

Bell, G. D., Halpert, M. S., Schnell, R. C., Higgins, R. W., Lawrimore, J., Kousky, V. E., … Artusa, A. (2000). Climate assessment for 1999. Bulletin of the American Meteorological Society, 81, s1–s50.

Bender, M. A., Knutson, T. R., Tuleya, R. E., Sirutis, J. J., Vecchi, G. A., Garner, S. T., & Held, I. M. (2010). Modeled impact of anthropogenic warming on the frequency of intense Atlantic hurricanes. Science, 327, 454–458.

Biasutti, M., Sobel, A. H., & Kushnir, Y. (2006). AGCM precipitation biases in the tropical Atlantic. Journal of Climate, 19, 935–958.

Blake, E. S., Rappaport, E. N., Jarrell, J. D., Landsea, C., & Center, T. P. (2007). The deadliest, costliest, and most intense United States tropical cyclones from 1851 to 2006 (and other frequently requested hurricane facts). NOAA/National Weather Service, National Centers for Environmental Prediction, National Hurricane Center Miami.

Blake, E. S., Kimberlain, T. B., Berg, R. J., Cangialosi, J. P., & Beven II, J. L. (2013). Tropical cyclone report hurricane Sandy. United States National Oceanic and Atmospheric Administration's National Weather Service.

Bond, N. A., Cronin, M. F., Freeland, H., & Mantua, N. (2015). Causes and impacts of the 2014 warm anomaly in the NE Pacific. Geophysical Research Letters, 42, 3414–3420.

Bove, M. C., O'Brien, J. J., Eisner, J. B., Landsea, C. W., & Niu, X. (1998). Effect of El Niño on U.S. landfalling hurricanes, Revisited. Bulletin of the American Meteorological Society, 79, 2477–2482.

Bruyère, C. L., Holland, G. J., & Towler, E. (2012). Investigating the use of a genesis potential index for tropical cyclones in the North Atlantic basin. Journal of Climate, 25, 8611–8626.

Camargo, S. J. (2013). Global and regional aspects of tropical cyclone activity in the CMIP5 models. Journal of Climate, 26, 9880–9902.

Camargo, S. J., Emanuel, K. A., & Sobel, A. H. (2007). Use of a genesis potential index to diagnose ENSO effects on tropical cyclone genesis. Journal of Climate, 20, 4819–4834.

Camargo, S. J., & Hsiang, S. M. (2015). From the influence of climate to their socioeconomic impacts. In Tropical Cyclones (pp. 303–342).

Camargo, S. J., Robertson, A. W., Barnston, A. G., & Ghil, M. (2008). Clustering of eastern North Pacific tropical cyclone tracks: ENSO and MJO effects. Geochemistry, Geophysics, Geosystems, 9, Q06V05.

Camargo, S. J., & Sobel, A. H. (2005). Western North Pacific tropical cyclone intensity and ENSO. Journal of Climate, 18, 2996–3006.

Camargo, S. J., Wheeler, M. C., & Sobel, A. H. (2009). Diagnosis of the MJO modulation of tropical cyclogenesis using an empirical index. Journal of the Atmospheric Sciences, 66, 3061–3074.

Caron, L.-P., Jones, C. G., & Doblas-Reyes, F. (2014). Multi-year prediction skill of Atlantic hurricane activity in CMIP5 decadal hindcasts. Climate Dynamics, 42, 2675–2690.

Chan, J. C. L. (2000). Tropical cyclone activity over the western North Pacific associated with El Niño and La Niña events. Journal of Climate, 13, 2960–2972.

Chan, J. C. L. (1985). Tropical cyclone activity in the Northwest Pacific in relation to the El Niño/Southern Oscillation phenomenon. Monthly Weather Review, 113, 599–606.

Chan, J. C. L. (2005). Interannual and interdecadal variations of tropical cyclone activity over the western North Pacific. Meteorology and Atmospheric Physics, 89, 143–152.

Chen, J.-H., & Lin, S.-J. (2013). Seasonal predictions of tropical cyclones using a 25-km-resolution general circulation model. Journal of Climate, 26, 380–398.

Colas, F., McWilliams, J. C., Capet, X., & Kurian, J. (2012). Heat balance and eddies in the Peru-Chile current system. Climate Dynamics, 39, 509–529.

Collins, J. M., & Mason, I. M. (2000). Local environmental conditions related to seasonal tropical cyclone activity in the northeast Pacific basin. Geophysical Research Letters, 27, 3881–3884.

Collins, J. M., & Mason, I. M. (2003). Seasonal environmental conditions related to hurricane activity in the northeast Pacific basin. N. Engl.–St. Lawrence Val. Geogr. Soc. Proc, 33, 44–50.

Corporal-Lodangco, I. L., Richman, M. B., Leslie, L. M., & Lamb, P. J. (2014). Cluster analysis of North Atlantic tropical cyclones. Procedia Computer Science, 36, 293–300.

Danabasoglu, G., Bates, S. C., Briegleb, B. P., Jayne, S. R., Jochum, M., Large, W. G., … Yeager, S. G. (2012). The CCSM4 ocean component. Journal of Climate, 25, 1361–1389.

Ding, H., Keenlyside, N. S., & Latif, M. (2012). Impact of the equatorial Atlantic on the El Niño Southern Oscillation. Climate Dynamics, 38, 1965–1972.

Elsner, J. B., Murnane, R. J., & Jagger, T. H. (2006). Forecasting U.S. hurricanes 6 months in advance. Geophysical Research Letters, 33, L10704.

Emanuel, K. A. (1986). An air-sea interaction theory for tropical cyclones. Part I: Steady-state maintenance. Journal of the Atmospheric Sciences, 43, 585–604.

Emanuel, K. A. (2005). Increasing destructiveness of tropical cyclones over the past 30 years. Nature, 436, 686–688.

Emanuel, K. A. (2007). Environmental factors affecting tropical cyclone power dissipation. Journal of Climate, 20, 5497–5509.

Emanuel, K. A. (2017). Assessing the present and future probability of Hurricane Harvey's rainfall. Proceedings of the National Academy of Sciences, 114, 12681–12684.

Emanuel, K. A., & Nolan, D. S. (2004). Tropical cyclone activity and the global climate system. In 26th Conference on Hurricanes and Tropical Meteorology. Miami, FL: American Meteorological Society.

Emanuel, K., Sundararajan, R., & Williams, J. (2008). Hurricanes and global warming: Results from downscaling IPCC AR4 simulations. Bulletin of the American Meteorological Society, 89, 347–368.

Fu, D., Chang, P., & Patricola, C. M. (2017). Intrabasin variability of East Pacific tropical cyclones during ENSO regulated by Central American gap winds. Scientific Reports, 7, 1658.

Fu, D. (2018). Central American gap wind impact on eastern North Pacific tropical cyclones. Texas A&M University Doctoral dissertation.

Goldenberg, S. B. (2001). The recent increase in Atlantic hurricane activity: Causes and implications. Science, 293, 474–479.

Graham, N. E., & Barnett, T. P. (1987). Sea surface temperature, surface wind divergence, and convection over tropical oceans. Science, 238, 657–659.

Gray, W. M. (1979). Hurricanes: Their formation, structure and likely role in the tropical circulation. Meteorology over the Tropical Oceans. Royal Meteorological Society, 155–218.

Gray, W. M., & Brody, L. R. (1967). Global view of the origin of tropical disturbances and storms. Citeseer.

Gray, W. M., & Sheaffer, J. D. (1991). El Niño and QBO influences on tropical cyclone activity. Teleconnections Linking Worldwide Climate Anomalies. Cambridge University Press.

Gray, W. M. (1984). Atlantic seasonal hurricane frequency. Part II: Forecasting its variability. Monthly Weather Review, 112, 1669–1683.

Gray, W. M. (1984). Atlantic seasonal hurricane frequency. Part I: El Niño and 30 mb Quasi-Biennial Oscillation influences. Monthly Weather Review, 112, 1649–1668.

Ham, Y.-G., Kug, J.-S., & Park, J.-Y. (2013). Two distinct roles of Atlantic SSTs in ENSO variability: North Tropical Atlantic SST and Atlantic Niño. Geophysical Research Letters, 40, 4012–4017.

Ham, Y.-G., Kug, J.-S., Park, J.-Y., & Jin, F.-F. (2013). Sea surface temperature in the north tropical Atlantic as a trigger for El Niño/Southern Oscillation events. Nature Geoscience, 6, 112–116.

Holland, G. J., & Webster, P. J. (2007). Heightened tropical cyclone activity in the North Atlantic: natural variability or climate trend? Philosophical Transactions of the Royal Society A: Mathematical, Physical and Engineering Sciences, 365, 2695–2716.

Holland, G. J. (2007). Misuse of landfall as a proxy for Atlantic tropical cyclone activity. Eos, Transactions American Geophysical Union, 88, 349–350.

Hunke, E. C., & Lipscomb, W. H. (2008). CICE: the Los Alamos sea ice model user's manual, version 4. Los Alamos National Laboratory Tech. Rep. LA-CC-06-012.

Hurrell, J. W., Holland, M. M., Gent, P. R., Ghan, S., Kay, J. E., Kushner, P. J., … Marshall, S. (2013). The Community Earth System Model: A framework for collaborative research. Bulletin of the American Meteorological Society, 94, 1339–1360.

Jien, J. Y., Gough, W. A., & Butler, K. (2015). The influence of El Niño–Southern Oscillation on tropical cyclone activity in the eastern North Pacific basin. Journal of Climate, 28, 2459–2474.

Jin, F.-F., Boucharel, J., & Lin, I.-I. (2014). Eastern Pacific tropical cyclones intensified by El Niño delivery of subsurface ocean heat. Nature, 516, 82–85.

Kalnay, E., Kanamitsu, M., Kistler, R., Collins, W., Deaven, D., Gandin, L., … Joseph, D. (1996). The NCEP/NCAR 40-Year reanalysis project. Bulletin of the American Meteorological Society, 77, 437–471.

Kanamitsu, M., Ebisuzaki, W., Woollen, J., Yang, S.-K., Hnilo, J. J., Fiorino, M., & Potter, G. L. (2002). NCEP–DOE AMIP-II Reanalysis (R-2). Bulletin of the American Meteorological Society, 83, 1631–1644.

Kang, S. M., Held, I. M., Frierson, D. M. W., & Zhao, M. (2008). The response of the ITCZ to extratropical thermal forcing: Idealized slab-ocean experiments with a GCM. Journal of Climate, 21, 3521–3532.

Kay, J. E., Deser, C., Phillips, A., Mai, A., Hannay, C., Strand, G., … Vertenstein, M. (2015). The Community Earth System Model (CESM) large ensemble project: A community resource for studying climate change in the presence of internal climate variability. Bulletin of the American Meteorological Society, 96, 1333–1349.

Klotzbach, P. J. (2011). The influence of El Niño–Southern Oscillation and the Atlantic Multidecadal Oscillation on Caribbean tropical cyclone activity. Journal of Climate, 24, 721–731.

Klotzbach, P. J. (2006). Trends in global tropical cyclone activity over the past twenty years (1986-2005). Geophysical Research Letters, 33, L10805.

Klotzbach, P. J., Bowen, S. G., Pielke, R., & Bell, M. (2018). Continental United States hurricane landfall frequency and associated damage: Observations and future risks. Bulletin of the American Meteorological Society, BAMS-D-17-0184.1.

Klotzbach, P. J., & Gray, W. M. (2008). Multidecadal variability in North Atlantic tropical cyclone activity. Journal of Climate, 21, 3929–3935.

Knapp, K. R., Kruk, M. C., Levinson, D. H., Diamond, H. J., & Neumann, C. J. (2010). The International Best Track Archive for Climate Stewardship (IBTrACS). Bulletin of the American Meteorological Society, 91, 363–376.

Knight, J. R., Folland, C. K., & Scaife, A. A. (2006). Climate impacts of the Atlantic Multidecadal Oscillation. Geophysical Research Letters, 33, L17706.

Knutson, T. R., Sirutis, J. J., Garner, S. T., Vecchi, G. A., & Held, I. M. (2008). Simulated reduction in Atlantic hurricane frequency under twenty-first-century warming conditions. Nature Geoscience, 1, 359–364.

Knutson, T., Landsea, C., & Emanuel, K. (2010). Tropical cyclones and climate change: a review. In Global perspectives on tropical cyclones: from science to mitigation (pp. 243–284). World Scientific.

Korty, R. L., Camargo, S. J., & Galewsky, J. (2012). Tropical cyclone genesis factors in simulations of the Last Glacial Maximum. Journal of Climate, 25, 4348–4365.

Korty, R. L., Camargo, S. J., & Galewsky, J. (2012). Variations in tropical cyclone genesis factors in simulations of the Holocene Epoch. Journal of Climate, 25, 8196–8211.

Kucharski, F., Parvin, A., Rodriguez-Fonseca, B., Farneti, R., Martin-Rey, M., Polo, I., … Mechoso, C. R. (2016). The teleconnection of the tropical Atlantic to Indo-Pacific sea surface temperatures on inter-annual to centennial time scales: A review of recent findings. Atmosphere, 7, 29.

Landsea, C. W., Franklin, J. L., & Beven, J. L. (2015). The revised Atlantic hurricane database (HURDAT2). United States National Oceanic and Atmospheric Administration's National Weather Service.

LaRow, T. E., Stefanova, L., Shin, D.-W., & Cocke, S. (2010). Seasonal Atlantic tropical cyclone hindcasting/forecasting using two sea surface temperature datasets. Geophysical Research Letters, 37, L02804.

Latif, M., Collins, M., Pohlmann, H., & Keenlyside, N. (2006). A review of predictability studies of Atlantic sector climate on decadal time scales. Journal of Climate, 19, 5971–5987.

Lawrence, D. M., Oleson, K. W., Flanner, M. G., Thornton, P. E., Swenson, S. C., Lawrence, P. J., … Slater, A. G. (2011). Parameterization improvements and functional and structural advances in Version 4 of the Community Land Model. Journal of Advances in Modeling Earth Systems 3.1.

Li, G., & Xie, S.-P. (2012). Origins of tropical-wide SST biases in CMIP multi-model ensembles. Geophysical Research Letters, 39, L22703.

Lin, I.-I., Black, P., Price, J. F., Yang, C.-Y., Chen, S. S., Lien, C.-C., … D'Asaro, E. A. (2013). An ocean coupling potential intensity index for tropical cyclones. Geophysical Research Letters, 40, 1878–1882.

Liu, H., Wang, C., Lee, S.-K., & Enfield, D. (2012). Atlantic warm-pool variability in the IPCC AR4 CGCM simulations. Journal of Climate, 25, 5612–5628.

Masunaga, H., Nakajima, T. Y., Nakajima, T., Kachi, M., & Suzuki, K. (2002). Physical properties of maritime low clouds as retrieved by combined use of Tropical Rainfall Measuring Mission (TRMM) Microwave Imager and Visible/Infrared Scanner 2. Climatology of warm clouds and rain. Journal of Geophysical Research, 107, 4367.

Murakami, H., Vecchi, G. A., Villarini, G., Delworth, T. L., Gudgel, R., Underwood, S., … Lin, S.-J. (2016). Seasonal forecasts of major hurricanes and landfalling tropical cyclones using a high-resolution GFDL coupled climate model. Journal of Climate, 29, 7977–7989.

Nobre, P., & Srukla, J. (1996). Variations of sea surface temperature, wind stress, and rainfall over the tropical Atlantic and South America. Journal of Climate, 9, 2464–2479.

Painemal, D., & Minnis, P. (2012). On the dependence of albedo on cloud microphysics over marine stratocumulus clouds regimes determined from Clouds and the Earth's Radiant Energy System (CERES) data. Journal of Geophysical Research: Atmospheres, 117, D06203.

Palmer, T. N., Alessandri, A., Andersen, U., Cantelaube, P., Davey, M., Délécluse, P., … Thomson, M. C. (2004). Development of a European multimodel ensembles system for

seasonal-to-interannual prediction (DEMETER). Bulletin of the American Meteorological Society, 85, 853–872.

Patricola, C. M., Chang, P., & Saravanan, R. (2016). Degree of simulated suppression of Atlantic tropical cyclones modulated by flavour of El Niño. Nature Geoscience, 9, 155–160.

Patricola, C. M., Li, M., Xu, Z., Chang, P., Saravanan, R., & Hsieh, J.-S. (2012). An investigation of tropical Atlantic bias in a high-resolution coupled regional climate model. Climate Dynamics, 39, 2443–2463.

Patricola, C. M., Saravanan, R., & Chang, P. (2017). A teleconnection between Atlantic sea surface temperature and eastern and central North Pacific tropical cyclones. Geophysical Research Letters, 44, 1167–1174.

Patricola, C. M., Saravanan, R., & Chang, P. (2014). The impact of the El Niño–Southern Oscillation and Atlantic Meridional Mode on seasonal Atlantic tropical cyclone activity. Journal of Climate, 27, 5311–5328.

Polo, I., Martin-Rey, M., Rodriguez-Fonseca, B., Kucharski, F., & Mechoso, C. R. (2015). Processes in the Pacific La Niña onset triggered by the Atlantic Niño. Climate Dynamics, 44, 115–131.

Rayner, N. A. (2003). Global analyses of sea surface temperature, sea ice, and night marine air temperature since the late nineteenth century. Journal of Geophysical Research, 108, 4407.

Reynolds, R. W., Smith, T. M., Liu, C., Chelton, D. B., Casey, K. S., & Schlax, M. G. (2007). Daily high-resolution-blended analyses for sea surface temperature. Journal of Climate, 20, 5473–5496.

Richter, I. (2015). Climate model biases in the eastern tropical oceans: causes, impacts and ways forward. Wiley Interdisciplinary Reviews: Climate Change, 6, 345–358.

Richter, I., & Xie, S.-P. (2008). On the origin of equatorial Atlantic biases in coupled general circulation models. Climate Dynamics, 31, 587–598.

Richter, I., Xie, S.-P., Behera, S. K., Doi, T., & Masumoto, Y. (2014). Equatorial Atlantic variability and its relation to mean state biases in CMIP5. Climate Dynamics, 42, 171–188.

Rodríguez-Fonseca, B., Polo, I., García-Serrano, J., Losada, T., Mohino, E., Mechoso, C. R., & Kucharski, F. (2009). Are Atlantic Niños enhancing Pacific ENSO events in recent decades? Geophysical Research Letters, 36, L20705.

Saha, S., Moorthi, S., Pan, H. L., Wu, X., Wang, J., Nadiga, S., … Behringer, D. (2010). NCEP climate forecast system reanalysis (CFSR) 6-hourly products, January 1979 to December 2010. Research Data Archive at the National Center for Atmospheric Research, Computational and Information Systems Laboratory, Boulder, CO.

Saha, S., Nadiga, S., Thiaw, C., Wang, J., Wang, W., Zhang, Q., … Xie, P. (2006). The NCEP climate forecast system. Journal of Climate, 19, 3483–3517.

Saha, S., Moorthi, S., Wu, X., Wang, J., Nadiga, S., Tripp, P., … Becker, E. (2014). The NCEP climate forecast system version 2. Journal of Climate, 27, 2185–2208.

Shuckburgh, E., Mitchell, D., & Stott, P. (2017). Hurricanes Harvey, Irma and Maria: how natural were these 'natural disasters'? Weather, 72, 353–354.

Skamarock, W. C., Klemp, J. B., Dudhia, J., Gill, D. O., Barker, D. M., Duda, M. G., … Powers, J. G. (2008). A description of the advanced research WRF version 3. NCAR Technical Note NCAR/TN-475+STR.

Small, R. J., Curchitser, E., Hedstrom, K., Kauffman, B., & Large, W. G. (2015). The Benguela upwelling system: Quantifying the sensitivity to resolution and coastal wind representation in a global climate model. Journal of Climate, 28, 9409–9432.

Smith, D. M., Eade, R., Dunstone, N. J., Fereday, D., Murphy, J. M., Pohlmann, H., & Scaife, A. A. (2010). Skilful multi-year predictions of Atlantic hurricane frequency. Nature Geoscience, 3, 846–849.

Tang, B. H., & Neelin, J. D. (2004). ENSO Influence on Atlantic hurricanes via tropospheric warming. Geophysical Research Letters, 31, L24204.

Taylor, K. E., Stouffer, R. J., & Meehl, G. A. (2012). An overview of CMIP5 and the experiment design. Bulletin of the American Meteorological Society, 93, 485–498.

Toniazzo, T., Mechoso, C. R., Shaffrey, L. C., & Slingo, J. M. (2010). Upper-ocean heat budget and ocean eddy transport in the south-east Pacific in a high-resolution coupled model. Climate Dynamics, 35, 1309–1329.

van Oldenborgh, G.J., Reyes, F.D., Drijfhout, S.S. and Hawkins, E. (2013). Reliability of regional climate model trends. Environmental Research Letters, 8, 14055.

Vecchi, G. A., Delworth, T., Gudgel, R., Kapnick, S., Rosati, A., Wittenberg, A. T., … Zhang, S. (2014). On the seasonal forecasting of regional tropical cyclone activity. Journal of Climate, 27, 7994–8016.

Vecchi, G. A., Msadek, R., Anderson, W., Chang, Y.-S., Delworth, T., Dixon, K., … Zhang, S. (2013). Multiyear predictions of North Atlantic hurricane frequency: Promise and limitations. Journal of Climate, 26, 5337–5357.

Vecchi, G. A., & Soden, B. J. (2007). Effect of remote sea surface temperature change on tropical cyclone potential intensity. Nature, 450, 1066–1070.

Vimont, D. J., & Kossin, J. P. (2007). The Atlantic Meridional Mode and hurricane activity. Geophysical Research Letters, 34, L07709.

Walsh, K. (1997). Objective detection of tropical cyclones in high-resolution analyses. Monthly Weather Review, 125, 1767–1779.

Wang, B., & Chan, J. C. L. (2002). How strong ENSO events affect tropical storm activity over the western North Pacific. Journal of Climate, 15, 1643–1658.

Wang, B., & Li, T. (1993). A simple tropical atmosphere model of relevance to short-term climate variations. Journal of the Atmospheric Sciences, 50, 260–284.

Wang, C., Dong, S., Evan, A. T., Foltz, G. R., & Lee, S.-K. (2012). Multidecadal covariability of North Atlantic sea surface temperature, African dust, Sahel rainfall, and Atlantic hurricanes. Journal of Climate, 25, 5404–5415.

Wang, C., & Lee, S.-K. (2009). Co-variability of tropical cyclones in the North Atlantic and the eastern North Pacific. Geophysical Research Letters, 36, L24702.

Wang, C., Li, C., Mu, M., & Duan, W. (2013). Seasonal modulations of different impacts of two types of ENSO events on tropical cyclone activity in the western North Pacific. Climate Dynamics, 40, 2887–2902.

Wang, C., Zhang, L., Lee, S.-K., Wu, L., & Mechoso, C. R. (2014). A global perspective on CMIP5 climate model biases. Nature Climate Change, 4, 201–205.

Wang, R., & Wu, L. (2013). Climate changes of Atlantic tropical cyclone formation derived from twentieth-century reanalysis. Journal of Climate, 26, 8995–9005.

Webster, P. J., Holland, G. J., Curry, J. A., & Chang, H.-R. (2005). Changes in tropical cyclone number, duration, and intensity in a warming environment. Science, 309, 1844–1846.

Whitney, L. D., & Hobgood, J. S. (1997). The relationship between sea surface temperatures and maximum intensities of tropical cyclones in the eastern North Pacific ocean. Journal of Climate, 10, 2921–2930.

Whyte, F. S., Taylor, M. A., Stephenson, T. S., & Campbell, J. D. (2007). Features of the Caribbean low level jet. International Journal of Climatology, 28, 119–128.

Wu, L., Tao, L., & Ding, Q. (2010). Influence of sea surface warming on environmental factors affecting long-term changes of Atlantic tropical cyclone formation. Journal of Climate, 23, 5978–5989.

Wu, L., & Wang, B. (2008). What has changed the proportion of intense hurricanes in the last 30 years? Journal of Climate, 21, 1432–1439.

Xu, Z., Chang, P., Richter, I., Kim, W., & Tang, G. (2014). Diagnosing southeast tropical Atlantic SST and ocean circulation biases in the CMIP5 ensemble. Climate Dynamics, 43, 3123–3145.

Xu, Z., Li, M., Patricola, C. M., & Chang, P. (2014). Oceanic origin of southeast tropical Atlantic biases. Climate Dynamics, 43, 2915–2930.

Yeager, S. G., & Robson, J. I. (2017). Recent progress in understanding and predicting Atlantic decadal climate variability. Current Climate Change Reports, 3, 112–127.

Yeager, S. G., Danabasoglu, G., Rosenbloom, N., Strand, W., Bates, S., Meehl, G., … Lovenduski, N. S. (2018). Predicting near-term changes in the Earth System: A large ensemble of initialized decadal prediction simulations using the Community Earth System Model. Bulletin of the American Meteorological Society, BAMS-D-17-0098.1.

Yeager, S., Karspeck, A., Danabasoglu, G., Tribbia, J., & Teng, H. (2012). A decadal prediction case study: Late twentieth-century North Atlantic ocean heat content. Journal of Climate, 25, 5173–5189.

Yokoi, S., & Takayabu, Y. N. (2009). Multi-model Projection of Global Warming Impact on Tropical Cyclone Genesis Frequency over the Western North Pacific. Journal of the Meteorological Society of Japan, 87, 525–538.

Yu, J.-Y., Kao, P., Paek, H., Hsu, H.-H., Hung, C., Lu, M.-M., & An, S.-I. (2015). Linking emergence of the Central Pacific El Niño to the Atlantic Multidecadal Oscillation. Journal of Climate, 28, 651–662.

Zaba, K. D., & Rudnick, D. L. (2016). The 2014-2015 warming anomaly in the Southern California Current System observed by underwater gliders. Geophysical Research Letters, 43, 1241–1248.

Zhang, G., Wang, Z., Dunkerton, T. J., Peng, M. S., & Magnusdottir, G. (2016). Extratropical impacts on Atlantic tropical cyclone activity. Journal of the Atmospheric Sciences, 73, 1401–1418.

Zhang, L., Wang, C., Song, Z., & Lee, S.-K. (2014). Remote effect of the model cold bias in the tropical North Atlantic on the warm bias in the tropical southeastern Pacific. Journal of Advances in Modeling Earth Systems, 6, 1016–1026.

Zhang, R., & Delworth, T. L. (2006). Impact of Atlantic multidecadal oscillations on India/Sahel rainfall and Atlantic hurricanes. Geophysical Research Letters, 33, L17712.

Zhang, W., Vecchi, G. A., Villarini, G., Murakami, H., Gudgel, R., & Yang, X. (2017). Statistical–dynamical seasonal forecast of western North Pacific and East Asia landfalling tropical cyclones using the GFDL FLOR coupled climate model. Journal of Climate, 30, 2209–2232.

Zhang, W., Vecchi, G. A., Villarini, G., Murakami, H., Rosati, A., Yang, X., … Zeng, F. (2017). Modulation of western North Pacific tropical cyclone activity by the Atlantic Meridional Mode. Climate Dynamics, 48, 631–647.

Zhao, M., Held, I. M., & Vecchi, G. A. (2010). Retrospective forecasts of the hurricane season using a global atmospheric model assuming persistence of SST anomalies. Monthly Weather Review, 138, 3858–3868.

Zhu, J., & Shukla, J. (2013). The role of air–sea coupling in seasonal prediction of Asia–Pacific summer monsoon rainfall. Journal of Climate, 26, 5689–5697.

Zuidema, P., Chang, P., Medeiros, B., Kirtman, B. P., Mechoso, R., Schneider, E. K., … Xu, Z. (2016). Challenges and prospects for reducing coupled climate model SST biases in the eastern tropical Atlantic and Pacific Oceans: The U.S. CLIVAR eastern tropical oceans synthesis working group. Bulletin of the American Meteorological Society, 97, 2305–2328.